Universitat Politècnica de Catalunya

TESIS DOCTORAL

NEW GENERATION FTTH ONU AND OLT DESIGN FOR UPSTREAM TRANSMISSION IN WDM PON INCLUDING OPTIMIZED COMBINATION OF ELECTRONICS AND OPTICS

MIREIA ESTHER OMELLA CANCER

2010

1. Introduction

The access network is the last segment of the operator network before reaching the subscriber. Current fixed access networks are mainly based on copper wires, which were originally installed for analogue telephone transmission in the lower frequency ranges. Due to their widespread availability, with the advent of data communication between computers, these copper cables were additionally used for digital signal transmission. But the capacity of copper cables is limited, and therefore the access part of the network became a bottleneck.

During many years, recurrent optimistic predictions have been made that soon fibre optic would be extended into the home, due to the high potential benefits of this technology. Unfortunately, these visions have been usually succumbed to the realities of economics, regulation and the interest from the main operators in the persistence of existing technologies.

As a mode of example, by using copper, a maximum of 200 Mb/s can be theoretically achieved up to 200 m, 100 Mb/s up to 450 m, while 60 km at 10 Gb/s can be transmitted simply, without problems, using an optical fibre. Another limitation of copper installed wires is that the technology does not allow symmetrical traffic.

Nowadays fibre to the home (FTTH) is becoming a reality with almost 40 million of subscribers worldwide.

New applications are waiting, ready for potential subscribers: video on demand, file sharing, Internet Protocol (IP) good quality telephony, and also broadcast in the form of IP television. The display format improves from the standard definition to high definition and even superhigh resolution video, also including 3D television and online gaming, and also videoconferencing of a much higher quality than we use today.

Standards for 3D video are already being formulated. Entry level 3D TV is currently appearing in the market; as its quality improves, so will increase the bandwidth required to transmit the video stream as it can be seen in Figure 1.1.

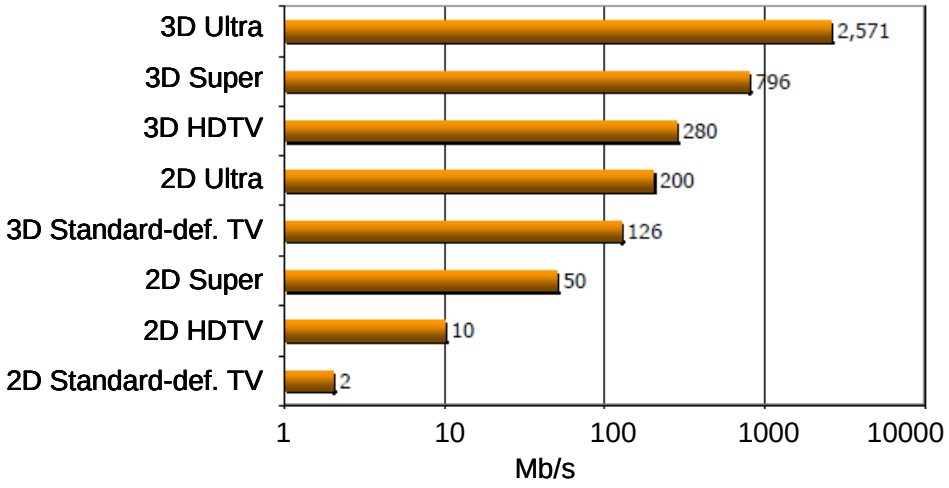

Figure 1.1 Bandwidth requirements for the different TV kinds and qualities

A standard definition television requires about 2Mb/s. A high definition HDTV needs around 4 Mb/s if the image is rather static (a journalist explaining the news for instance), but in fast actions it requires around 8 Mb/s, and 3D immersive HDTV between 50 and 300Mb/s. If uncompressed, 3D television would require Gb/s.

Entertainment is not the only use for bandwidth, also social and environmental benefits can be obtained from a broadband infrastructure: telemedicine, e-learning, Internet-connected security cameras and remote energy monitoring services. Telehealth gives residents instant access to medical specialists via conferencing from the home to the fitness centre or a community room. The videoconferencing may be integrated with internet-enabled diagnostic devices (blood pressure cuffs, respiration measurement, etc), electronic medical record systems, and online prescription services (See Figure 1.2).

Figure 1.2 Telehealth videoconference

More applications can appear in the near future, capable to improve the human life quality. Innovation will continue, bandwidth needs will keep on growing and only fibre to the home with its superior reliability and plentiful upstream capacity will be able to keep delivering the bandwidth requested.

Nowadays there is no technical reason why everyone could not have Gb/s of data to their home using optical access systems which are commercially available today, the obstacles are purely economic. Cost effective solutions must be developed to be able to offer future-proof broadband connections to end users at a reasonable cost.

Currently, in the access networks, passive optical networks (PONs) constitute the most cost effective solutions for practical fibre to the home deployment. A PON consists of an optical line terminator (OLT) located at the Central Office (CO) and a set of associated optical network terminals (ONT), also known as optical network units (ONU) to terminate the fibre. In at FTTH deployment, the ONU is located at the customer's premise but in the other FTTx approaches, ONUs are located in an intermediate point between the CO and the end users. PON gets its name because instead of using powered electronics (switches) in the outside plant (which is done in active networks), it uses passive splitters and couplers to divide up the bandwidth among the end users. Other advantages are the bit rate and modulation transparency and the easy upgrade; only requiring changes in the optoelectronics at the OLT and /or ONU premises. In addition, passive networks can be extended to all available optical bands.

As in PONs there is a shared resource (the fibre), used by all users to connect to the CO, a Media Access Control (MAC) needs to be established in order to guarantee the integrity of the information that is exchanged between the CO and each of the ONUs connected to the network. There are many ways to multiplex different users on a common transmission channel. Time Division Multiplexing (TDM) and Wavelength Division Multiplexing (WDM) are the most common techniques in access PON, although also SCM and OFDM are currently being the focus of strong investigation. Hybrid solutions combining two or more techniques are possible as well.

This thesis is focused on low cost solutions to improve the performance of high speed signals in WDM PONs with minimum infrastructure. The necessity to simplify the transmission components in the FTTH access network also introduces new optical fibre transmission limitations to overcome, which would not be present if it were possible to have redundancy.

Optimized combination of electronics and optics will allow joining the enormous bandwidth that optics can offer in colourless systems, with the cost effectiveness, the potential intelligence, and the processing capability of electronics; being a key solution to the increasing demand of scalability and efficient use of the available resources which are two main goals of access Passive Optical Networks (PON).

1.1. Standardization. Current Status

There have been several generations of PON technologies up to date. Two different organizations, the International Telecommunications Union (ITU-T) in collaboration with the Full Service Access Network association (FSAN) on one side, and the Institute of Electrical and Electronic Engineers (IEEE) on the other, have proposed several standards as a guide to operators, manufacturers and vendors [Hajduczenia09].

From FSAN/ITU-T the three main standards completely developed are ATM-PON (APON), using symmetrical 155Mb/s, Broadband-PON (BPON) with 625 Mb/s down and 155 Mb/s upstream and Gigabit-PON (GPON) with 2.5Gb/s down and 1.25 Gb/s upstream, while 10G-PON is currently finishing its standardization proposing symmetrical 10 Gb/s but allowing a first intermediate migration with 2.5 Gb/s upstream. From IEEE, Ethernet-PON (EPON) appeared as an alternative to GPON with symmetrical 1 Gb/s and, at present, 10G-EPON has just been standardized aiming also symmetrical 10 Gb/s with and intermediate stage allowing 1Gb/s in the upstream, as it can be seen in Figure 1.3.

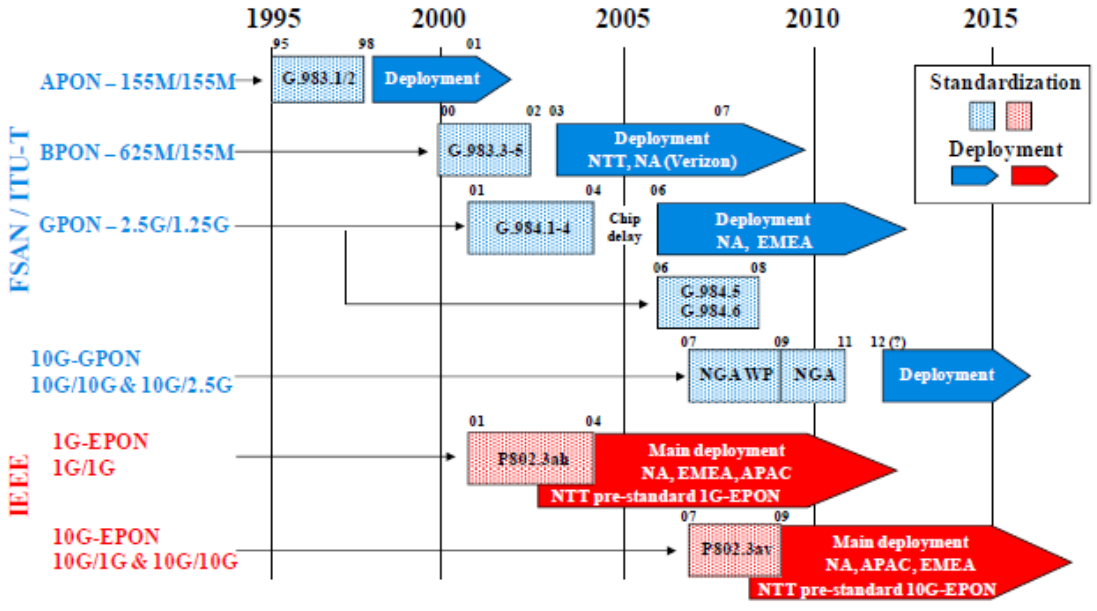

Figure 1. 3. IEEE and FSAN/ITU-T PON systems and their standardization status / timelines

1.1.1. GPON & 1G-EPON Standards

Currently the deployed PONs are based either in GPON (supported by the ITU-T and FSAN) or EPON standards (supported by the IEEE- Ethernet group). Perhaps the highest distinction between the two protocols is a marked difference in architectural approach. GPON provides ATM for voice, Ethernet for data, and proprietary encapsulation for other services. EPON, on the other hand, uses IP to carry data, voice, and video.

A multiprotocol transport solution supports the GPON structure. Using ATM technology, virtual circuits are provisioned for different types of services sent from a central office location primarily to business end users. This type of transport provides high-quality service, but involves significant overhead because virtual circuits need to be provisioned for each type of service. Additionally, GPON equipment requires multiple protocol conversions, segmentation and reassembly (SAR), virtual channel (VC) termination and point-to-point protocol (PPP).

EPON [Kramer04] provides seamless connectivity for any type of IP-based or other "packetized" communication. Since Ethernet devices are ubiquitous from the home network all the way through to regional, national and worldwide backbone networks, implementation of EPONs can be highly cost-effective.

These are the main characteristics of both standards:

- GPON:
  - Uses Generic Encapsulation Method (GEM) protocol layer to support Ethernet, ATM and TDM over point to multipoint PON network topologies
  - 1.25 Gb/s upstream and 2.5 Gb/s downstream bandwidth
  - Includes mechanisms for network Operations, Administration and Maintenance (OAM)
  - Supports Class of Service (CoS) operation for time-sensitive transport of data payloads
  - Supports TDM using circuit emulation services or transport over GEM
  - Supports voice services with Voice over IP (VoIP)

- EPON:
  - Combines Ethernet transport protocols with point to multipoint PON network topologies
  - Also called Ethernet in the First Mile or EFM
  - 1 Gb/s symmetrical upstream and downstream bandwidth
  - Includes mechanisms for network Operations, Administration and Maintenance (OAM)

- Supports Class of Service (CoS) operation for time-sensitive transport of data payloads such as video where video frames must be delivered in sequence and in time to prevent visible glitches
- Supports TDM only using circuit emulation services
- Supports voice services with Voice over IP (VoIP)

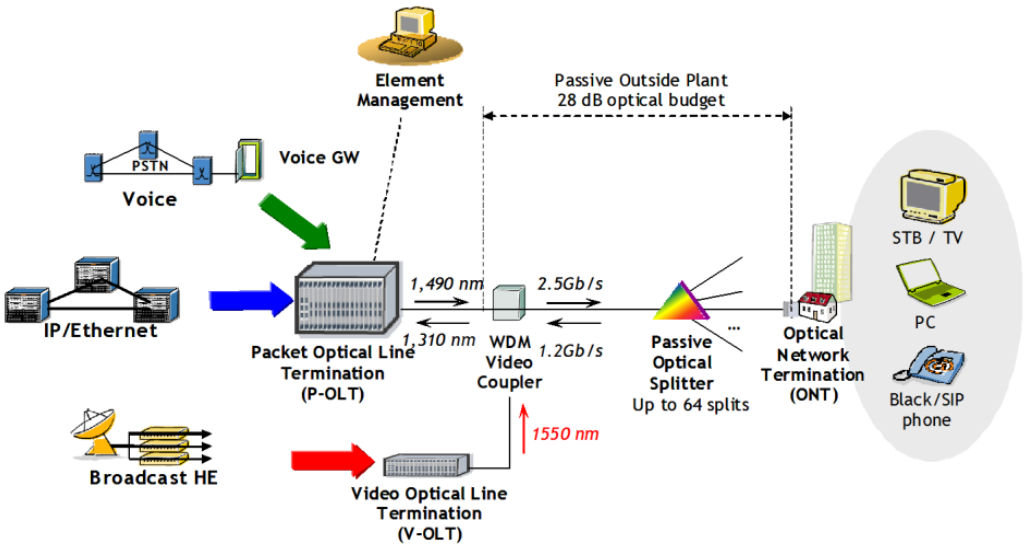

Figure 1.4 Schematic diagram of a GPON Network [FTTH council]

During the elaboration of this thesis new standards have been approved, 10G-GPON and 10G-EPON, which are explained in following section.

1.1.2. 10G-GPON & 10G-EPON standards

IEEE 10G-EPON

The 10G-EPON standardization (defined as IEEE Std 802.3av) was started with the target of adding the 10-Gbit/s physical layer specifications to the GEPON standard. To achieve a smooth upgrade, it is assumed that the following three types of ONUs can coexist in the same PON. [Hajduczenia10, Tanaka10]

(1) Symmetric 10G-EPON ONU (10G/10G),
(2) Asymmetric 10G-EPON ONU (1G/10G),
(3) GE-PON ONU (1G/1G).

1G/10G downstream signals are transmitted in different wavelength bands (i.e., 1480–1500 nm for 1G and 1575–1580 nm for 10G) at the OLT, and the ONU selects one signal or the other by using a wavelength filter.

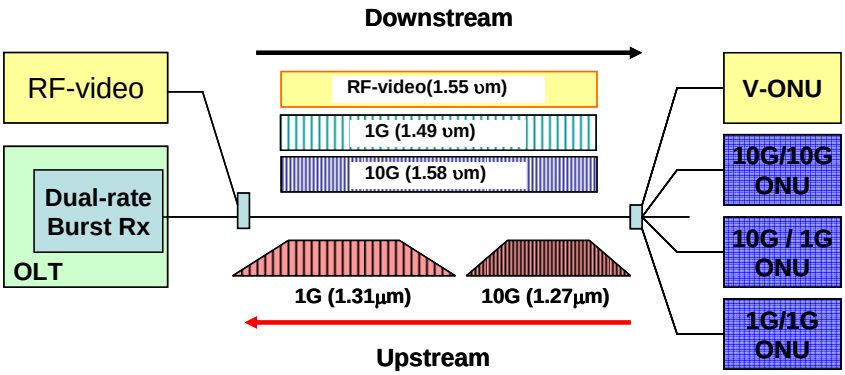

Figure 1.5. Wavelength distribution and possible ONU bit rates in 10G-EPON based networks

1G/10G upstream signals are transmitted within the same/overlapped wavelength band (1260–1360 1G and 1260–1280 nm 10G) at ONUs, but the signal from each ONU is transmitted so as to arrive at the OLT at a different timing from the others under the OLT's control: this scheme is called time-division multiple access (TDMA). To receive consecutive upstream signals having different speeds (i.e., 1G or 10G) and different powers from each other, a dual rate burst receiver is necessary in OLT (see Figure 1.5).

Radio-frequency (RF) video overlayed onto PON (using 1550–1560 nm) is considered in 10G-EPON as well as in GE-PON. 10G-EPON uses a high-gain forward error correction (FEC) code, called Reed-Solomon (255, 223), to make possible low-cost optical transceiver modules. The coexistence of 10G-EPON and GE-PON can be achieved by utilizing these specifications as well as a dual-rate dynamic bandwidth allocation algorithm, which is out of the scope of the standard, so that network operators can smoothly upgrade PON systems.

ITU-T XG-PON

ITU-T Q2/15 is studying XG-PON with the focus on 2.5 Gb/s upstream and 10 Gb/s downstream at this moment. It is planning to develop four Recommendations (G.987.1 to G.987.4). The following items are under discussion: high-speed Internet access, emulation and/or simulation of legacy services, IPTV (Internet protocol television), and mobile backhauling (which requires time synchronization between the OLT and ONU). Smooth migration from the Gigabit-class PON is one of the important requirements. The maximum reach between the OLT and ONU is 20 km, and its extension to 60 km is to be added in a revised version. The wavelength allocation of XG-PON is the same allocation as IEEE 10G-EPON (i.e., 1260–1280 nm upstream and 1575–1580 nm downstream), so that the optical components can be common with IEEE.

Although it is previewed that the margin of the new wavelengths to be used by the XG-PON could be increased to fill also the 1290-1330 region for the upstream and the 1480-1500nm for the downstream.

In any case wavelength allocation has to allow XG-PON and G-PON to coexist in the same fibre when WDM without wavelength overlaps between them.

Like in IEEE 10G-EPON, the issue of how to implement FEC to achieve a high loss budget is one of the important issues under study.

The maximum optical loss between the OLT and ONU, i.e., the loss budget, is being discussed on the basis of the existing fibre infrastructure that many network operators have already deployed for the current-generation PON.

1.2. FTTH Deployment. State of the Art

EPON represented the 60% of the market in 2008 as it can be seen in Figure 1.6 up. This is in large part due to Asia-Pacific's almost exclusive use of EPON, with both Japanese and South Korean carriers backing the technology (see Figure 1.6 bottom).

Breakdown of the FTTx technologies worldwide – end of 2008

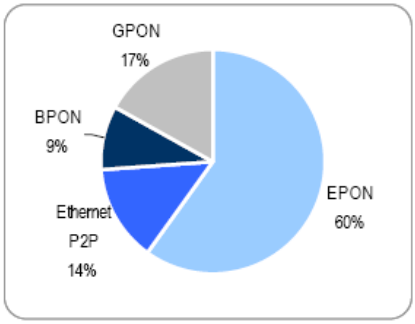

Source: IDATE

Breakdown of FTTx technologies by region (subscribers) – end of 2008

	EPON	GPON	BPON	Ethernet P2P
Asia Pacific	91%	-	-	9%
China	*100%*			
North America	5%	74%	12%	9%
Europe	-	19%	-	81%

Source: IDATE and Broadband Properties for North American figures

Figure 1.6. Percentage of the different FTTx technologies wordwide (up) and types of technology used by region (down)

However, this percentages change with time. China that at the end of 2008 was deploying EPON is nowadays deploying both EPON and GPON. According to a recent report by market research firm Dell'Oro Group, first quarter 2010 GPON equipment revenues from both optical line terminals and optical networking terminals surpassed EPON revenues for the first time and hit a record level, growing almost 70 percent over the year ago period.

Regarding the current number of subscribers, more than 6 million consumers now use direct fibre optic connections to the home or building in the United States, more than 17 million in Japan, and 10 million in Korea. In all Europe (EUR36), the number of subscribers is nowadays around 3.5 million (IDATE). At 2006, the 97% of the subscribers were concentrated in five countries (Sweden, Italy, Denmark, the Netherlands and Norway), where competition from alternative and cable operators was strongest. At end 2009, 4 countries have entered the Global Ranking, meaning that more than 1% of households have subscribed to a FTTH/B service: France, Czech Republic, Portugal and Bulgaria, and the majority of subscribers (around 67% of FTTH/B subscribers) is concentrated in 7 countries in Western and Northern Europe: Sweden, Italy, France, Norway, The Netherlands, Denmark and Germany.

Rank	Operator	Country	Main technology & architecture	FTTx subscribers
1	NTT	Japan	FTTH/B GEPON	11 793 000
2	China Telecom (1)	China	FTTH - FTTx+LAN EPON LAN/DSL	11 160 000
3	KT	South Korea	FTTB EPON/GEPON	3 555 644
4	Verizon	USA	FTTH BPON/GPON	3 100 000
5	SK Broadband	South Korea	FTTB/LAN GEPON	2 733 141
6	AT&T	USA	FTTN VDSL2	1 585 000
7	LG Powercom	South Korea	FTTH/B EPON/GEPON	1 504 090
8	Chunghwa Telecom	Taiwan	FTTB GEPON	1 342 000
9	KDDI	Japan	FTTH/B EPON/GEPON	1 211 000
10	Beeline	Russia	FTTB EP2P	724 000

(1) of which 560,000 FTTH subscribers and 10.6 million FTTx/LAN subscribers

Source: IDATE

Figure 1.7. Top 10 FTTx players around the globe as of mid-2009

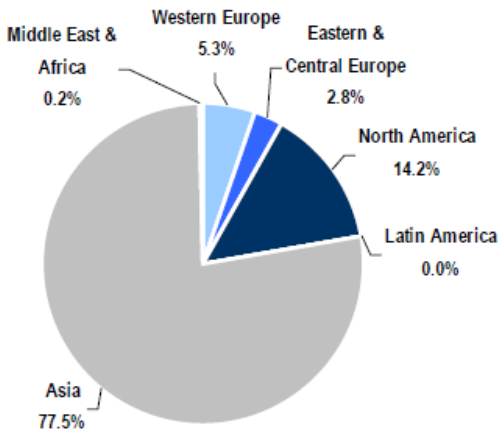

Figure 1.8 Distribution of FTTH/B subscribers around the world as of mid-2009

	FTTH/B	VDSL	FTTLA	FTTx + LAN	Total FTTx
Western Europe (1)	1 806 515	1 645 350	20 000	0	3 471 865
Eastern & Central Europe (1)	962 165	34 000	225 393	0	1 221 558
North America (2)	4 805 500	1 585 000	na	0	6 390 500
Latin America	2 000	0	na	0	2 000
Asia	26 293 000	1 500	na	16 900 000	43 194 500
Middle East & Africa	66 100	0	0	0	66 100
TOTAL World	**33 935 280**	**3 265 850**	**245 393**	**16 900 000**	**54 346 523**

Figure 1.9. FTTx subscribers as of mid-2009, by geographical area. (1) Western, Eastern and Central Europe includes the EU-27, Norway, Switzerland, Iceland, Andorra, Luxembourg, Croatia and Russia. (2) USA, Canada & Mexico.

1.3. NG Passive Optical Networks: SARDANA network

The elaboration of this thesis has been involved in the FP7 strep SARDANA project. As its name indicates, Scalable Advanced Ring-based Dense Access Network Architecture, SARDANA pursues the goals and requirements of next-generation passive optical networks:

Single-fibre bidirectional access to the user simplifies the outside plant and cable management, also reducing microbending risks at user premises. The use of colourless identical ONUs avoids coloured laser sources at the end-user side, thus dismissing maintenance and inventory issues.

SARDANA is based on a WDM double-fibre-ring with single-fibre wavelength-dedicated trees (TDM) connected to the main ring at the Remote Nodes (RN). Remote amplification is introduced at the RN by means of Erbium Doped Fibres (EDFs) for compensating Add/Drop and filtering losses. Pump for the remote amplification is provided by the pumping lasers located at the Central Office (CO). The CO uses a stack of tuneable lasers for serving the different tree network segments on a TDM basis. Tunable lasers can be shared among different network segments with agile WDM tuning for routing and using Geographical Bandwidth Allocation (GBA) techniques to concentrate the resources at the more demanding networks sections. It can be noticed that the complexity of the network is concentrated at the CO, since its cost is shared among the many users of the PON, while the ONUs are kept simple and the external plant fully passive. The schematic architecture can be seen in Figure 1.10.

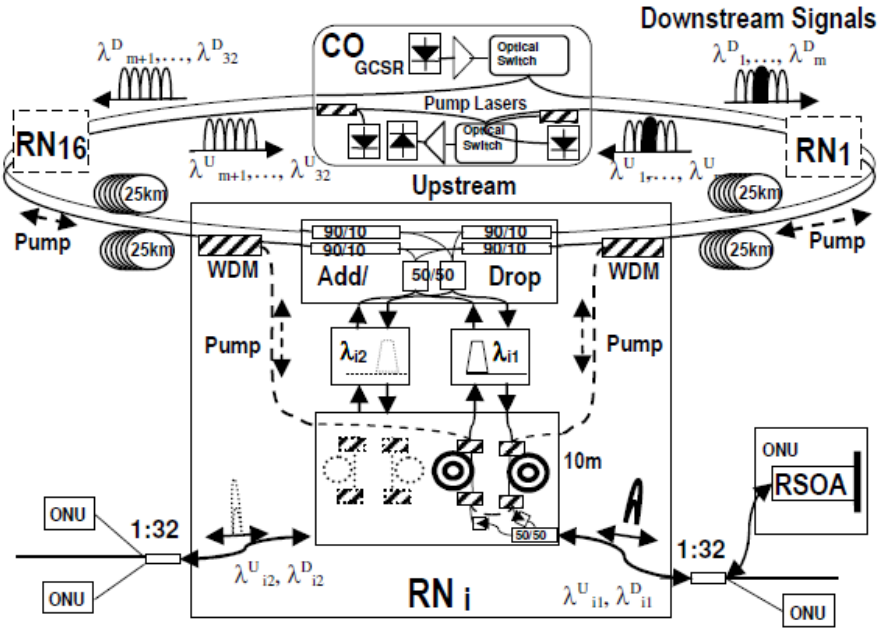

Figure 1.10. SARDANA architecture

Centralized wavelength generation and control are requirements of network operators. High user density and scalability, in terms of user addition, and transparent OADM addition together with distance extension and geographical flexibility capabilities are other interesting features that advanced topologies should implement, and are included in SARDANA. All these concepts together allow the convergence between metro and access, simplifying the outside plant and reducing the equipment at the RNs.

The FP7 strep SARDANA project includes university and industrial partners from different European countries: Universitat Politècnica de Catalunya (UPC) from Barcelona (Spain) as a coordinator, France-Telecom/Orange from Lannion (France), Tellabs in Espoo (Finland), Athens Institute of Technology (AIT) and IntraCOM from Athens (Greece), Instituto de Telecomunicaçoes (IT) in Aveiro (Portugal) and Istituto Superiore delle Comunicazioni (ISCOM) from Rome (Italy).

1.4. References of Chapter 1.

[Desurvire06] E. B. Desurvire “Capacity Demand and Technology Challenges for Lightwave Systems in the Next Two Decades” J. Lightwave Technol, vol. 24, no. 12, Dec. 2006

[FTTH council] “Fiber to the Home. Advantages of optical access” 4th Edition/Spring 2010. www.FTTHCouncil.org

[Hajduczenia09] M. Hajduczenia et al., “Next Generation PON Systems – Current Status”, in proc. ICTON 09, paper Tu.B5.2, Madeira (Portugal), June 2009

[Hajduczenia10] M. Hajduczenia et al., “IEEE 802.3av™-2009 10G-EPON and Support for Loss Budgets beyond 29dB”, in proc. OFC10, paper NWB2, San Diego USA, March 2010

[IDATE] http://www.idate-research.com/en/Research/FTTx-Watch-Service

[Lázaro 2006] J. A. Lázaro et al., “Remotely Amplified SARDANA: Single-fibre-tree Advanced Ring-based Dense Access Network Architecture” In proc. ECOC’06, Cannes, paper We3.P.169 September 2006

[Song10] H. Song et al., “Long-Reach Optical Access Networks: A survey of Research Challenges, Demonstrations, and Bandwidth Assignment Mechanisms”, IEEE communications surveys and tutorials, vol. 12, no.1, pp. 112-122, March 2010

[Tanaka10] K. Tanaka, A. Agata, and Y. Horiuchi “IEEE 802.3av 10G-EPON Standardization and Its Research and Development Status”. J. Lightw. Technol., vol. 28, no. 4, Feb 2010 pp. 651-661

[Kramer04] G. Kramer, "Ethernet Passive Optical Network s," McGraw-Hill Professional, 2004 , ISBN: 0071445625

2. Photo-Detection & Chromatic Dispersion Mitigation

2.1. Introduction

In single mode fibres, the group velocity associated with the fundamental optical mode is frequency dependent because of chromatic dispersion (CD). The frequency dependence of the group velocity leads to pulse broadening simply because different spectral components of the pulse disperse during propagation and do not arrive simultaneously at the fibre output.

CD is originated into the optical fibre. In fact it is a linear effect, over the optical field. However, at the fibre end, the signal passes through the photodetector to be transformed into electrical signal. The obtained electrical signal is proportional to the optical power, due to the square-law characteristic of the photodiode, and becomes non-linear with the optical field.

A simple module capable to perform the mathematical function "square root" (SQRT) has been designed, simulated and experimentally implemented using microstrip and MMIC technologies. As it will be explained in the following subchapters, this module can partially compensate for the square-law characteristic of the photodiode and improve the performance in analogue and digital systems. Although the phase is lost, a more linear relationship is present between CD and the received signal, improving the performance in Radio over Fibre (RoF) systems and also in digital transmission when an electronic post-equalizer is used.

The same way a photodiode detects optical power, also direct modulated laser and external modulators at transmission transform the electrical signal linearly into optical power. A new technique to transmit data proportional to the optical field has been studied and experimentally tested, and combined with the square root equalization.

Finally, a study of the optimum non linear function to allow a Gaussian photodetection, under spontaneous emission noise (ASE) as the dominant impairment, is presented.

Although this thesis in mainly focused in access networks based in WDM PON systems, the work done in this chapter has also been applied to long haul (SQRT with MLSE) as a complementary demonstration of the channel linearization capability of the SQRT.

2.2. State of the art

Chromatic dispersion compensation can be classified into optical (ODC) and electronic (EDC) solutions.

ODC

Between the optical solutions, dispersion compensating fibres (DCF) [Vengsarkar93] and Fibre Bragg Gratings (FBG) [Marti97] [Brooks95] are the most known. DCF is currently used as the standard solution for dispersion compensation in long-haul transmission links, since it yields colourless, slope matched dispersion cancellation with negligible cascading impairments. Typical DCF has negative dispersion and produces a negative slope, with nominal values that are typically ten times higher than those of the fibre to compensate for. Therefore, for example, to adequately compensate for the dispersion in 90 km of G.652 fibre, approximately 9 km of DCF must be installed (this is a general rule). However, DCF is also limited in optical input power to avoid nonlinear impairments. In addition, the typical attenuation found in a DCF is three times higher than in standard fibre, and the polarization mode dispersion (PMD) coefficient is about double. In bidirectional systems DCF presents more Rayleigh Backscattering effects and it is bulky.

Chirped FBGs could possibly replace DCF as the standard solution for in-line dispersion compensation. Chirped FBGs have a negligible nonlinearity, low insertion loss and small size [Hill97] [Fews06]. The main drawback of FBGs is that they suffer from distortions in their phase response, better known as the group delay ripple (GDR) [Veljanovski06]. This is caused by imperfections in the gratings fabrication process and limits the number of FBGs that can be cascaded.

Another main limitation present in both solutions is their stiffness, at compensating a specific amount of dispersion or fibre length. However, variable dispersion compensators have been also reported like in [Doerr05], where the adaptability is achieved by a variable curvature reflecting membrane. Also special integrated tuneable fibre gratings have been reported [Eggleton2000].

Nowadays, commercial optical tuneable dispersion compensators have been developed for applications of dynamic dispersion compensation up to 40Gb/s in long haul transmissions. Also commercial programmable filters are appearing, capable to be adapted in wavelength, amplitude and phase to the requirements of the network over the entire C or L-band, flexible enough to be

adapted according to changes in the network or the source used as a transmitter [Omella_ANIC10].

EDC

Electronic compensators can be used directly or together with an optical compensation. The advance of high-speed microelectronics, has enabled the application of EDC in optical communication systems at 10 Gb/s. Compared to its optical counterpart, it is more flexible, cost-effective, and easier to integrate into transmitters or receivers. Receiver-side EDC, which can adapt quickly to changes in link conditions, is of particular value for future transparent optical networks where the reconfiguration of add- and drop-nodes can cause the transmission paths to vary. However, as it has been previously mentioned, the performance of conventional EDC using direct detection (DD EDC) is limited by the loss of the signal phase information and photodetection non-linearity. In addition, the transformation of linear optical impairments arising from chromatic dispersion (CD) into nonlinear impairments after square-law detection notably increases the operational complexity of the DD EDC.

EDC based on coherent detection can access both the intensity and the phase of the optical field, thus allowing full CD compensation. However, it requires additional tight-specification optical components, and signal polarization and phase tracking or recovery [Cai08]. Other sophisticate receivers try to recover the full optical field after receiver [Ellis06] [Zhao08] [Zhao10]. Using a single asymmetric Mach–Zehnder interferometer (AMZI) prior to balanced photo-detection and a separated branch of DD allows recovering phase and amplitude although it can be also done by a balanced photodetector with differential outputs. The recovered information properly adjusted is afterwards sent to a conventional offline EDC like a simple dispersive transmission line, Decision Feedback-Feed-Forward Equalizer DFE-FFE, or maximum likelihood sequence estimation (MLSE) [Zhao10] in the electrical domain. In recent papers, the amplitude information after reception is passed through a digital off-line square root mathematical transformation, before processing it [Zhao08] [Zhao10].

A third approach is to modify the transmission format where the baseband signal spectrum is compressed using baseband line coding in order to reduce the effective bandwidth required to transmit or receive the data [May94]. For example, amplitude modulated phase shift keyed (AM-PSK) duobinary [Yoneaka95] or phase shaped binary transmission (PSBT) [Penninckx97] achieve bandwidth reduction at the electric field level, which reduces the impact of dispersion as compared to regular binary signalling. These methods avoid multiple optical power or detected levels by uniquely encoding the data and biasing the amplitude modulator at 90º or

270º. Other forms of multilevel signalling which transmit multiple optical power levels provide some dispersion immunity over straight binary signalling as well; however, maintaining the multiple levels at the optical power level is generally more susceptible to noise. Another modulation method called dispersion supported transmission (DST) [Bungarzeanu94] may also be classified into this group since it uses a combination of amplitude and phase modulation to limit the effects of dispersion.

A special technique used to minimize the effects of CD is the Optical Single Sideband (OSSB) generation [Fonseca06] [Sieben99]. Dispersion makes upper and lower sideband subcarrier experience different phase shift. When RF frequency is produced by beating of optical carrier and subcarrier at receiver, these phase differences result in power degradation at the RF frequency. So, OSSB transmission that transmits only one of two sidebands is a good solution to overcome CD effects.

In this thesis, the focus has been on a low cost strategy in the electrical domain to compensate the quadratic response of the photodetector, evaluating also the signal statistics in combination or not with a special transmission that is linear with the optical field. Regarding off-line processing in MLSE, as an alternative to the SQRT function, studies in [Franceschini07, Bosco08, Hueda07] have also proposed other non linear n-root concave functions.

2.3. SQRT module

In this subchapter, a low cost technique to partially compensate the non-linear effect of the photodiode is proposed. It consists of an equaliser which deals with the intrinsic square-law function of the photodiode between the optical field amplitude and the generated current, an effect that limits the effectiveness of the electronic equalisers.

If optical field amplitude could be detected instead of optical power, a more linear relationship between linear impairments in the optical domain (like CD, ASE noise, PMD or Rayleigh Backscattering) and the received signal could be used. This idea has been implemented in this thesis work, either digitally or with a memoryless electronic circuit, which tries to approximate the response of the SQRT mathematical function with the use of a simple electronic circuit applied at the physical transport layer, overcoming the transmission limitation in the electrical domain.

Unlike other solutions, SQRT combined with conventional EDC does not depend on the exact distance of the optical fibre to be compensated, and it could be integrated in chip form with the photodiode. The good accuracy between the ideal and the circuit approximation SQRT response has been demonstrated by measurements and simulations. In fact, it provides better results than a digital SQRT mathematical function for low and medium levels of quantisation and almost the same results for a high level of quantisation. More details and application results for this type of equaliser are provided in following sections.

2.3.1. Statistical Model

The optical channel under study, using an on–off keying (OOK) modulation, is generally assumed to be Gaussian during optical fibre transmission. However, in optically amplified transmissions and because of amplified spontaneous emission (ASE) and CD, noise statistics after photodetection are non-Gaussian and signal dependent. A non-central chi-square statistic constitutes a proper model of the optical OOK noise-corrupted channel [Proakis] [Sahuguede09].

Considering the detected signal as the sum of squared signal and noise, that has an in-phase and in-quadrature components:

$Y = X_1^2 + X_2^2$, where X_1 and X_2 are statistically independent Gaussian random variables with means m_i, i = 1, 2 and common variance σ^2. *Y* presents a non-central chi-square distribution with 2 degrees of freedom and with non-centrality parameter $s^2 = m_1^2 + m_2^2$. The PDF of Y is [Proakis]

$$p_Y(y) = \frac{1}{2\sigma^2} e^{-(s^2+y)/2\sigma^2} I_0\left(\sqrt{y}\frac{s}{\sigma^2}\right), \quad y \geq 0 \quad (2.1),$$

where $I_0(x)$ is the 0^{th} order Bessel function of the first kind. By applying the square root module over the detected signal, the distribution becomes Ricean. Defining the random variable R, where $R = \sqrt{Y}$, the PDF of the resultant distribution can be obtained by a simple change of variable as:

$$p_V(v) = \frac{1}{2\sigma^2} e^{-(s^2+v^2)/2\sigma^2} I_0\left(\frac{v \cdot s}{\sigma^2}\right), \quad v \geq 0 \quad (2.2)$$

The particular case of Rice distribution where the mean values are zero is called Rayleigh distribution, and it is used to characterize another important effect in optical fibres that will be explained in next chapter: the Rayleigh Backscattering [Gysel90]. The PDFs of a Gaussian (2.3), Ricean (2.2) and Chi-square (2.1) distributions have been plotted for comparison. In Figure 2.1 left the plot compares these distributions for values of σ^2=4 and variables (y, v and x) close to zero. In Figure 2.1 right, the rice distribution for different values of v is presented. It can be seen that for *v* values higher than 2, the PDF are Gaussian like, with similar variances.
The expression for Gaussian distributions is:

$$p_X(x) = \frac{1}{\sqrt{2\pi}\sigma} e^{-(x-m_x)^2/2\sigma^2} \quad (2.3)$$

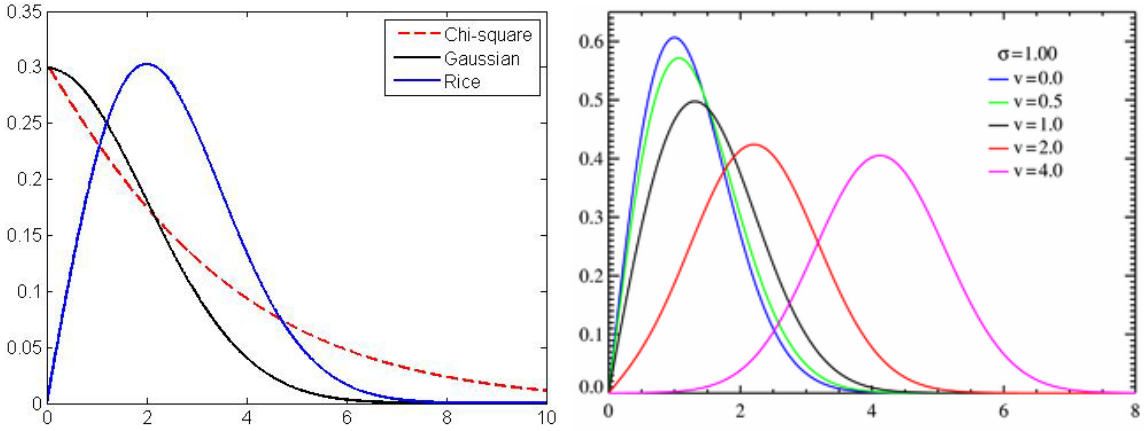

Figure 2.1 Chi-square, Gaussian and Rice distributions comparison and Rice PDF evolution for different values of its variable v.

In [Foggi06], it is stated that the received signal statistics after photodetection in CD and Polarization Mode Dispersion (PMD) dominant systems can be approximated as a Gaussian if a SQRT operation is performed, but in the case of low signal to noise ratios only the right hand tail is Gaussian.

2.3.2. 1st Electronic Implementation: Discrete Microstrip Prototype

To develop an electronic circuit capable to perform the mathematical function SQRT, a non – linear element was needed. A diode is a two terminal semiconductor device having a non-linear V-I relationship. This nonlinearity has been already exploited for functions of signal detection, demodulation, switching, frequency multiplication and oscillation [Hines84]. The Schottky barrier diode is the diode which presents lower junction capacitance and, for this reason, is the more suited for high frequency applications.

The Schottky diode can be modelled as a non-linear resistor, with a small signal V-I relationship expressed as (2.4) and Figure 2.21:

$$I(V) = I_s(e^{\frac{qV}{nkT}} - 1) \quad (2.4)$$

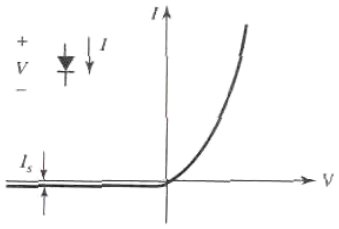

Figure 2.2 I-V response of a schottky diode

where I_s is the saturation current (typically between 10^{-6} to 10^{-15} A), n is a number close to 1.0, usually between 1.05 and 1.25, called the slope parameter or ideality factor, q is the charge of an electron , k the Boltzmann's constant and T the temperature in Kelvin degrees.

Instead of using the diode in series, it can be also used in parallel to the transmission line, driving it controlling the current and detecting the resulting voltage. It has been seen that isolating the voltage with respect to the current (2.5), the behaviour can be approximated to the SQRT controlling the elements of the electronic circuit and the associated parasitic effects of the diode.

$$V = \frac{nkT}{q} \cdot \left[\ln\left(\frac{I}{I_s} \right) + 1 \right] \quad (2.5)$$

In practical implementations, the infinite slope of a SQRT that is present in the zero cannot be achieved. In our case, the dynamic range of the device will be equivalent to the maximum extinction ratio (ER) that can present the incoming signal to be optimally linearised. Signals with very low ER will not achieve much improvement from the SQRT because the slope of the response will not change very much and could be approximated by a linear response. If a DC coupled photodetector is used, the gain in the automatic gain control (AGC) can be adjusted to fit the device diode requirements without modifying the ER of the signal, simply measuring the DC level at the input of the SQRT if the ER of the signal is between the dynamic ranges of the device.

The implemented non-linear circuit that approximates the SQRT function is based on 2 Schottky diodes in parallel and two resistors in series. The values of the resistors have been optimized by using the Advanced Design System, including also the specific electrical model of the chosen diodes. The electrical scheme can be seen in Figure 2.3.

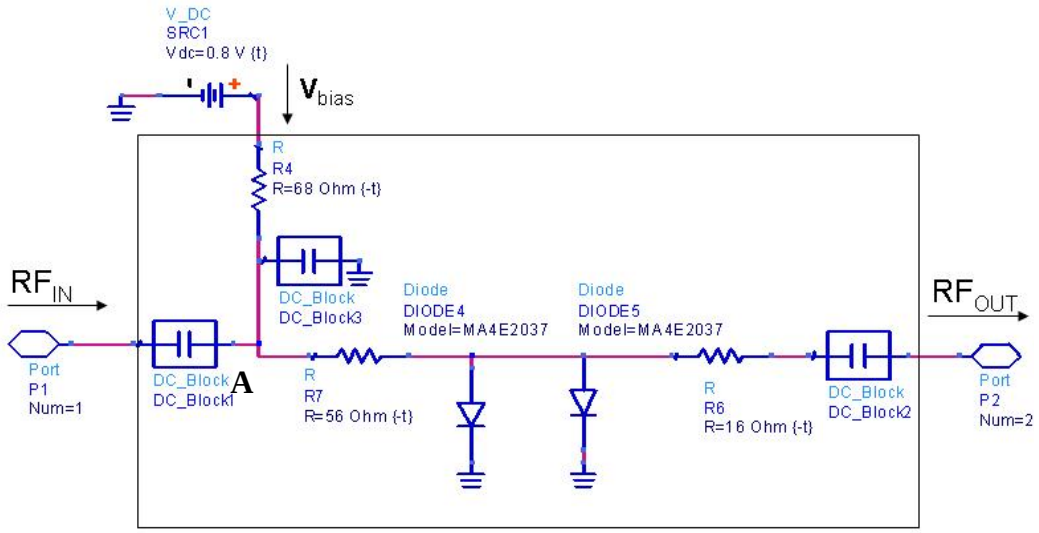

Figure 2.3 ADS electrical circuit which performs the mathematical function SQRT based in two diodes

Main characteristics

As it can be observed, the circuit is AC-coupled and the operation is then performed around a bias point, by applying a bias voltage after the DC block. The DC level of the input signal is adjusted to the Schottky diode working conditions.

The best way to adjust the optimum DC bias for the diodes is introducing a triangular signal to the device and observing the form of square root at the output with an oscilloscope, as shown in Figure 2.4 at 3MHz. We only had triangular shape signal generators up to some MHz at that time. Nowadays commercial arbitrary waveform generators (AWGs) are appearing in the market capable to be programmed to create special waveforms with repetition rates of several GHz.

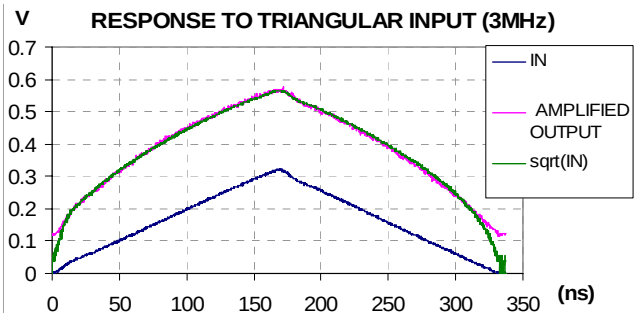

Figure 2.4. Circuit response to triangular input

In order to check the circuit's behaviour at higher frequency, a network analyzer (NA) can be used; the process is summarized in Figure 2.5. The S_{21} parameter is measured with the NA from 130 MHz to 10 GHz, introducing a very small RF signal and changing the DC voltage (V_{cc}). All the traces are captured and stored in a computer by using a GPIB connector, and then processed to evaluate the performance of the device compared with an ideal SQRT.

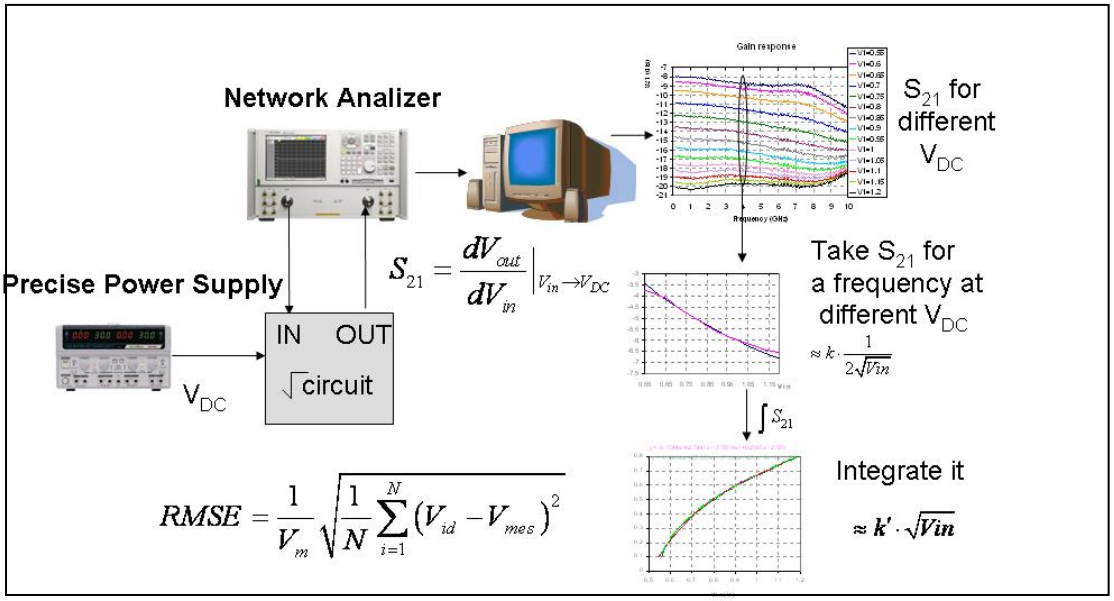

Figure 2.5 Set up and process to evaluate the SQRT circuit behaviour at high frequencies

The captured S21 traces are presented in Figure 2.6. For a voltage bigger than the diode threshold, as the bias voltage increases, the gain of the device decreases, showing the non-linear compression effect.

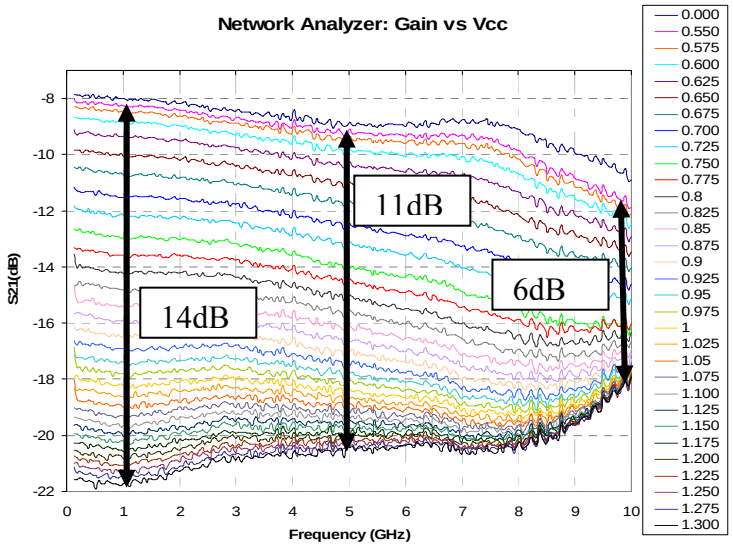

Figure 2.6. Gain versus Vcc measured with a network analyzer

Using an external resistor, we have been able to measure de current that goes (for each voltage) through the bias path in order to know the real voltage V_{in} in the point marked as "A" in Figure 2.3. As it can be seen in the graph, the shape of the S_{21} changes from 8GHz to 10GHz due to the microstrip and diode bandwidth limitations and does not allow more than 6dB of variation of gain in this upper margin.

Taking the values of the different traces for a specified frequency (in this case 5GHz), translating the dB data to linear measurement, and doing the integration of the data, (the network analyzer shows the gain or first derivative of the signal) we can obtain the shape of the signal, taking an equivalence between the variation in amplitude of the RF data, and the variation of the Vin (point A in Figure 2.3) because of changing V_{cc} doing trapezoidal integration with the excel samples.

$$\int dV_{out} = \int S_{21}(V_i)dV_i =$$
$$= \int S_{21}(V_{i-1})dV_{i-1} + (V_i - V_{i-1})10^{(S_{21}(V_{i-1})/20)} + (V_i - V_{i-1})(10^{(S_{21}(V_{i-1})/20)} - 10^{(S_{21}(V_i)/20)})/2 \qquad (2.6)$$

In Figure 2.7, the results show that the response of the circuit can be approximated to the SQRT of a voltage that is the result of the input voltage subtracted by 0.615. Summing a constant or multiplying the signal by a constant constitute linear operations that do not affect to the non-

linear effect of the square root. In the graph, the adjusted measurement corresponds to multiply the measured data by 9.58 and after sum -1.75.

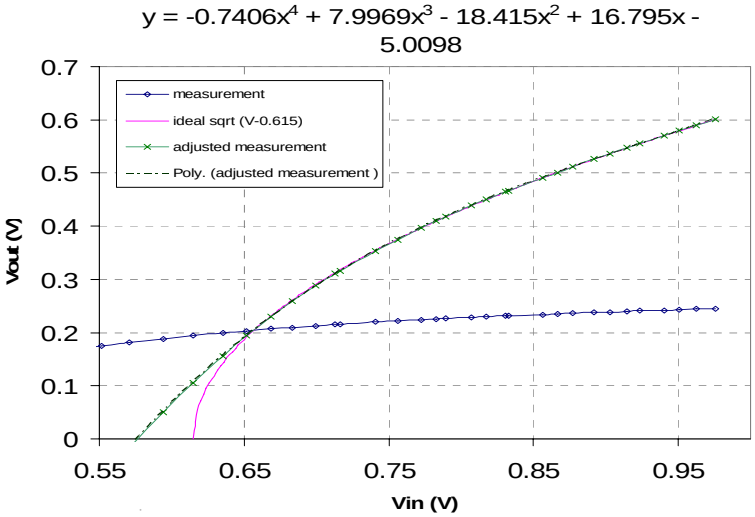

Figure 2.7. Circuit response comparison to ideal SQRT

The Root Mean Square Error (RMSE) has been calculated. It is defined as

$$RMSE = \frac{1}{V_m}\sqrt{\frac{1}{N}\sum_{i=1}^{N}\left(V_{id} - V_{mes}\right)^2} \qquad (2.7)$$

Where V_{id} means the ideal voltage at the output, and V_{mes} means V measured and Vm is the medium voltage: $\sqrt{(\text{DC voltage in A})}$. Table 2.1 presents the achieved results showing the penalty increases notably from ER bigger than 10 dB, as it was expected due to the maximum compression of 11dB at 5GHz shown in Figure 2.6. Figure 2.8 shows a picture of the device in a microstrip circuit mounted technology based in CuClad substrate (Right). Figure 2.8 left shows the low frequency cut-off (around 25 KHz) due to the DC blocks used in the circuit.

RMSE ER= ∞ dB	RMSE ER= 12.5dB	RMSE ER= 10dB	RMSE ER= 8.2dB	RMSE ER= 6dB
0.0468	0.00686	0.00225	0.00184	0.00163

Table 2.1. RMSE for different values of ER

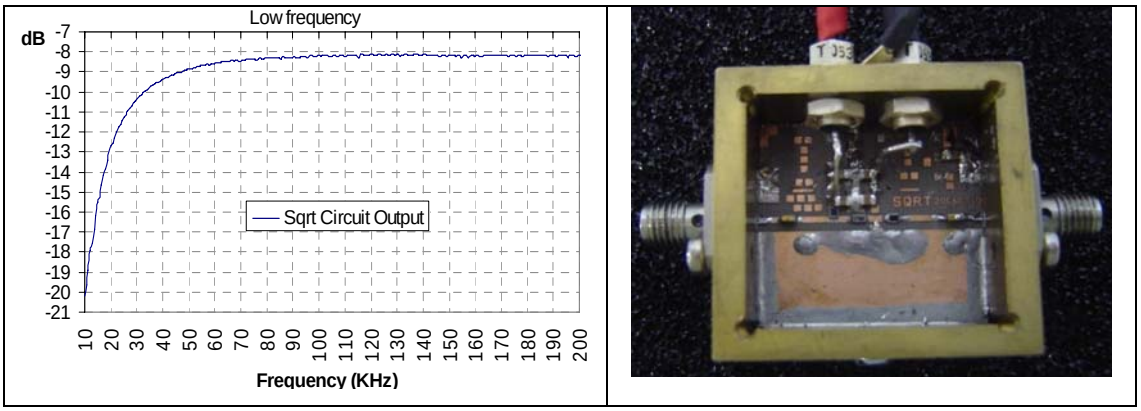

Figure 2.8 Left: Low frequency cut-off. Right: photograph of a SQRT module microstrip implementation.

2.3.3. 2nd Electronic Implementation: MMIC Prototype

The first SQRT circuit, that approximates the response of the square root mathematical function with the use of two Schottky diodes, introduced in previous subchapter, demonstrated its performances in digital and RoF systems experimentally as it will be shown. However, its bandwidth was limited to 7GHz due to the microstrip mounting of the discrete diodes and the rest of the microwave circuit.

Here, the design and implementation of this non-linear circuit in Monolithic Microwave Integrated Circuit (MMIC) chip form is presented. This is the result of a mobility that took place in the Instituto de Telecomunicaçoes (IT) in Aveiro (Portugal) with the finality of studying the potential of this non linear electronic equalizer and its possible integration in a photo-receiver, together with the preamplifier.

2.3.3.1. ADS circuit design considerations

The Ommic design kit ED02AH from Advance Design Software (ADS) from Agilent has been used in order to design the MMIC chip, which has been implemented using GaAs 0.2um technology. This tool allows the implementation of circuits up to 40GHz , although the layout requires some considerations.

Regarding the available area to be implemented, there were 2 different fixed area sizes: 1.5 mm^2 and 3 mm^2. Using the first option 15 dies could be produced while for the second case only 12 dies were included. The first chip area was too small for our design, the second was too big, but this allowed the possibility to include 3 different designs in order to make a comparison between them.

Following the same idea as the used with the microstrip circuit, of approximating the SQRT nonlinear behaviour by utilizing the voltage response with respect to the current of a diode, there were two possibilities of implementation: by means of designs based in the Gate Metal (GM) diode or based in the non linear transistor Pseudomorphic - High Electron Mobility Transistor (P-HEMT).

The non linear model of the GM diode is shown in Figure 2.9. The GM diodes can be composed by several fingers in order to adjust its parasitic effects. The Table of Figure 2.9 presents the

relationship between resistance, capacity and inductance effects with respect to the number of fingers. The diode must be oriented with the active GM side parallel to the X axis. Its main parameters are Wu (unit electrode width in μm), Nbd (number of fingers) and W (total electrode width in μm = Nbd×Wu.)

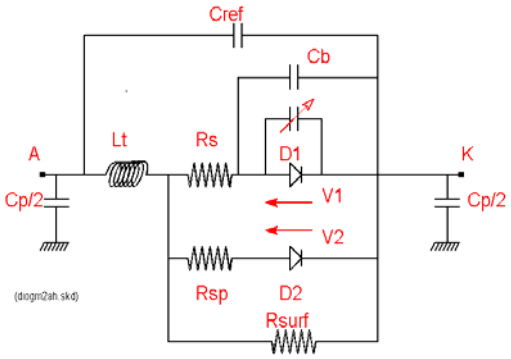

Parameter description	Name (unit)	Value and Scaling (W in um)
Series Inductance	Lt(pH)	Wu/Nbd + Wu/2.5
Series Resistance	Rs(Ohms)	$0.1\times W/Nbd^2+450/W+14/Nbd$
Series Resistance	Rsp(Ohms)	600/Nbd
Fringing capacitance	Cb(fF)	W/2
Coupling capacitance	Cref(fF)	0.047×W + 2.5×Nbd
Surface losses	Rsurf(Ohms)	1.0E12/W

Figure 2.9. ADS GM diode Model

Regarding the transistor option, the ED02AH process offers two different P-HEMTs, the Field Effect Transistor (FET)-off and the FET-on with two different threshold voltages, one negative and one positive (with the choice between two values), available simultaneously on the same chip. For the required non-linear response, we found that the appropriate model is the FET-on.

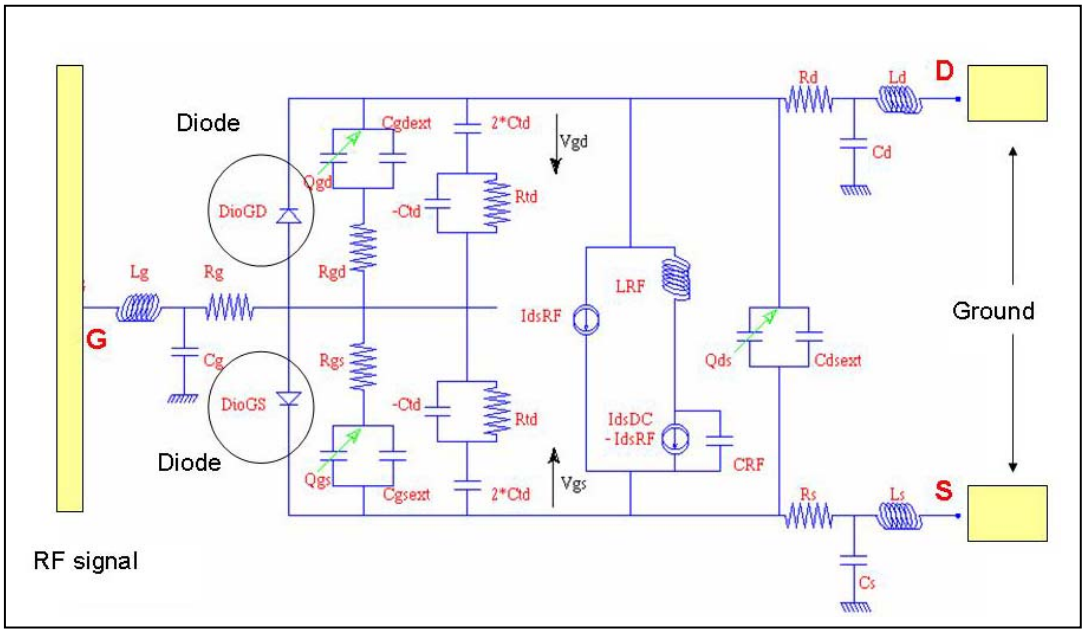

Figure 2.10. ADS ED02AH FET-on Model

The model of this transistor is shown in Figure 2.10. With the gate connected to the RF in-out line and the Drain (D) and Source (S) connected directly to ground, the circuit is equivalent to have two schottky diodes in parallel to ground, but with better bandwidth than with the discrete diodes used in the microstrip prototype.

To increase the DC current and the output power of the FETs, the total gate width must be increased. A wide FET could be laid, with a single wide gate finger; but in that case, the gate resistance is high so that the maximum available gain decreases, and the noise increases. Using several fingers in parallel avoids this drawback. The number of gate fingers is usually even to have a source pad on each side of the FET. If more than 2 fingers are used, then the source pads must be interconnected (see Figure 2.11).

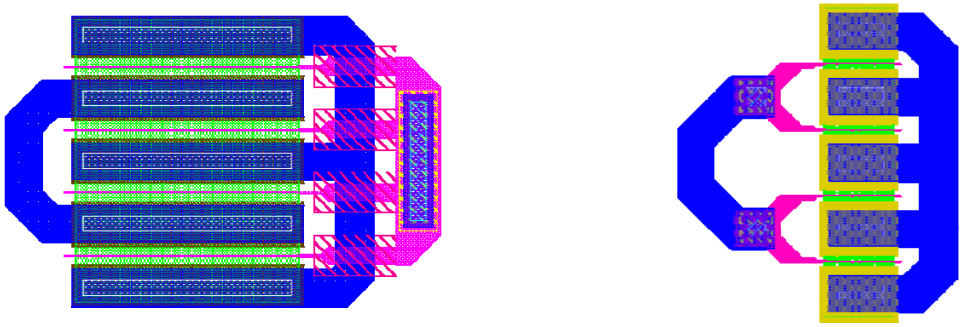

Figure 2.11. Examples of layout mask of a multifinger P-HEMT (left) and a GM diode (right)

When connecting the connect the D and S to ground, the first limitation is found: it is not possible to connect directly gates with drains or sources of the same transistor, because of the layout rules which affect to the lift-off technique needed for the GM (gate metal), OH (ohmic contact), and the rest of the layers. The shape of the FET layout cannot be completely closed, as it can be seen in Figure 2.12. This forces the design to have separated ground connections for D and S. Another rule for this technology is that minimum separation between connections to ground is 0.2 um. This will be translated into longer paths to ground in the design, as it will be seen later.

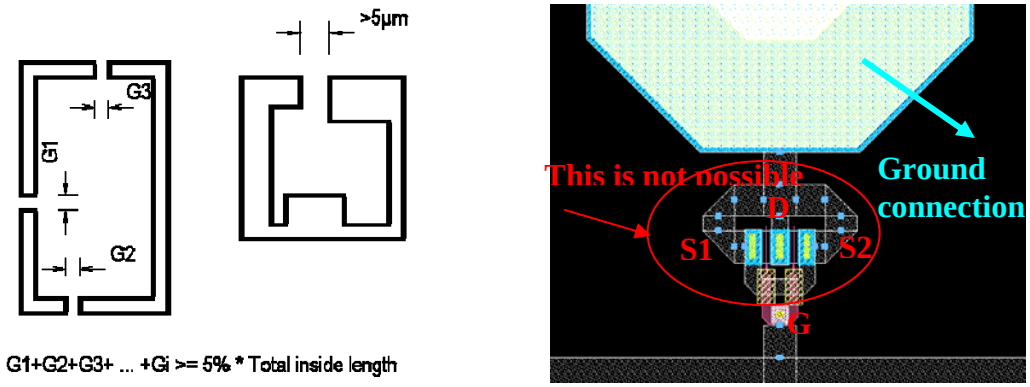

Figure 2.12. Dimension opening rules for the FET design and an example of a wrong layout design

The following aspects have also had to be considered when designing the electronic circuit:

- Capacitors: implementation of DC blocks in GaAs MMIC technology is not possible, the maximum value is about 10pF
- Bonding and packaging: it is important to include parasitic effects in the schematic; the bonding is simulated with a small inductance of 0.4nH.

2.3.3.2. ADS design simulations

According to all the limitations and requirements, 2 different circuits have been designed, one using a P-HEMT based configuration and another one with the GM diodes solution. Taking the maximum advantage of the available area, a third circuit was introduced, maximizing its performance for applications up to 10GHz. All 3 circuits are implemented in the same chip:

2.3.3.2.1. Circuit 1: 6- HEMT configuration

The first topology is based in 6 HEMT's with the gate connected to the RF in-out line and the D and S connected directly to ground. Here Nbd=1 and Wu=10um for the transistors. The distance requirement between grounds and the RF line defined the minimum path length from the transistor to ground that cannot be reduced, however the simulations predict a good circuit performance. Figure 2.13 shows the ADS schematic.

According to the simulation results shown in Figure 2.14, this circuit allows to achieve high level of non-linearity and SQRT response accuracy, with more than 14dB of ER. Moreover, the device is designed to be matched to 50 Ohms with S11 and S22 parameter under 13 dB in the entire frequency margin. The change in slope for a triangular signal (signal linear with time) is also presented. The layout of this first SQRT circuit configuration can be seen in Figure 2.15.

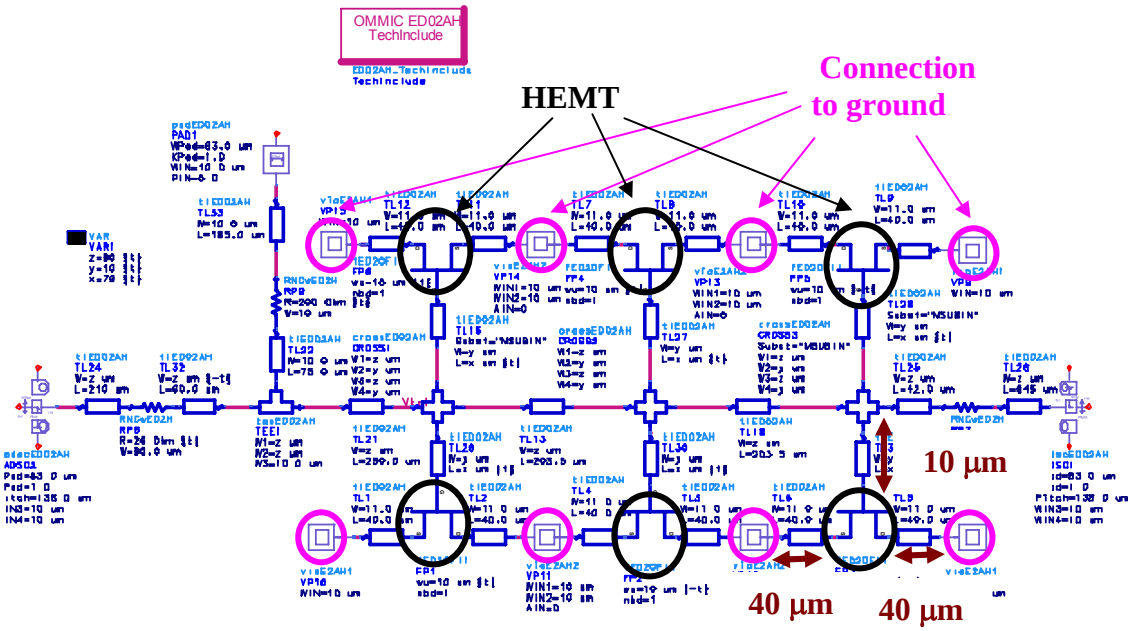

Figure 2.13. SQRT MMIC ADS schematic based in 6-HEMT configuration

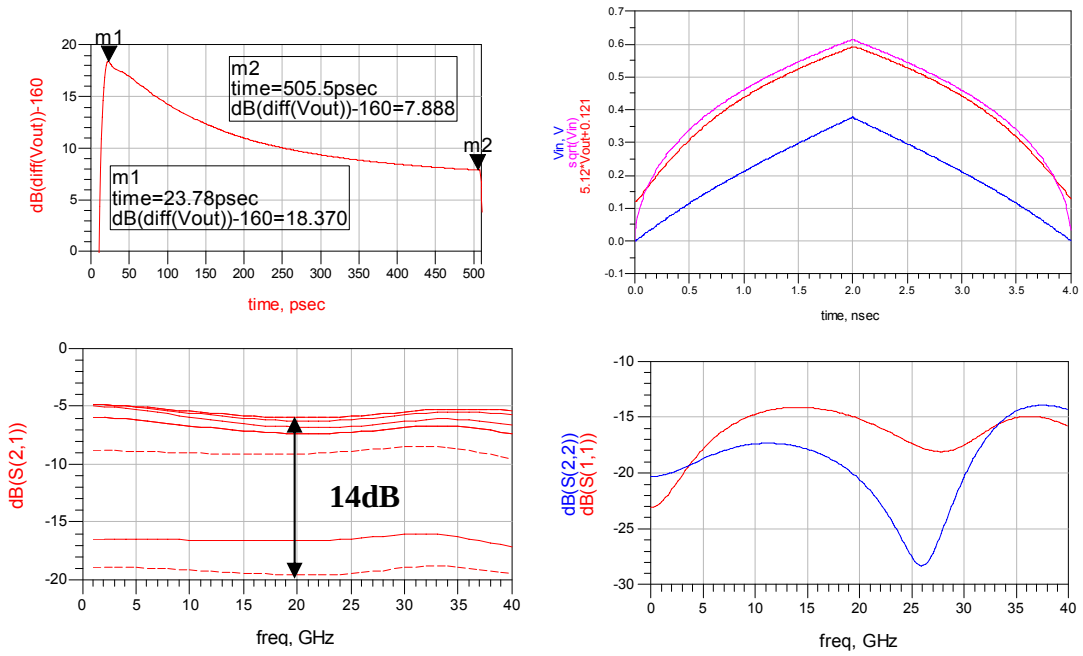

Figure 2.14 Change in the slope of the signal (up-left). Comparison Vout vs. sqrt(Vin) (up right). Change in gain vs. DC (bottom left). S11 and S22 matching.(bottom right).

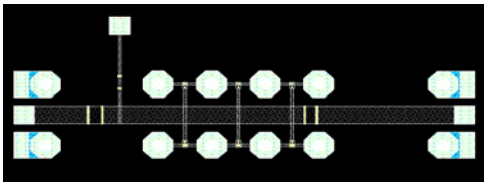

Figure 2.15. Layout of the 6-HEMT based configuration SQRT circuit

2.3.3.2.2. Circuit 2: 6-diodes configuration

This circuit is based in 6 GM diodes. The number of fingers for the diodes, Nbd is equal to 2, and the electrode width Wu is of 15um. The schematic can be seen in Figure 2.16 and the layout and results are shown in Figure 2.17. By using this configuration the ground paths can be located closer to the diodes, compared to the previous case.

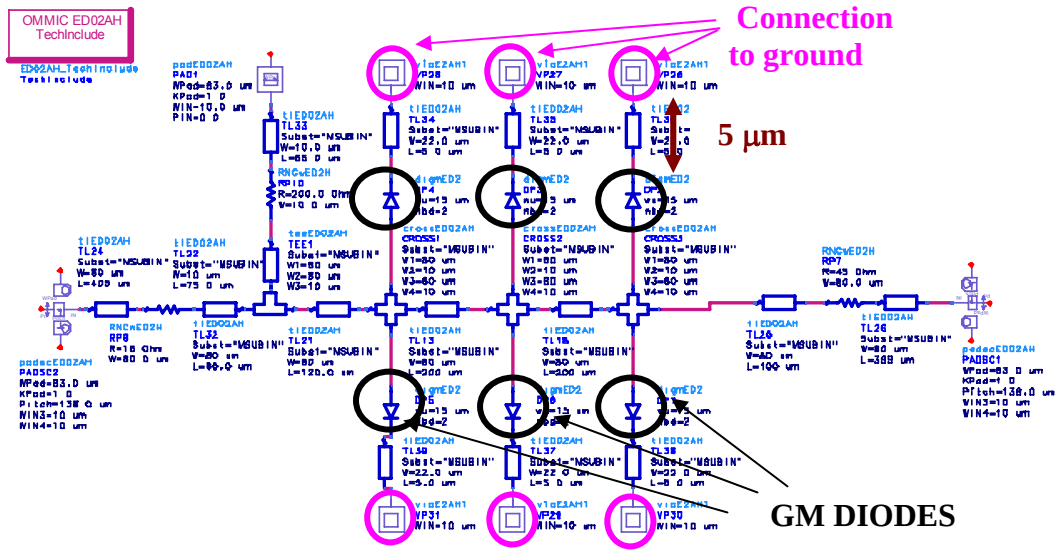

Figure 2.16. SQRT MMIC ADS schematic based in 6-diodes configuration

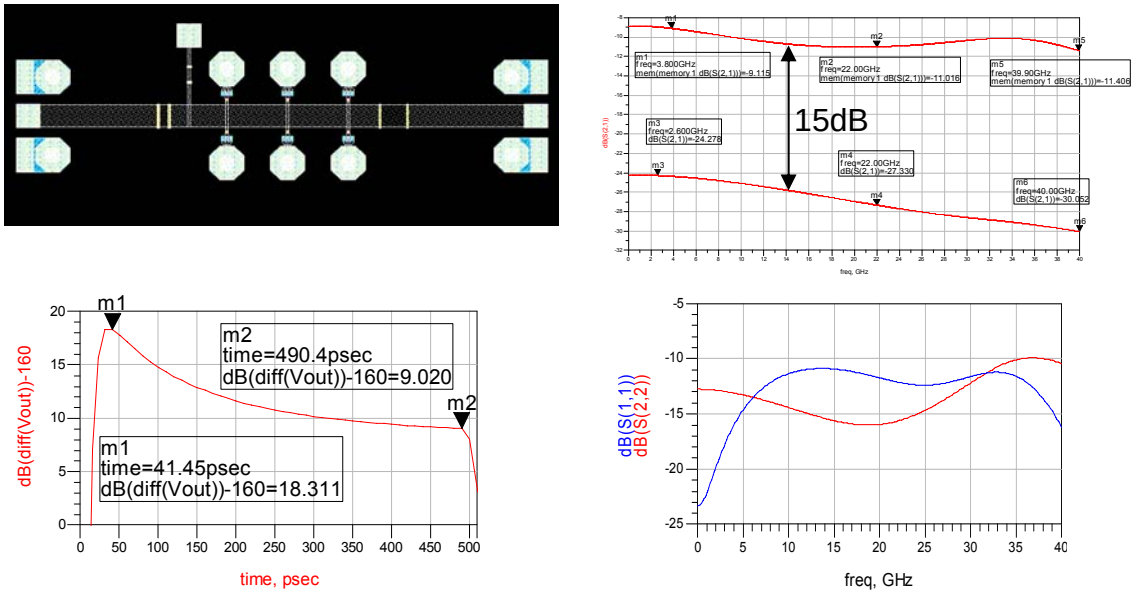

Figure 2.17. Layout (left up), Change in gain vs. DC (right up). Change in the slope of the signal (down-left). S11 and S22 matching.(bottom right).

2.3.3.2.3. Circuit 3: 2-diodes configuration

In order to take advantage of all the chip area, a third circuit has been considered. It is a based on only 2 diodes with their non-linearity maximized and matched to work up to 10GHz. Here Ndb= 6 and Wu =22 um. The results show more than 16 dB of ER up to 10GHz. Figure 2.18 presents the ADS schematic and Figure 2.19 the layout and results.

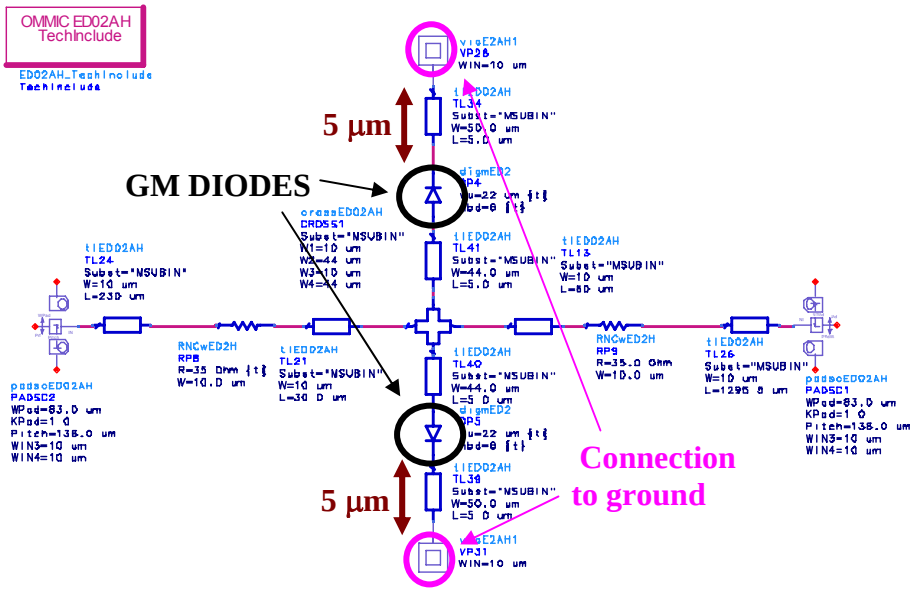

Figure 2.18. SQRT MMIC ADS schematic based in 2-diodes configuration

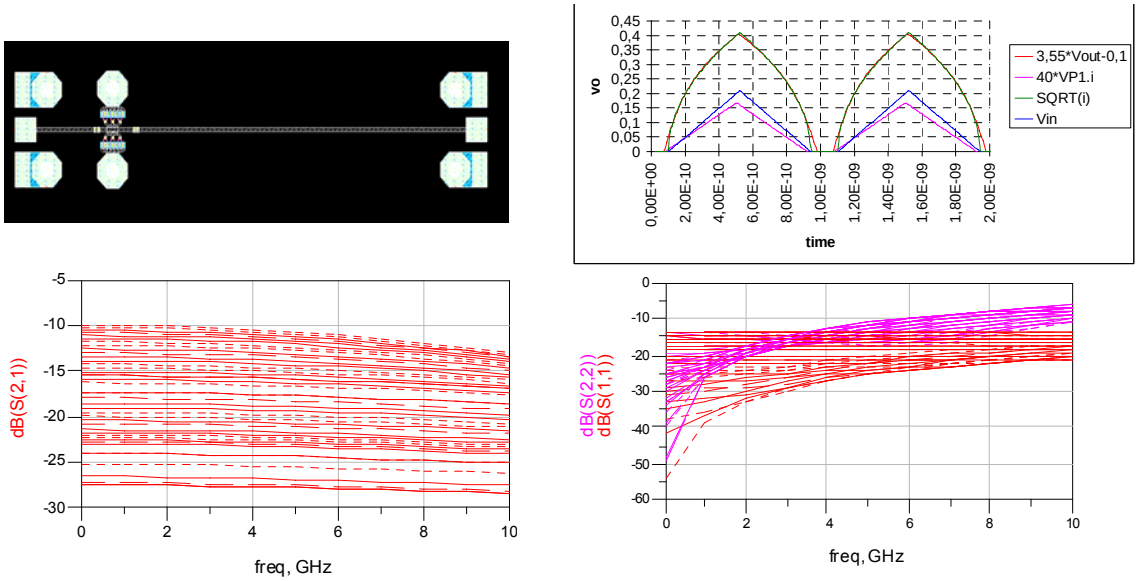

Figure 2.19. Layout (left up), Response to a triangular signal (righ up) Change in S21gain vs. DC (left down). . S11 and S22 matching.(bottom right).

In the final layout the three circuits have been introduced, sharing the grounds in the RF IN OUT pads, taking into account all the requirements of this MMIC technology. Figure 2.20 shows the finished layout and Figure 2.21 the implemented device.

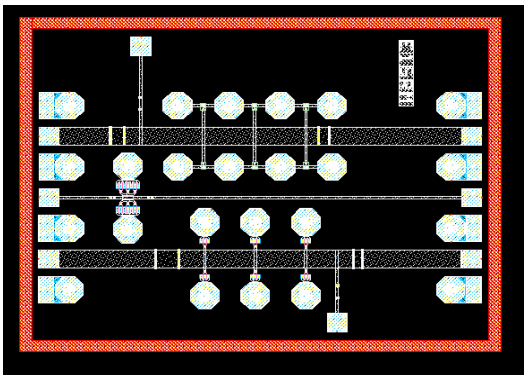

Figure 2.20. MMIC chip layout for SQRT operation.

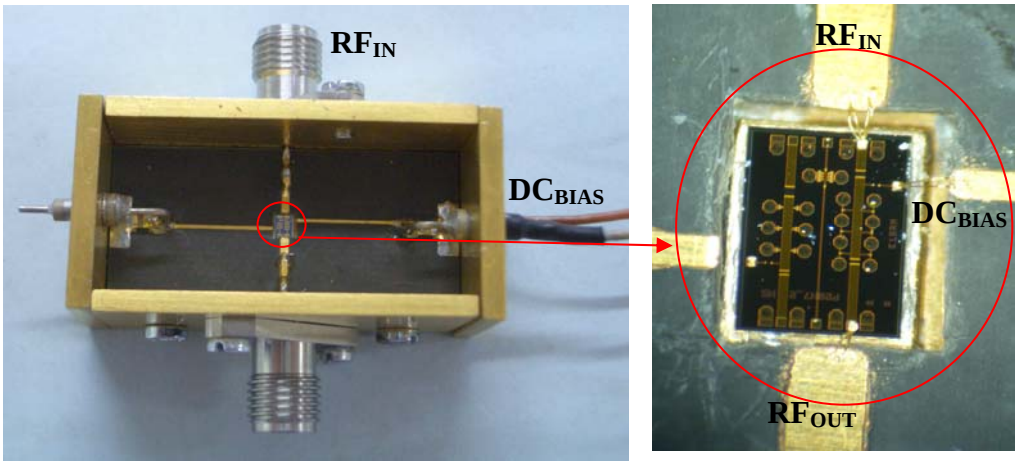

Figure 2.21. MMIC SQRT implemented device

2.3.3.3. Experimental circuit validation

Testing has been done at UPC, in our lab we do not have technology to test at 40GHz, but with a Network Analyzer which operates up to 20GHz.

Results for 6-HEMT based circuit

Although the Network Analyzer only works up to 20GHz looking at the curves tendency, it can be inferred in the following Figure 2.22 that the bandwidth at 3dB would be around 20-25GHz for the 6-HEMT circuit, while in the simulations it was more than 40GHz, however the compression level around 14-13dB fits the simulation previews. The reduction in bandwidth could be associated in part with any effect created by the chip packaging and bonding, being very critical at so high frequencies.

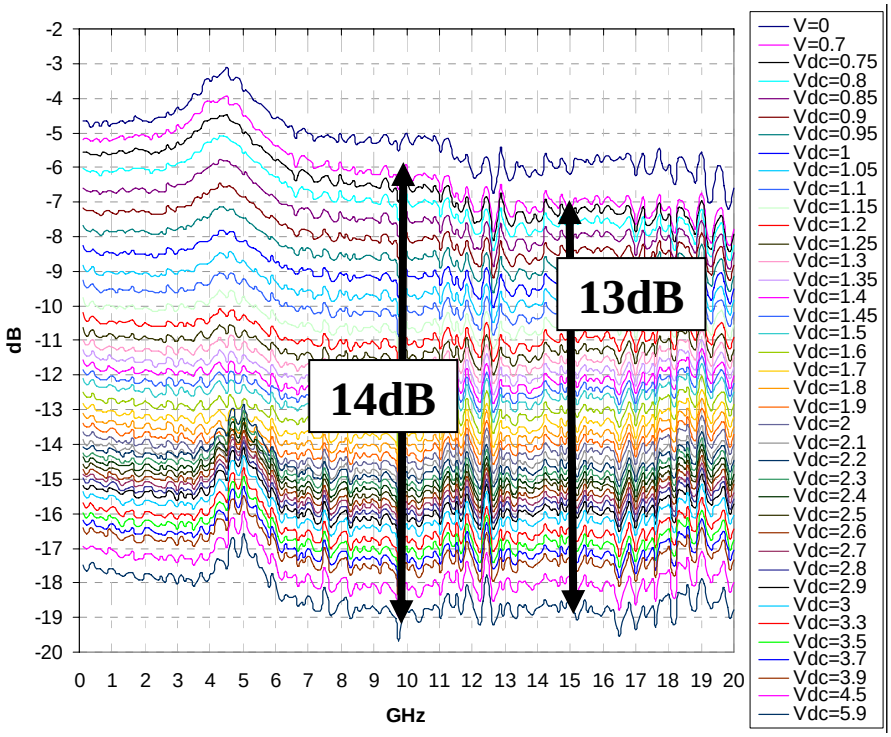

Figure 2.22. Experimental measurements of S21 with respect of VDC for the 6-HEMT based SQRT circuit

In Figure 2.23, the fitting response to an ideal SQRT can be evaluated. The circuit presents behaviour very close to the ideal SQRT from around an input of 0.2 Volts to about 2.2 V.

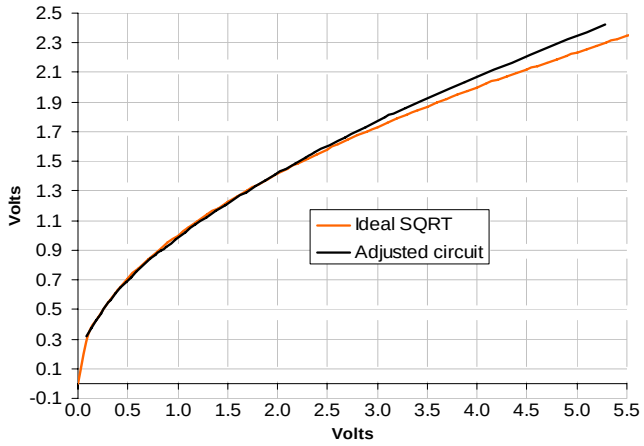

Figure2.23. Comparison between ideal SQRT response and in 6-HEMT based circuit response

Results for 6 GM Diode circuit

The S21 results obtained with this configuration also present a transmission peak at 5GHz, as with the 6-HEMT configuration, but after that the response roll-off is higher for low values of

Vbias. However, as it can be seen in Figure 2.24, the achievable non-linearity or compression is as high as 21dB, when it was predicted around 15dB in the simulations.

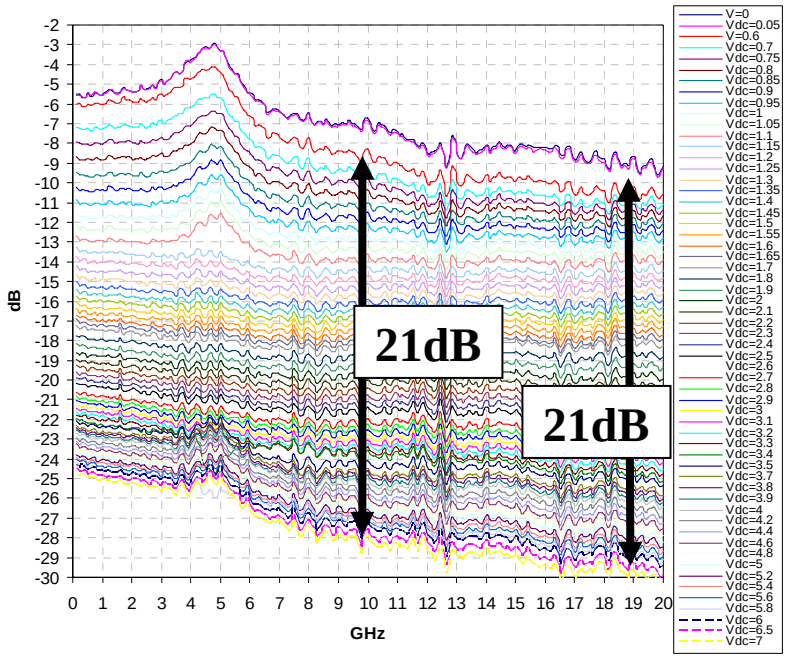

Figure 2.24. Experimental measurements of S21 with respect of VDC for the 6-GM diodes based SQRT circuit

Figure 2.25, shows the fitting response to an ideal SQRT. The circuit presents behaviour very close to the ideal SQRT from around an input of 0.2 Volts to about 5.3 V. The fitting curves of both circuits have been obtained by taking the S21 points at 10GHz, and numerically integrating them.

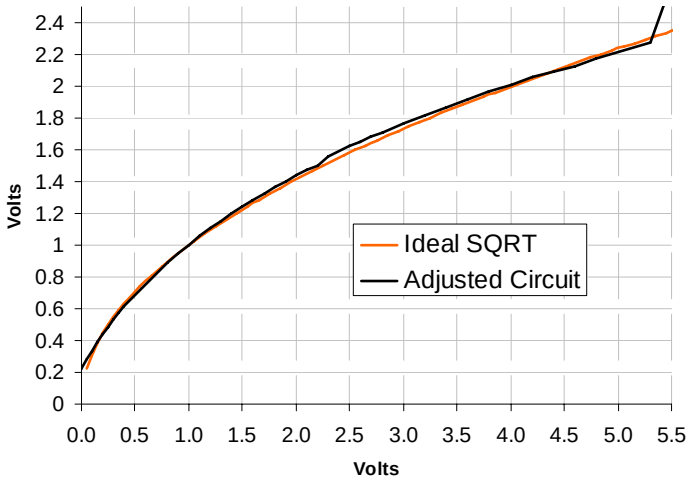

Figure 2.25. Comparison between ideal SQRT response and in 6-GM diodes based circuit response

2.3.4. Intensity Modulation (IM) & Amplitude Modulation (AM)

While a photodetector linearly detects optical power rather than the optical field, lasers and (in principle) commercial amplitude modulators modulate power as well (photon–electron conversion). In terms of the field, the signal is modulated in intensity although it could be desirable to have it modulated in field amplitude. Because of that, the optimum results with the SQRT are obtained when a real amplitude modulation (AM) is applied instead of intensity modulation (IM), as it is presented in Figure 2.26, when the optical field amplitude is proportional to applied voltage because the complete system becomes more linear.

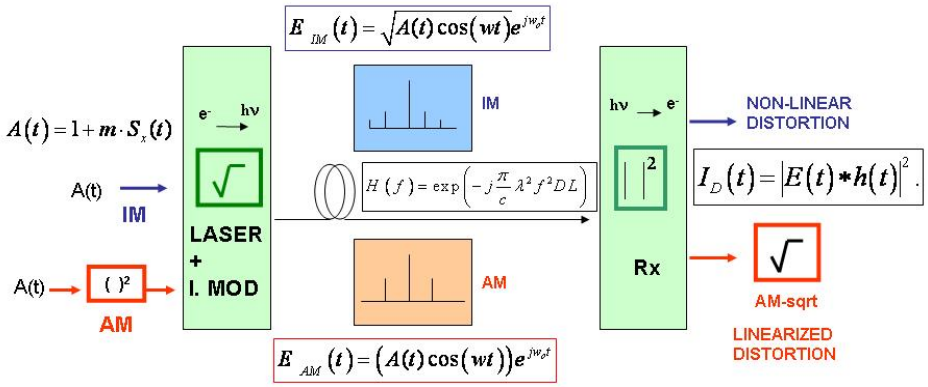

Figure 2.26. AM IM modulation schematic.

Defining the input signal as:

$$A(t) = A \cdot (1 + m \cdot S_x(t)) \tag{2.8}$$

where m is the modulation index which determine the extinction ratio (ER) of the signal. And $S_x(t)$ can be a digital or an analogue data.

If, instead of entering the signal directly to an intensity modulator, it is squared, this signal is modulated in terms of amplitude instead of intensity, then having an optical field proportional to the input signal. Comparing both expressions, what is obtained at the output of an intensity modulator in both cases are:

$$E_{IM} = \sqrt{A(t)} \cdot \cos(w_0 t + \phi(t)) \tag{2.9}$$

$$E_{AM} = A(t) \cdot \cos(w_0 t + \phi(t)) \tag{2.10}$$

Between the transmitter and the receiver, a link of standard single mode fibre (SMF) with length *L* and coefficient of chromatic dispersion *D* is considered. Its transfer function is determined by the known expression [Agrawal]:

$$H_F(f) = \exp\left(-j\frac{\pi}{c}\lambda^2 f^2 DL\right) \tag{2.11}$$

The detected current, in the electrical domain, is obtained by the convolution between the optical field of the transmitted signals and the response of the fibre, modulus squared, like it follows:

$$I_D(t) = \left|E(t) * h_F(t)\right|^2 \tag{2.12}$$

Thus, for the case of SQRT-AM and IM direct detection (IM-DD) the expressions are:

$$I_{D_{AM}}(t) = A\left(\left(1 + m \cdot s_x(t) * \mathrm{Re}\left(h_F(t)\right)\right)^2 + \left(m \cdot s_x(t) * \mathrm{Im}\left(h_F(t)\right)\right)^2\right) \tag{2.13}$$

$$I_{D_{IM}}(t) = A\left(\sqrt{1 + m \cdot s_x(t)} * \mathrm{Re}\left(h_F(t)\right)\right)^2 + \left(\sqrt{1 + m \cdot s_x(t)} * \mathrm{Im}\left(h_F(t)\right)\right)^2 \tag{2.14}$$

Comparing the detected current after passing through the SQRT with the conventional IM-DD for a sinusoidal signal as data, the expressions are:

$$\sqrt{I_{D_{AM}}(t)} = \sqrt{A\left(\left(1 + m \cdot \cos(w_x t) \cdot \cos(\chi)\right)^2 + \left(m \cdot \cos(w_x t) \cdot \sin(\chi)\right)^2\right)} \tag{2.15}$$

$$I_{D_{IM}}(t) = A\left(\sqrt{1 + m \cdot \cos\left(w_x t\right)} \cdot \cos(\chi)\right)^2 + \left(\sqrt{1 + m \cdot \cos\left(w_x t\right)} \cdot \sin(\chi)\right)^2 \tag{2.16}$$

where $\chi = -j\frac{\pi}{c}\lambda^2 f^2 DL$ (2.17)

The maximum error can be calculated for a specific ER. Considering an ER of 10dB, the equivalent modulation index is m = 0.52. The worse case for both received signal would be for cos (χ) = 0, the expressions are reduced to:

$$\sqrt{I_{D_{AM}}(t)} = \sqrt{A\left(\left(1\right)^2 + \left(0.52 \cdot \cos(w_x t)\right)^2\right)} \tag{2.18}$$

$$I_{D_{IM}}(t) = A\left(\sqrt{1 + 0.52 \cdot \cos\left(w_x t\right)}\right)^2 \tag{2.19}$$

Due to the imaginary part, in the first case the maximum error will be $\frac{\sqrt{1+0.52^2}-1}{\sqrt{1+0.52^2}}=11.2\%$, when for the second case, it will be $\frac{1+0.52^2-1}{1+0.52^2}=34\%$, denoting that CD induces a non-linear error, much higher in IM-DD than in AM-SQRT.

2.3.5. SQRT in RoF Systems: Harmonic & Intermodulation

Transmission of microwave and millimetre-wave signals over optical fibre [radio-over-fibre (RoF)] is an area of intense research activity mainly driven by the need of low-cost antenna terminals and the increase in operative frequencies. Applications of the fibre antenna feeder solutions are growing in a variety of wireless cellular, fixed broadband access, satellite, and radar systems. In order to keep the remote antenna stations simple, the microwave carrier to be emitted through the radio channel is directly modulated over the optical wavelength. This incurs in severe harmonic distortion caused by optical fibre CD which degrading effect on the received signal scales as the square of the radio carrier [Curri04]. To cope with it, a variety of equalization techniques both into the optical and into the electrical domain have been proposed [Marti97], [Stahl04], [Curri04], with great emphasis devoted recently to electronic equalization, due to higher adaptability and lower cost [Curri04].

2.3.5.1. SQRT Effect in RoF: Mathematical analysis

In RoF, it can be shown that using the SQRT after direct detection is also a simple way to reduce the intermodulation distortion. In order to better show the linearity level of the detected signals, let's consider the data $S_x(t)$ of (2.7) as a sinusoidal tone:

$$S_x(t)=\cos(w_x t) \tag{2.20}$$

Here the noise will not be taken into account. Taking the variable χ as in (2.16), from the expression (2.12), it can be derived that the detected current in the AM case is:

$$I_{AM}(t)=1+\frac{m^2}{2}+2m\cos(\chi)\cos(w_x t)+\frac{m^2}{2}\cos(2\chi) \tag{2.21}$$

It can be observed that the linear distortion caused by chromatic dispersion could be compensated for by linear equalizers if it was not for the nonlinearity coming from the square

law detection process which gives a term at the second harmonic frequency (2χ). After the SQRT we obtain, up to order m^3:

$$\sqrt{I_{AM}(t)} \cong 1 + \frac{m^2}{4}\sin^2(\chi) + m\cos(\chi)\cos(\omega_x t) + \\ + \frac{m^2}{4}\sin^2(\chi)\cos(2\omega_x t) - \frac{m^3}{8}\cos(\chi)\sin^2(\chi)\cos(3\omega_x t) \tag{2.22}$$

For conventional intensity modulation and direct detection (IM-DD) systems we may approximate the photodiode current, developing the expression (2.14) with (2.20) and (2.21) up to m^3 terms, as:

$$I_{IM}(t) \cong 1 + m\cos(\chi)\cos(\omega_x t) + \\ + \frac{m^2}{4}\sin^2(2\chi)\cos(2\omega_x t) - \frac{m^3}{8}\cos(3\chi)\sin^2(3\chi)\cos(3\omega_x t) \tag{2.23}$$

The factors 2 and 3 in (2.23) that do not appear in the cosines and sinus arguments for the case of AM-SQRT detection (2.22), indicate that with AM-SQRT, the same signal can be transmitted twice the distance to have the same level of a second harmonic ($\sqrt{2}$ in terms of frequency), and three times the distance ($\sqrt{3}$ in terms of frequency) to have the same level of a third harmonic.

2.3.5.2. SQRT Effect in RoF: Simulations and experiments

The electronic microstrip based SQRT analogue circuit designed in sub-chapter 2.3.2 has been used to test the improvement in terms of transmission link linearity achievable with the use of the SQRT module.

2.3.5.2.1. One-Tone analysis

In this section, the second and third harmonics created by the optical fibre due to chromatic dispersion are evaluated. To do that, a sinusoidal signal is introduced in a MZM and transmitted through a long distance (in our case 100Km). The frequency of this sinusoidal signal is swept from low frequency up to 7GHz. After reception, the levels of the transmitted frequency (F1) and the levels at twice and three times F1 (F2 and F3 respectively) are measured.

A system like the presented in Figure 2.27 has been first simulated for a TX Extinction Ratio (ER) of 10 dB. The optical link consists of 100km of standard single mode optical fibre. The first simulations are considering ideal AM and SQRT operation after detection (AMSR in the

following Figures). The second takes into account the response of the M-Z modulators and the electrical SQRT circuit response.

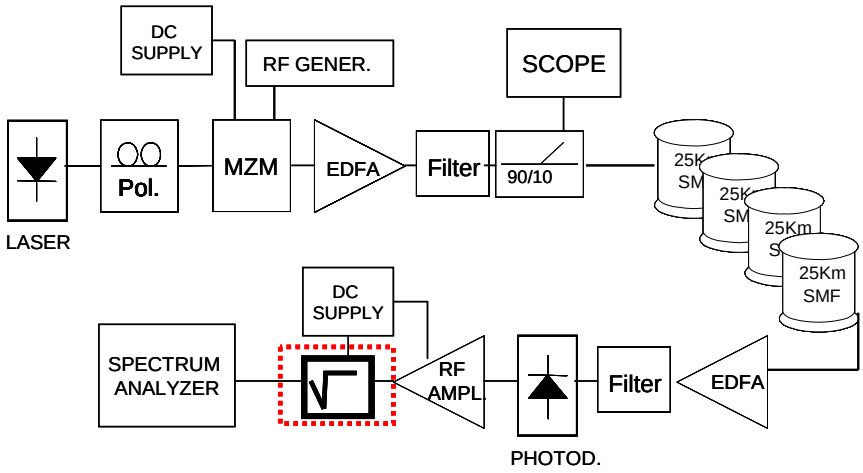

Figure 2.27 RoF experimental set-up used for harmonic analysis.

The first simulations results are shown in Figure 2.28 .The linearizing capabilities of the SQRT in the radiofrequency band are demonstrated, in terms of harmonics level attenuation. As a quantitative example, for the 100km link with chromatic dispersion constant D=16ps/nmKm and considering a maximum tolerance of -40dB of harmonics level, we could extend the operative frequency band from 1.67GHz for the conventional IM-DD system up to 2.40GHz with the AM-SR where it is limited by the second harmonic reaching the -40dB level or even up to 3.64GHz where the third harmonic gets that level, confirming a little more than the expected $\sqrt{2}$ and $\sqrt{3}$ improvement for the 10dB extinction ratio considered.

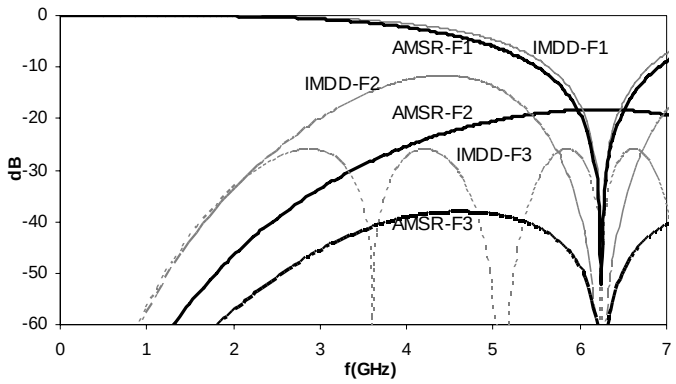

Figure 2.28. Comparison of harmonic power levels with (SR) and without (DD) the Square Root Module. The power levels are normalized to low-freq F1 with respect to modulating frequency for 100Km of standard SMF with D=16ps/(nm.Km) and ER=10dB.

In the practical setup, the IM modulation is obtained by biasing the MZ modulator around the quadrature (90º) point, as it is common practice, while for the AM a bias closer to the zero transmission point (135º) is used as shown in Figure 2.29. Around this point, the modulator input–output characteristic (voltage–optical power) tends to a quadratic function, and thus it is approximately linear with the optical field amplitude. The point of 180º is impractical because of the high attenuation and the ambiguity distortion (change of polarity beyond), so 135º is a good compromise between AM approximation and feasibility.

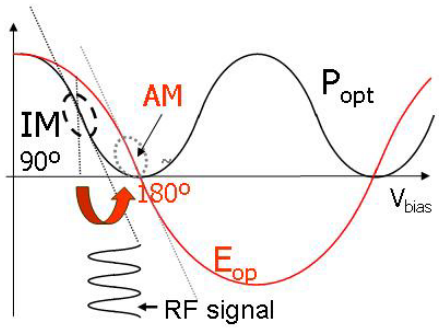

Figure 2.29. M-Z modulator input/output characteristic (voltage/optical power)

Simulations have been also correspondingly carried out for the practical setup in Figure 2.27, taking the MZ transfer function and the nonlinear memoryless input–output relationship of the diode circuit The resulting nonlinear harmonic power levels are shown in Figure 2.30, comparing the IM-like system (MZ at quadrature and DD) with the system with MZ biased at 135º and receiver with SQRT circuit. We observe that the results are very similar to the ideal cases. The greater differences are found at low frequencies which characterize the back-to-back intrinsic system nonlinear behaviour due to the nonlinear transfer functions of modulator and detector and where the AM-SR system yields a higher F2, (-25.6dB respect to the F1).

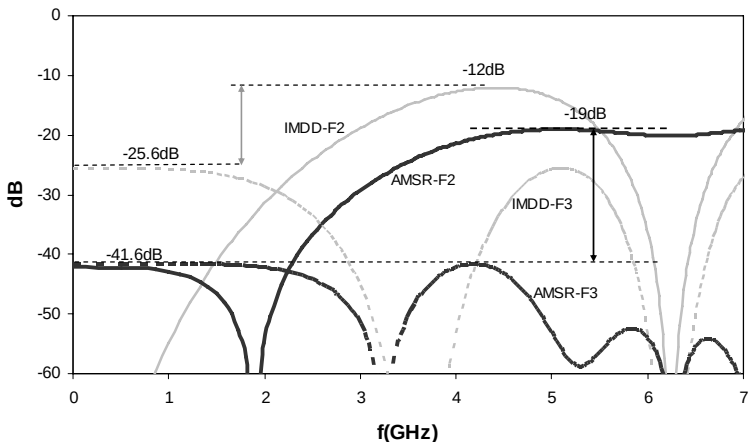

Figure 2.30. Harmonic power levels obtained by simulation of the practical setup, Figure3, with the diode circuit model instead of the ideal sqrt mathematical function, and proper biasing of the MZ; IM: 90º, AM:135º, and with 100 km SSMF, ER=10 dB

The low-frequency levels are in any case well below the pass band values and should not entail a significant reduction of performance. More importantly, at high frequencies, the AM-SR approach maintains its linearity advantage in front of the conventional system.

Experiments

An analogue optical transmission system of 100 Km of standard SMF (D=16 ps/nmKm) operating at 1550 nm has been set up (scheme in Figure 2.27). The SQRT module has been biased at 0.65V. The harmonics power for the same ER=10 dB in the margin of electrical modulating frequencies from 200 MHz up to 7 GHz has been measured, Figure 2.31. The levels present the same basic frequency dependence as the simulation predictions and confirm the linearization capabilities of the AM-SR approach. At frequencies above 2GHz, the harmonic levels of the proposed system are well below those of conventional IM-DD systems. The non-linearity reduction in the worst case margin (around 4GHz of fundamental) is about 5dB. The low-cost SQRT circuit is bandwidth-limited; causing to work with very low powers at the higher frequencies (4GHz of F3 means operation at 12GHz). Normalization at these frequencies produces a noise amplification effect and some deviation from simulated results in Figure 2.30. Still, the predicted linearity improvement in the pass-band frequencies up to 5GHz is seen.

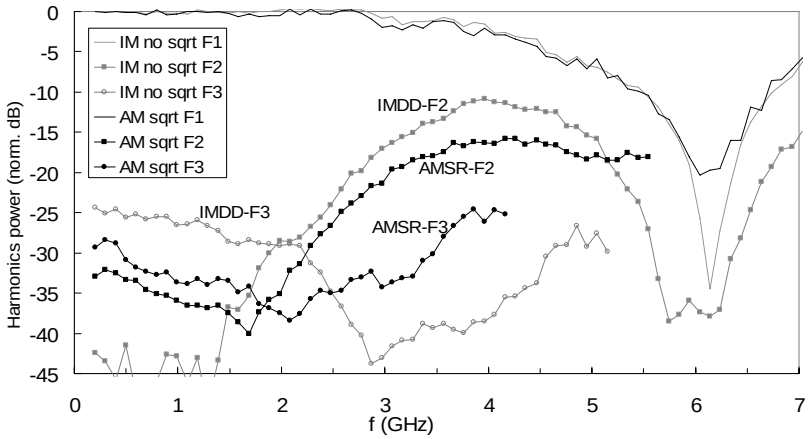

Figure 2.31. Measured harmonic power levels (F2 and F3) normalized to low-frequency F1 power, for a 100Km SSMF and ER=10dB, as a function of modulating frequency.

2.3.5.2.2. Two tones analysis

The main idea is to introduce two analogue tones in 100Km of optical fibre in order to analyze the dispersion improvement that can be obtained with the use of the square root equalizer, compared to the IM classical transmission for different configurations. Third order intermodulation can be particularly troublesome because the distortion components can fall within the band of interest and so will not be filtered away.

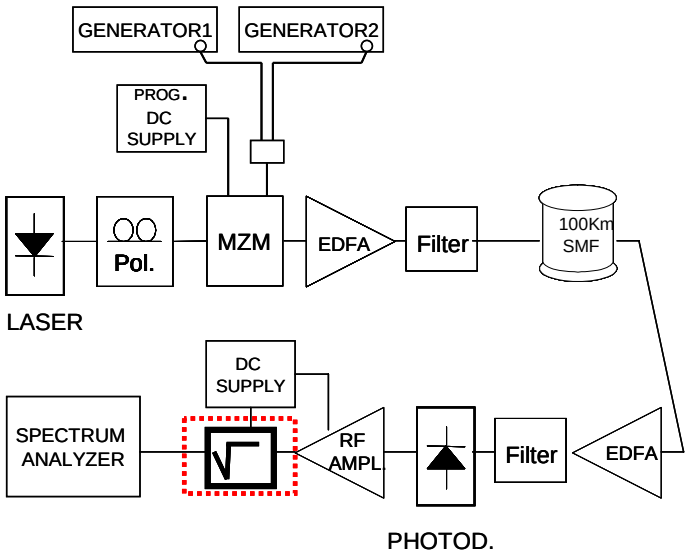

Figure 2.32. Set up used for two tone analysis.

For the two-tone intermodulation distortion analysis, both composite second order (CSO) ($f_1 \pm f_2$) and composite triple beat (CTB) distortions ($2f_1 \pm f_2$ and $2f_2 \pm f_1$) are considered.

Two tones are generated simultaneously according to Figure 2.32, with frequencies $f_a=4f_u$ and $f_b=5f_u$ respectively, where f_u is a reference or unit frequency which will vary from 200 MHz to 1.4GHz. So CSO will be measured at $9f_u$ and $1f_u$. CTB will correspond to the frequencies $3f_u$, $6f_u$ and also $13f_u$ and $14f_u$, but in this case we only will take into account the first two because they are closest to the inputs f_a and f_b.

Figure 2.33 shows the results. There is a 30dB reduction in CTB at frequencies up to 3GHz and CSO with a -48dBc quality threshold up to 3.5GHz with AM-SR. Here, $C9=f_a+f_b$, $C1=f_b-f_a$, $C3=2f_a-f_b$ and $C6=2f_b-f_a$.

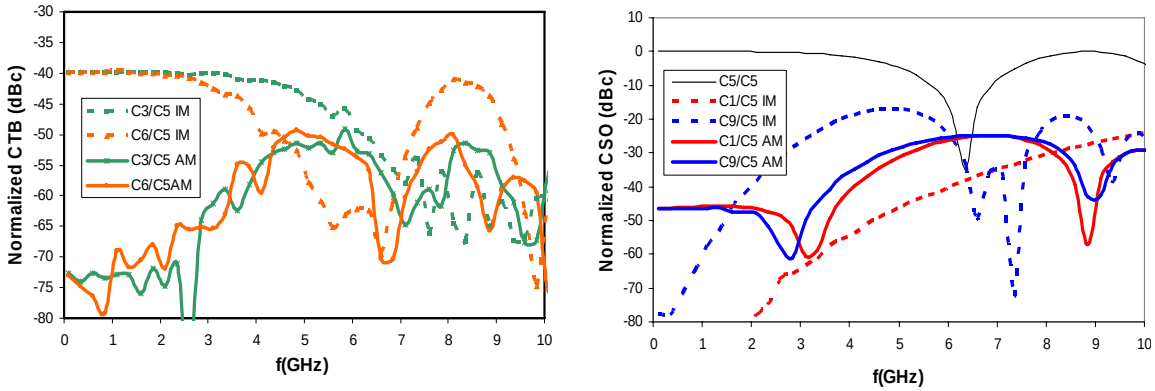

Figure 2.33. Two tones simulation results

2.3.6. Digital. Multilevel

Using a simulation software called Virtual Photonics Inc. (VPI), a four level amplitude PAM-4 signal has been transmitted in three different kinds of scenarios: one in which the dominant impairment was ASE noise, other with only CD and a third one with a combination of ASE and CD. The effect of the square root placed after the photodiode can be seen in the eye diagrams, which are more symmetrical with the SQRT module, and in the signal distribution density graphics, where more equally power distributed symbols can be observed (Figure 2.32).

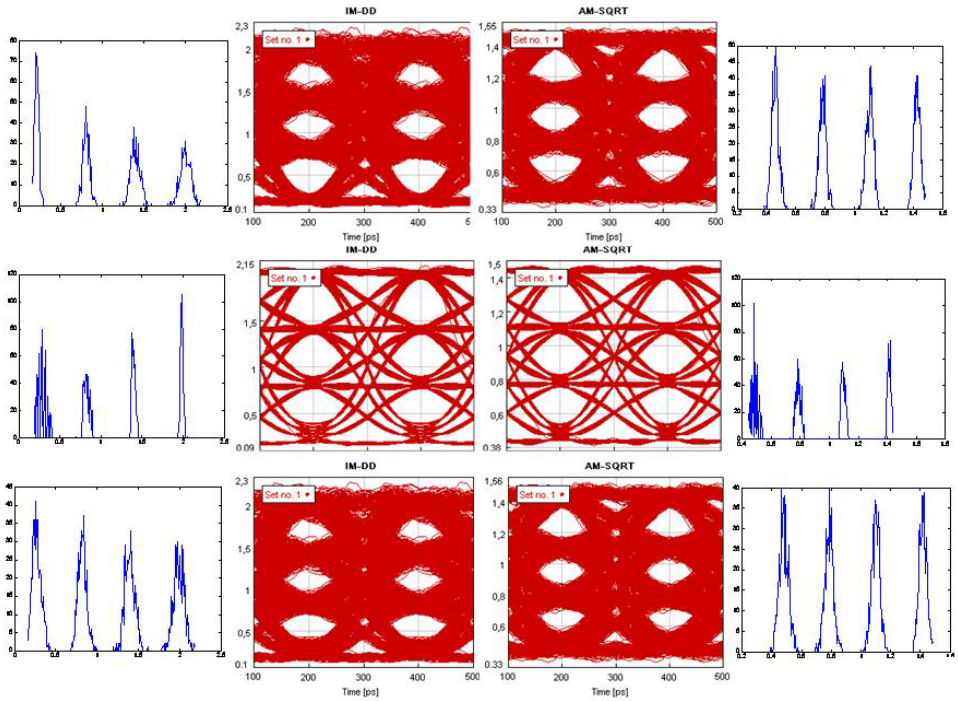

Figure 2.32. PDF distribution and eye diagrams for a PAM 4 ER 10dB for IM DD (left) and AM-SQRT (right) For 3 cases: only ASE noise (top), only CD (middle) and ASE noise +CD

2.3.7. SQRT with Electronic Equalizer

In digital systems, placing the SQRT module does not improve the performance by itself. The non-linear transformation changes the probability density function (PDF) of the photo-detected signal and shifts the optimum decision threshold, but the BER may remain unchanged if the detection settings are adjusted. The last post-equalizer block is fundamental to improve the performance of the IM-DD system with the non-linear function included. Most of the EE were firstly developed to improve the performance of radio and copper cable systems. When applying them to optical networks the outputs did not achieve the equivalent performance.

In systems where ASE noise is dominant and with ideal filtering processes, the detected signal statistics is (as shown in section 2.3.1) chi-square [Marcuse 1991, Humblet 1991, Cai 2003, Bosco 2001]. Applying square root (SQRT) mathematical function over the detected signal, the signal is transformed into a Rice distribution, which is more similar to the Gaussian, so the resulting eye diagram is more symmetrical, as shown before.

For digital transmissions, two different equalizers have been taken into account, FIR (Finite Impulse Filter), with different number of coefficients and delays in a linear Feed Forward distribution (FFE), and Maximum Likelihood Sequence Equalizer (MLSE).

2.3.7.1. FFE equalizer

In this type of equalizer, the data signal is delayed by a taped delay line [Proakis01]. If the delay is of one bit period per stage, then it is called a synchronously spaced FFE. If the delay is of less than one bit period, then the FFE is told to be fractionally spaced. This delayed data signal is tapped and weighted by the tap coefficients C_n and superimposed in a summing unit, as depicted in the next Figure 2.35.

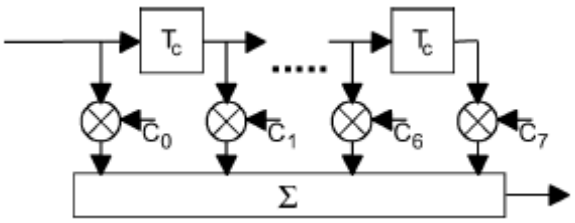

Figure 2.35 - Schematic of a feed forward equalizer, in this particular case having eight adjustable taps

By tuning each of the weighted tapped coefficients, the $H_{comp}(f)$ is built. The device works as a linear filter, capable of compensating linear distortions. Typically, the system transfer function has a low-pass characteristic, which causes the equalizer to have a high-pass characteristic.

Simulation studies were targeted on examining the achievable improvement in the transmission distance and in terms of Q penalty when the SQRT module is combined with a linear FFE equaliser [Prat05]. Figure 2.36 shows the eye opening improvement for various distances. Figure 2.37 compares the results with and without SQRT revealing an increase in transmission distance by more than 50% without optical dispersion compensator with 14 and 28 taps, up to 165km at 2dB penalty at a BER of 10^{-10}

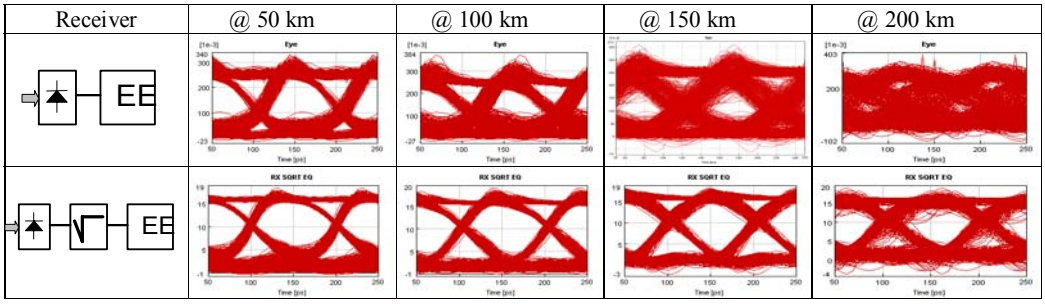

Figure 2.36 Eye opening improvement due to SQRT for various distances

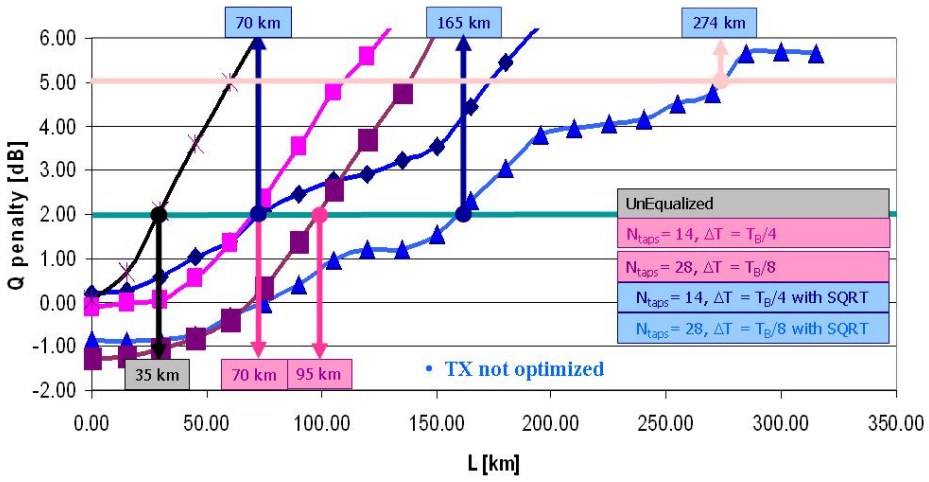

Figure 2.37. Transmission performance with and without SQRT in terms of Q penalty

2.3.7.2. MLSE

Maximum Likelihood Sequence Estimation (MLSE) makes the decision to choose the most probable sequence of symbols among all sequences that could be transmitted, being in this way a popular method to, dynamically, estimate channel characteristics and its compensation [Yu06]. The mathematical concept relies in Maximum Likelihood Estimation (MLE), a statistical method useful to make inferences about parameters of the underlying probability distribution from a given data set.

That is, for a fixed data set and underlying probability model, maximum likelihood takes the values of the model parameters which make the data "more likely" than any other parameters values [Haykin00]. Applying the MLE principle, the demodulation of digital information is sequence based. To the constellation of possible received sequences, it is associated a likelihood function which returns, for each sequence, a measure of its probability of transmission [Castellini97].

Graphically, it uses a tree-like structure called trellis to illustrate state transitions as a function of time. It consists of a set of nodes that represent the states that characterize the memory of the channel (or a sequence of received bits) at different instants in time. In the IMDD systems using the MLSE, the required complexity quickly becomes very large with accumulate dispersion. For this reason complexity must be minimized as much as possible. Processor requirements depend on:

- Number of Trellis States (nodes in the trellis diagram)
- Amount of processing per state

Processing per state is related with the branch metric used. The best trade-off between computational complexity and OSNR performance has to be ensured.

The MLSE algorithm is typically implemented through a Viterbi processor. At each processor iteration, the metric m_n for each branch should be evaluated as

$$m_n = -\sum_{k=1}^{K} \ln\left\{ f_{y_{n,k}}(y) \right\} \qquad (2.24)$$

where *n* is an index running from 1 to the total number *2N* of branches in the trellis, *k* is an index running from 1 to the total number of samples per bit, $y_{n,k}$ is the random variable (RV) associated to the noisy signal samples, conditioned on the transmitted signal being that of the

*n*th branch and the *k*th sample, is the probability density function (pdf) of $y_{n,k}$ and *y* is the actual noisy signal sample taken on the photo-detected electrical signal *y(t)*.

Exact Metric

Equation (2.24) shows that the branch metric should be based on the exact statistical distributions $f_{y_{n,k}}(y)$ of the signal samples across the trellis. Unfortunately, such pdf's are not analytically available in optical systems using postdetection filters. However, it is possible to accurately estimate them by using semi-analytical techniques based on the Karhunen–Loève (KL) expansion of noise [Lee94].

One way to employ the KL metric in simulations is to precompute the 2N·K functions $-\ln\left\{f_{y_{n,k}}(y)\right\}$, for sufficiently densely-spaced values of *y*, and then store the results in look-up Tables. The KL-derived metric constitutes the theoretically best-performing one and can be used as benchmark for all others.

In the commercial MLSE unit, trellis branch metric calculations are done via histograms. This is theoretically effective in terms of performance, but complex. A simplified metric is the variance stationary Gaussian approximation, where all the variances are considered identical, but it is inaccurate in conventional conditions where CD and ASE noise are dominant, in front of shot, thermal and electrical noises.

SQRT metric

The SQRT Data transformation can be applied as a pre-processing technique carried out to reduce data variation to ensure that data follows a normal distribution or to try to make data more "Gaussian". Power transformation is such a kind of conversion, being the square-root a special case that can only be performed in non-negative data. As it has been thoroughly during this chapter, the square-law characteristics of the photodiode can be compensated by a square-root module, and then apply the SQRT metric.
This metric is based on the following assumptions [Bosco08A].

- The random variables (RV's) $\sqrt{y_{n,k}}$, obtained after taking the square-root of the received signal samples $y_{n,k}$, have Gaussian pdf's.
- The variance is identical for all RV's $\sqrt{y_{n,k}}$.

Under these assumptions, the resulting branch metric can be simply written as

$$m_n = -\sum_{k=1}^{K}\left(\sqrt{y} - \mu'_{n,k}\right)^2 \text{, where } \mu'_{n,k} = E\left\{\sqrt{y_{n,k}}\right\} \quad (2.25)$$

With this new metric we can be more confident for assuming the noise statistics as Gaussian or normal distributed. Only two parameters are needed to characterize a normal pdf: mean and variance. Thus we have to estimate these two values for each branch from the received data samples. However, assuming all the variances identical, besides its very low computational complexity, the SQRT metric needs only one parameter per branch metric, namely the average value of the received signal sample. The nature of this parameter allows tracking its changes (i.e., tracking the channel changes) very fast, especially as compared to the histogram approach. Then, using the SQRT metric may simplify the implementation of large processors with many states.

Despite the simplicity of the SQRT metric, the preliminary results of [Poggiolini06A] hinted at a very good performance, with essentially negligible OSNR penalty with respect to more sophisticated metrics like the chi-square metrics [Foggi06].

Subsequently, the SQRT metric was used in long-haul off-line experiments, with good results. In [Poggiolini06B][Savory07] the signal was introduced to a re-circulating loop with 80-km span length. The fibre was standard single-mode G.652. The signal was recirculated 13 times, for a total distance of 1040 km (D=17,680 ps/nm). The average power launched into the loop was -3dBm. No DCF was installed in the loop. The experimental set up is presented in figure 2.38 It was possible to transmit 1040 km at 10 Gb/s with a penalty of 3.8 dB with respect to back-to-back with 4096 states and two samples per bit [Poggiolini06B], and even transmission using an MLSE of only one sample/bit over this distance [Savory07].

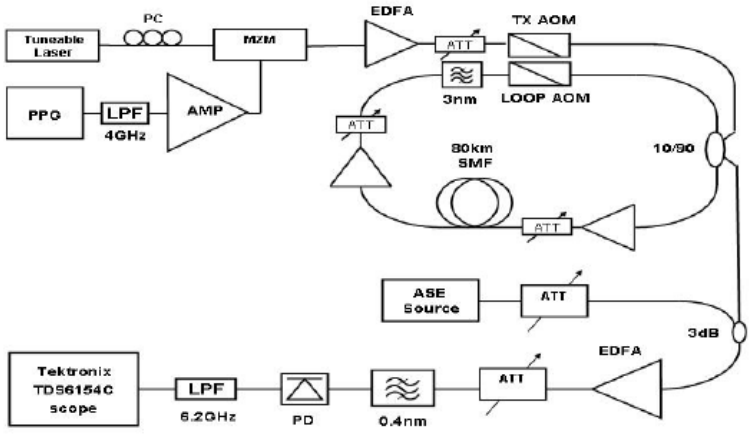

Figure 2.38. Recirculating loop used to emulate a transmission through 1040 km.

As a mode of example, in Fig 2.39, the required OSNR to maintain BER of 10^{-4} with respect to the distance is compared for different metrics. A commercial solution from Core-Optics has also been added to the comparison. As it can be seen, the best results are obtained for the chi-square metric and the square root metric, with almost identical performances.

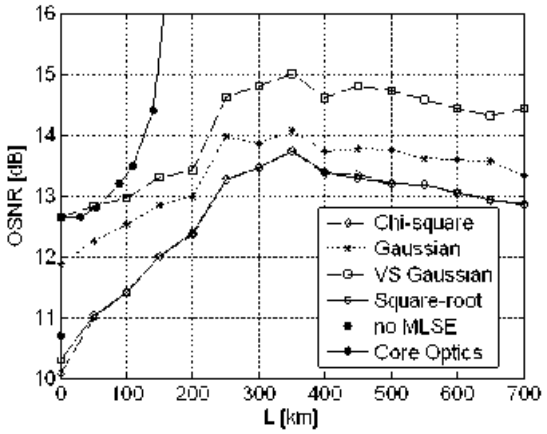

Figure 2.39. Required OSNR to maintain BER of 10^{-4} with respect to the distance is compared for different metrics

The SQRT can be effectively implemented either analogically, before the A/D converter or built in the A/D converter itself by making the quantisation levels unspaced.

2.3.7.2.1. Digital and analogue SQRT comparison:

Using a Matlab program, which takes simulation transmission results done with OPTSIM, a comparative between a digital SQRT ideal function after quantification and the behaviour of our analogue SQRT has been performed.

Simulation details:

Transmitter: NRZ rectangular pulses at a bit rate of 10.7 Gbit/s filtered by a 5-pole Bessel filter with bandwidth 7.5 GHz. ER: infinite or 12 dB for the results at 400km

Fibre: Modelled by an ideal fibre Bragg grating with total dispersion D·L, taking the values of D=17 ps/nm/km and L=400km to simulate the optical fibre.

Receiver: 2nd order Super-Gaussian optical filter with bandwidth 35 GHz. Post-detection filter (electrical): 5-pole Bessel filter with bandwidth 7.5 GHz. Electrical signal sampled using 4 samples per bit

First the signal has to be prepared before entering into the circuit: an amplitude peak to peak (App) and a DC voltage (Vdc) has to be chosen. Then apply normalization (scaling) and biasing :

```
Vppi=max(y)-min(y);
Ginput=(Vpp/Vppi);
y=y*Ginput;
mi=mean(y);
y=(y-mi)+Vdc;
```

After that, the action of the circuit is defined: the circuit acts as a non-linear device (SQRT) from 0.55V to 0.98V; out of this margin its behaviour is linear.

```
if (y<0.55)
 y=3.0397*y-1.75
elseif (y>0.98)
y=0.8627*y - 0.2404;
else
y=-0.0773*(y.^4)+0.8348*(y.^3)-1.9222*(y.^2)+1.7531*y-0.3403;
 y=(y*9.58)-1.75;
end
```

In fact, the equation y=(y*9.58)-1.75, does not affect to the results.

Generally, with optical amplification, the received data presents more noise in the ones than in the zeros. Because of it, the necessary Vdc to adjust the signal to the useful margin is lower than the middle value between the max and the min of the signal. The idea is to maintain the major part of the signal into the non-linear margin, although some noisy points are out of it. The best

results are obtained with the entire margin whatever the signal is of ER=12 or infinite dB. Taking a file with OSNR equal to 13dB and a number of states equal to 128, using App=0.85V and Vdc=0.6V, BER has been calculated for different levels of quantization with the following results in Table 2.2, where *Nq* is the number of quantization bits (*Nq*=0 means no quantization). As it can be observed, analogue SQRT is better for low number of quantization bits.

	With ER= 12 dB			With ER=∞	
Nq	**BER (digital)**	**BER (analogue)**	**Nq**	**BER (digital sqrt)**	**BER (analog sqrt)**
3	0.0124734156	0.0018254	3	0.016838491	0.0035497
4	0.0010538362	0.00063135	4	0.00245291111	0.0012732
5	0.000433932582	0.00043203	5	0.00119689095	0.00093558
6	0.000325211004	0.00037004	6	0.000921272207	0.00087836
7	0.000309951836	0.00036908	7	0.00083734683	0.00086596
0	0.000305183348	0.00038244	0	0.000832578342	0.0008364

Table 2.2. BER comparison of using digital or analogue SQRT for different number of quantification bits

In [Bosco08B] the system performance is evaluated in terms of required OSNR to obtain a BER equal to 10^{-3} as a function of the number of quantization bits for a transmission over 400km and 256 states. As it was found with A/D infinite resolution, the performance of the MLSE-RX employing either the exact, chi-square or the digital SQRT metric is virtually the same. For the sake of clarity, in Figure 2.40, only one curve (solid line) is shown for these three metrics. The minimum number of bits needed to ensure no excess penalty is 5, for all metrics. When 4 bits are used, digital SQRT, exact and chi-square show a 0.5 dB excess penalty, whereas Gaussian is impacted much more seriously (1.5 dB). Interestingly, the analogue SQRT shows almost no excess penalty. With 3 bits, it is the only one that still works, though with a 0.8-dB penalty. These results prove that the SQRT metric retains its near-identical performance with respect to the exact metric even under realistic quantization. In addition, it shows that by means of predistorting the signal in the analogue domain according to a square-root law, a better tolerance to quantization can be obtained when the number of bits gets low.

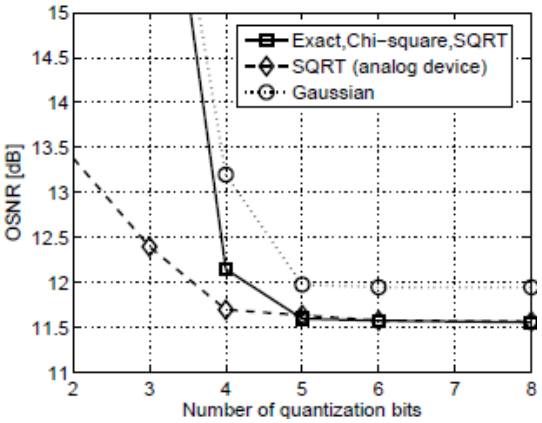

Figure 2.40. Required OSNR to obtain a BER = 10^{-3} versus quantization bits for a 400km link and 256 states.

Clipping

As it has been shown in previous section, the advantage in using the analogue SQRT is that it in some way optimizes the quantization process, because the mathematical operation is done before the A/D converter.

We found that penalty can be reduced by decreasing the upper limit of the quantization interval, which corresponds to performing a “clipping” of the high end of the received signal. The new quantization range was [ymin, ymax/Kclip], where *k* is the clipping factor. Quantization is assumed to be uniform over this new range.

Clipping introduces a sort of "error floor" in the BER while using the analogue device this error floor shouldn't be present. As MLSE usually works at FEC limit ($BER=10^{-3}$), clipping constitutes a good strategy at reducing excess penalty due to low number of quantification bits although generate complex trade-offs, since clipping may reduce penalty at high BERs but typically generates BER floors as well [Bosco08A].

2.3.8. Other SQRT applications

Although the SQRT module was originally designed to compensate the square law characteristic of the photodiode, to linearise the optical system, its non linear behaviour can be applied to other aspects, more related with the upstream transmission in PON: the downstream cancellation and remodulation and the burst mode transmission, this will be explained in detail in Chapter 4.

2.4. Optimum non-linear function

As it has been commented in previous subchapter, in systems where ASE noise is dominant and with ideal filtering processes, the detected signal statistics are chi-square [Marcuse 1991, Humblet 1991, Cai 2003, Bosco 2001]. Applying square root (SQRT) mathematical function over the detected signal, the signal is transformed achieving a Rice distribution which is more similar to the Gaussian, so the resulting eye diagram is more symmetrical. The worst case is in the IM/DD systems with very high ER (Extinction Ratio) where the symbol '0' presents very low signal energy, because Rice distribution separates from the Gaussian shape in the region close to the origin.

As an alternative to the SQRT function, works in [Franceschini07, Bosco08, Hueda07] propose other non linear n-root concave functions: in [Franceschini07] cube root is found to be a better function to improve the required Optical Signal to Noise ratio (OSNR) in specific chromatic dispersion conditions. In [Bosco08A] the MLSE's suggested branch metric is $m_m=((y_m)^{\alpha}-\mu_m)^2$, with $0.3<\alpha<0.4$, where y_m is a sample of the received signal, α is the nonlinear distortion exponent , m is an index running overall possible branches and sampling instants, and μ_m is the estimated mean value of those $(y_m)^{\alpha}$ that belong to the branch and samples corresponding to index *m*.

In this work, the non-linear transformation function that provides Gaussian statistics after the photodetector of an IM-DD system with dominant optical ASE noise is derived mathematically, without restriction to a predefined function form, for any value of ER, thereby overcoming the Rice distribution limitations in ASE dominant systems [A. JimenezMT].
The main goals of the optimum non-linear function are:

A. Noise with Gaussian statistics.
B. Signal mean proportional to the optical field amplitude, instead to the optical power.
C. Equal variances independently on the signal mean value.

2.4.1. System model

The system is composed of the following elements, conventional of a IM-DD system scheme: an optical bandpass filter, a photodetector, an electrical filter, the non-linear function and a post equalizer (Figure 2.41).

The ASE noise, generated by the optical amplification is modelled as an AWGN channel (Additive White Gaussian Noise) and we follow the conventional analysis of [Marcuse 1991] where the received optical signal is composed by the data with On-Off keying modulation and Non-return to Zero impulses. We consider a rectangular optical filter with large bandwidth B_0 before the receiver.

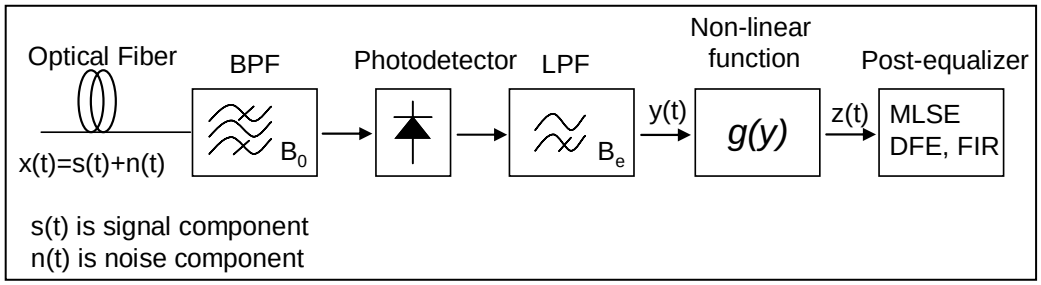

Figure 2.41. General set-up.

The photodetector converts the optical signal to its electrical counterpart. A low-pass electrical filter with bandwidth B_e further filters out the ASE noise. We assume here that this filter does not disturb the signal waveform. Next module represents the non-linear transformation g(y), object of this work, whose main goal is to convert the chi-square distributed signal into Gaussian distribution. Finally, after this non-linear equalization, an electronic equalizer like MLSE, FIR, or analogue, follows this module in order to compensate the dispersion introduced by the channel. A summary of these techniques can be found in [Hahn 1994].

Obtaining a Gaussian output does not improve the digital system performance by itself, as it was commented previously in this thesis at the introduction of the SQRT module. The non-linear transformation changes the probability density function (PDF) of the photo-detected signal and shifts the optimum decision threshold but the BER may remain unchanged if the detection settings are adjusted. The last post-equalizer block is not analyzed in this work, but its operation is fundamental to improve the performance of the IM-DD system with the non-linear function included.

It is important to note that although here the work is focused mainly on digital systems, the reference to RoF systems is also relevant, because the goal of making the system response more linear is related to the goal of obtaining Gaussian statistics, independent of the signal level.

2.4.2. Hastings-Dillard non-linear approximation

To find the non-linear function, we have chosen a method that uses the inverse method from the random variable conversion theory. This method can be found in [Hueda 2007, Hahn 1994, Devroye 1986] and it is based on the general non linear transformation of a Chi-square Random Variable (RV) y in Gaussian RV z by:

$$g(y) = F_{z|s}^{-1}\left(F_{y|s}(y)\right) \tag{2.26}$$

where $F_{y|s}(\cdot)$ and $F_{z|s}(\cdot)$ are the conditional cumulative distribution functions (CDF) of *y* and *z*, respectively, when the noise-free signal *s* is received. First the chi-square distribution is translated to a uniform distribution one via $F_{y|s}(\cdot)$ and then the uniform is transform to a Normal distribution via $F_{z|s}^{-1}(\cdot)$. From the tendency of the distribution functions, note that *g(y)* is also a monotonically non-decreasing function. As the received signal is Chi-square, then the CDF of the RV *y* is given by the following expression [Proakis01]:

$$q = F_{y|s}(y) = 1 - Q_{pM}\left(\sqrt{\frac{2E_s}{N_0}}, \sqrt{\frac{2y}{N_0}}\right), \ \text{y} \geq 0 \tag{2.27}$$

where $Q_m(a,b)$ is the Marcum Q function, E_s is the signal energy, N_0 is the power spectral density of the ASE noise, M is the relationship between the electrical and optical bandwidth ($M=B_o/2B_e$) and *p* is an integer that indicates the existence (p=1) or non existence (p=2) of a polarizer at the receiver input. To simplify the calculation of Marcum Q function, we have used an expression derived from the Dillard recursive algorithm [Dillard 1973, McGee 1970]:

$$Q_M(a,b) = e^{-a^2/2} \cdot e^{-b^2/2} \cdot X_M(a,b) \tag{2.28}$$

where

$$X_M(a,b) = \sum_{k=0}^{\infty} p_k n_k$$

$$n_k = n_{k-1} + d_k, \quad d_k = \frac{1}{2}\frac{b^2 d_{k-1}}{k+M-1}, \quad p_k = \frac{1}{2}\frac{a^2 p_{k-1}}{k}, \quad P_0 = 1$$

$$d_0 = \frac{\left(\frac{b^2}{2}\right)^{M-1}}{(M-1)!}, \quad n_0 = \sum_{j=0}^{M-1}\frac{\left(\frac{b^2}{2}\right)^{j}}{j}$$

The only limitation of this algorithm is that it only allows integer numbers, although we have proved that this quantification gives negligible error. For the second part of (2.26), the inverse conditional CDF of the normal RV z, $F_{z|s}^{-1}(\cdot)$ does not have an analytical closed-form. Then, an approximation is used. Among the different techniques that can be used, there are numerical methods such as bisection, secant or Newton-Raphson [Devroye 1986] and analytical approximations as Odeh & Evans, C. Hastings and Chebyshev polynomial interpolation [Devroye 1986, McGee 1972]

Although Odeh & Evans solution has been demonstrated to give the lowest error [Devroye 1986], here, C. Hastings approximation is used because it gives low error (ε(q) is lower than $4.5\cdot10^{-4}$) with moderate complexity. Its expression is given by:

$$F_{z|s}^{-1}(q) = \begin{cases} \eta_1 - \left\{\dfrac{a_0 + a_1\eta_1 + a_2\eta_1^{\,2}}{1 + b_1\eta_1 + b_2\eta_1^{\,2} + b_3\eta_1^{\,3}}\right\} + \varepsilon(q), & 0 < q \le 0.5 \\ -\eta_2 + \left\{\dfrac{a_0 + a_1\eta_2 + a_2\eta_2^{\,2}}{1 + b_1\eta_2 + b_2\eta_2^{\,2} + b_3\eta_2^{\,3}}\right\} + \varepsilon(q), & 0.5 < q \le 1 \end{cases} \tag{2.29}$$

where
$$\eta_1 = \sqrt{-2\cdot\ln(q)} \tag{2.30}$$

and
$$\eta_2 = \sqrt{-2\cdot\ln(1-q)} \tag{2.31}$$

and q represents an uniform RV distributed in interval (0,1). The constants of the expression (2.29) are shown in the Table 2.3.

a_0 = 2,515517	b_1 = 1,432788
a_1 = 0,802853	b_2 = 0,189269
a_2 = 0,010328	b_3 = 0,001308

Table *2.3:* Hastings coefficients

Note that the C. Hastings approximation (2.29) transforms a uniform RV q distributed between (0,1) into a normal RV N(0,1) with zero mean and unity variance.

Using both Dillard (2.28) and C. Hastings (2.29) algorithms in expression (2.26), we can obtain the non-linear function $g(y,\gamma,\delta,n_e)$ which is composed of the following parameters:

- **Noise parameter γ**: variance of the ASE noise $\gamma = \sqrt{\overline{N_0}/2}$, where $\overline{N_0}$ is an estimator of the power spectral density N_0.
- **Estimated non-centrality parameter δ**: it is used for a fine tuning of the function in order to achieve the best trade-off between minimum BER and Gaussian shape. It is related to the non-centrality parameter of the input signal $\lambda=2E_s/N_0$ [Urkowitz 1967]. Ideally, $\delta = \lambda$.
- **Modal parameter n_e** ratio between the optical and electric filter bandwidths. It is an integer number because of the Dillard algorithm limitations. n_e is an estimator of the chi-square degrees of freedom $n = 2pM$.

According to the inverse method, the q value in (2.29) is given by the non central chi-square CDF (2.27) with n_e degrees of freedom, as it is shown in (2.32).

$$\begin{aligned} q = F_{y|s}(y) &= 1 - Q_{n_e/2}\left(\sqrt{\delta}, \frac{\sqrt{y}}{y}\right) = \\ &= 1 - e^{-\delta/2} \cdot e^{-y/2\gamma^2} \cdot X_{n_e/2}\left(\sqrt{\delta}, \frac{\sqrt{y}}{y}\right) \end{aligned} \tag{2.32}$$

Using this q value (2.32) as argument in (2.29), then η_2 in (2.31) can be simplified as:

$$\begin{aligned} \eta_2 &= \sqrt{2 \cdot \ln\left(e^{-\delta/2} \cdot e^{-y/2\gamma^2} \cdot X_{n_e/2}\left(\sqrt{\delta}, \frac{\sqrt{y}}{\gamma}\right)\right)} = \\ &= \sqrt{\frac{y}{\gamma^2} + \delta - 2 \cdot \ln\left(X_{n_e/2}\left(\sqrt{\delta}, \frac{\sqrt{y}}{\gamma}\right)\right)} \end{aligned} \tag{2.33}$$

However, η_1 in (2.30) cannot be simplified, and it is given by

$$\eta_1 = \sqrt{2 \cdot \ln\left(1 - e^{-\delta/2} \cdot e^{-y/2\gamma^2} \cdot X_{n_e/2}\left(\sqrt{\delta}, \frac{\sqrt{y}}{\gamma}\right)\right)} \tag{2.34}$$

Finally, the results in (2.33) and (2.34) have been substituted in the Hastings approximation (2.29). Then, the obtained non-linear function $g(y,\gamma,\delta,n_e)$ is (2.35):

$$g(y,\gamma,\delta,n_e) = \begin{cases} \gamma\sqrt{\delta} - \gamma\eta_1 + \gamma \dfrac{a_0 + a_1\eta_1 + a_2\eta_1^2}{1 + b_1 + b_1\eta_1 + b_2\eta_1^2 + b_3\eta_1^3}, & 0 \le y \le y_U \\ \gamma\sqrt{\delta} + \gamma\eta_2 - \gamma \dfrac{a_0 + a_1\eta_2 + a_2\eta_2^2}{1 + b_1 + b_1\eta_2 + b_2\eta_2^2 + b_3\eta_2^3}, & y > y_U \end{cases} \tag{2.35}$$

where y_U can be extracted from the following transcendent function:

$$0.5 = e^{-\delta/2} \cdot e^{-y_U/2\gamma^2} \cdot X_{n_e/2}\left(\sqrt{\delta}, \frac{\sqrt{y}}{\gamma}\right) \tag{2.36}$$

In order to modify the zero mean and unity variance of normal RV z obtained with C. Hastings approximation, note that (2.29) has been multiplied by the standard deviation γ, and then the mean term $\gamma\sqrt{\delta}$ has been added.

The expression (2.35) can be normalized by the variance. This process allows working in normalized mode. Note that the noise parameter γ can be removed of the expression (2.31) (replacing in (2.35) γ=1). Figure 2.42 represents the comparison between the slope of the normalized non-linear function $\bar{g}(y, \delta, n_e)$ (in solid line) with n_e=10 and the SQRT (in dashed line) for the different cases of δ. It can be seen that the non-linear function presents a more abrupt slope than the SQRT close to the origin while for high values of y both lines tend to have the same slope. This discards all the previously proposed functions y^{α} since they diverge for high values (or low values in case of α = 0.5).

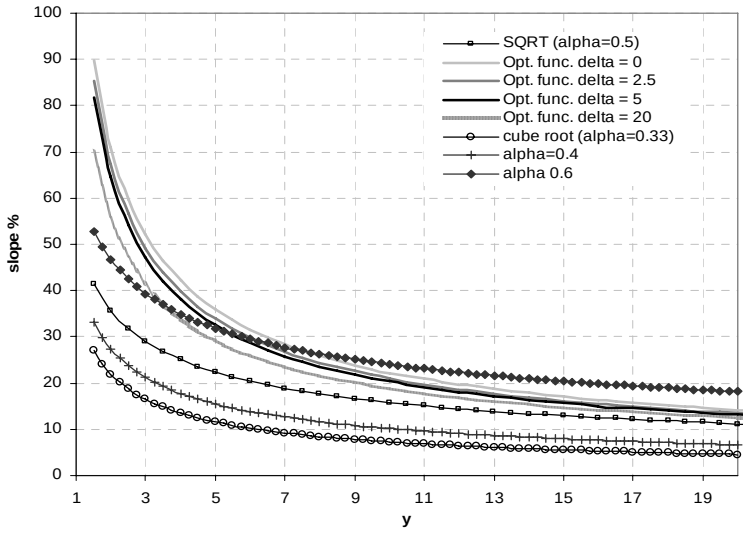

Figure 2.42. Comparison between the slopes of normalized optimum function with n_e=10 , for different estimated non-centrality parameter δ and functions of the form yα where α is 1/3, 0.4, 0.5 and 0.6.

2.4.3. Non-linear function analysis

As it has been explained in the previous section, the non-linear function depends on the three parameters n_e, γ , and δ. The first two can be estimated from the IM/DD systems using the MoM [Agazzi 2005] defined as:

$$\overline{N_0} = \frac{v_1 - v_0}{2(m_1 - m_0)},\ \overline{pM} = \frac{6m_0\overline{N_0}^2 - q_0}{4\overline{N_0}^3}$$
$$n_e = 2\overline{pM},\qquad \gamma = \sqrt{\overline{N_0}/2} \tag{2.37}$$

where $v_1 = \mathrm{var}\{X_1\}$ and $m_1 = E\{X_1\}$ with $X_1 = \{1,1...,1\}$ is the training sequence of the bit 1, $v_0 = \mathrm{var}\{X_0\}$, $m_0 = E\{X_0\}$ with $X_0 = \{0,0...,0\}$ the training sequence of the bit 0 and q_0 is the third order central moment for sequence '0'. Another method for estimate the number of spectral modes M, it is to use the approximation $M=B_0/2B_e$. The function is exact when the estimated non-centrality parameter δ is well estimated and coincides with signal non-centrality parameter λ (δ is an estimator of λ). This implies that for an IM/DD system with binary alphabet $\{0,1\}$, the received symbol has to be estimated in order to specifically set its non-centrality parameter. Monitoring or training sequence initialization can be applied in order to fix the non-centrality parameter. If in real conditions, δ is fixed to a suitable value the function is not exactly the optimum with a limited error, which in general is not substantial.

In order to choose the convenient value, two different analyses have been done. The first one consists of a BER versus estimated non-centrality parameter δ study for different scenarios and the selection of the best value (Figure 2.43). The second procedure is related to the behaviour of the statistical moments for different values of δ. (Figures 2.44-2.45)

2.4.3.1. BER simulation vs. estimated non-centrality parameter

For the BER computation, a Monte Carlo simulation with 10^7 transmitted pulses and infinite ER has been used in an ideal system without chromatic dispersion and with only ASE noise. The bandwidths for the optical and electrical filters are, respectively, B_0=40 GHz and B_e=8 GHz. The signal to noise ratio is chosen to be E_b/N_0=15 (in linear) at the photodetector input, since it is required to achieve a BER close to 10^{-3}, that can be supported using FEC coding. Note that the relationship between E_b/N_0, the non-centrality parameter λ, and the OSNR is (only for OOK system with infinite ER):

$$\lambda = \frac{2E_s}{N_0} = \frac{4E_b}{N_0} = 8\,OSNR \cdot T \cdot B_0 \tag{2.38}$$

The obtained BER for different estimated non-centrality parameters δ is plotted in Figure 2.43. The region $\delta \in [4, 7]$ is where the best results are obtained, and the minimum BER is achieved with δ =5.

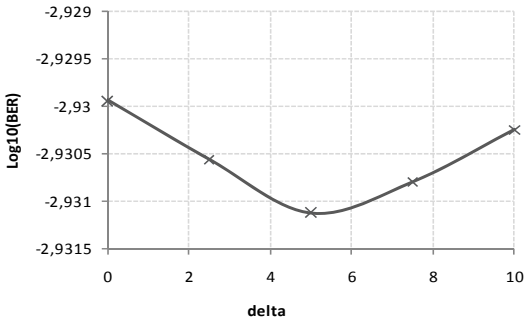

Figure 2.43. Logarithmic BER versus estimated non-centrality parameter for MC simulation with 10^7 transmitted pulses and infinite ER, Eb/N_0=15, n=10 spectral modes (the same for the function) and normalized noise system ($\gamma = \sigma = 1$).

2.4.3.2. Analysis of statistical moments

For the statistic analysis of the obtained distribution after the non-linear transformation, 100 iterations of the Dillard algorithm, and n = 10 spectral modes (same for modal parameter n_e) have been considered for different values of δ in an ideal normalized noise system. Note that for a Gaussian distribution with mean $\mu = 0$ and variance σ^2, the moments can be generalized as [Hahn 1994]:

$$E\{x^n\} = \begin{cases} 0, & n = 2k+1 \\ 1 \cdot 3 \cdot (n-1)\sigma^n, & n = 2k \end{cases} \tag{2.39}$$

The statistic parameters that have been studied are the mean, the variance, the Skewness S and the Excess Kurtosis EK. The two last ones are derived from the third and fourth order moments respectively [Hahn 1994]. In an ideal Gaussian distribution, both S = 0 and EK = 0.

Figure 2.44 shows the mean of the non-linear function for different values of estimated non-centrality parameter δ versus the square root of the signal non-centrality factor $\sqrt{\lambda} = \sqrt{2E_s / N_0} = s/\sigma$, where $s = \sqrt{E_s}$ is the signal mean in optical domain and $\sigma = \sqrt{N_0 / 2}$ the standard deviation of the ASE noise. The square root of the non centrality factor has been taken as the variable in abscissa axis, instead of directly the non centrality factor, in order to show the linearity of the function better in terms of field amplitude instead of optical power. In radio systems the received signal mean is always linear with (i.e. proportional to) the amplitude mean of the electric field. This is the ideal behaviour which the non-linear function is looking for. So, this hypothetical mean has been printed in order to compare the performance of the non-linear function. As it can be observed in Figure 2.44, with a value of $\delta = 5$ the system is more lineal than with the SQRT. The cube root highly deviates at $s/\sigma > 5$.

In Figure 2.45 left, the variance with respect to s/σ is presented for the cases of SQRT, normalized non-linear function with different values of δ, and cube root. The SQRT slightly deviates from the expected constant value (the functions are normalized to the variance of ASE noise so the output should be equal to unity) for low values of s/σ. The SQRT tends faster to the unity level than the other y^{α} function family.

In Figures 2.45 right, a comparison of the Skewness (S) is shown between the SQRT, cube root and the normalized non-linear function for different values of δ. The Excess Kurtosis (EK) has

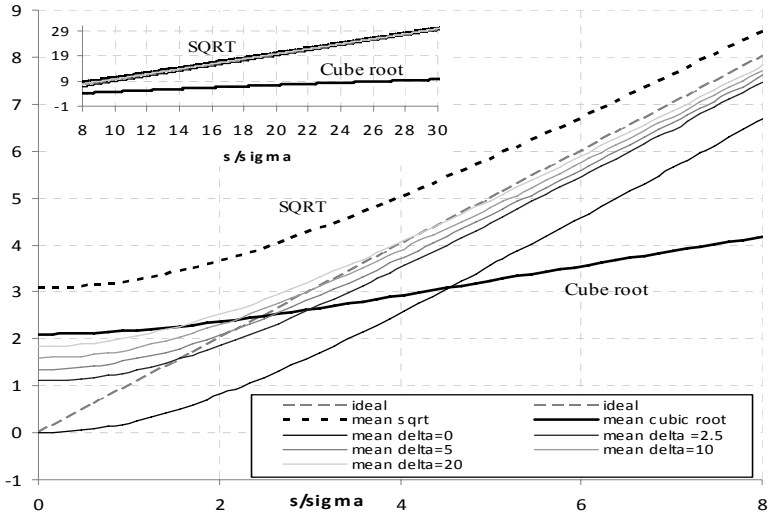

Figure 2.44. Function mean versus s/σ for n=10 and different values of estimated non-centrality parameter $\hat{\delta}$, in a normalized noise system. The curves obtained for the SQRT, cube root and ideal mean cases are also depicted.

also been measured. It is always lower than 0.06 and lower than 0.03 for s/sigma major than 0.5 for all the cases. Note that in Gaussian case S = EK = 0. High levels of δ produce the movement away from the optimum Gaussian case for signals with low means. In fact, by increasing this parameter, the function tends to behaviour similar to the SQRT. The best statistical results are obtained with δ ~5, both in convergence rate and in value deviation.

From these tests, we can conclude that the obtained non-linear equalizer function provides statistics that are nearly constant, and the variance remains practically the same with the mean optical power variation with little error.

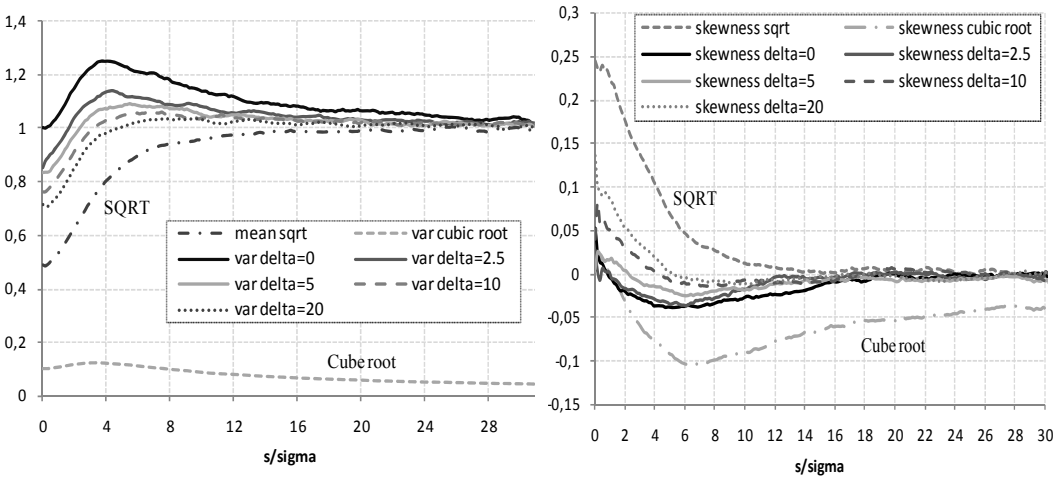

Figure 2.45. Function variance (left) and Function Skewness (right) versus s/σ for n=10 and different values of estimated non-centrality parameter δ, in a normalized noise system. The curves obtained for the SQRT and the cube root are also depicted.

2.4.3.3. System BER calculation

Two procedures have been developed to compute the BER and test the function behaviour. First one is based on Monte Carlo simulation in an ideal system with only ASE noise. The second uses a MLSE simulator which implements Viterbi algorithm.

2.4.3.3.1. Monte Carlo BER Analysis with only ASE Noise

For this study we used the same parameters than in section IV. Some assumptions have been taken: only ASE noise is present, the resultant distribution is Chi-square with n = 10 degrees of freedom, the system is not polarized (p = 2) and the optical and electrical filter bandwidths are B_o = 40 GHz and B_e= 8 GHz, respectively. Assuming infinite ER, in Figure 2.46 left, the BER logarithm versus 10log (Eb/N_0) is printed for five different cases: in triangles for the normalized non-linear function (n_e=10 and δ=5), in squares for the radio system Gaussian stationary (AWGN channel with constant variance), in circles for the SQRT, in crosses for the cube root, and in diamonds for the case without function. About the symbol decision, Gaussian approximation (with different mean and variance for bit "1" and bit "0") has been used to obtain the threshold. For the ideal Gaussian stationary BER computation the expression of the ASK modulation of two levels has been used [Proakis01]

$$BER = \frac{1}{2} erfc\left(\sqrt{E_b \big/ 2N_0}\right) \tag{2.40}$$

The difference in BER between the non-linear function, the SQRT and the cube root is very low.

However, the first always give slightly better results, although it is far from the stationary Gaussian. From the last results, Figure 2.46 right top) shows the PDFs for the bit "0" and the bit "1" in log scale for the non-linear function (solid line) and the ideal Gaussian (dashed line), with Eb/N_0 = 13.01 dB and assuming infinite ER. As it can be observed, the non-linear function gives good results of Gaussianity.

Finally, as explained in the section 2.3.4, while a photodetector linearly detects optical power rather than the optical field, lasers and (in principle) commercial amplitude modulators modulate power as well (photon–electron conversion). In terms of the field, the signal is modulated in intensity although it is desirable to have it modulated in field amplitude. Because of that, the optimum results with the SQRT are obtained when a real amplitude modulation (AM) is applied instead of intensity modulation (IM).

A four-level transmission system with IM-DD, AM-SQRT and AM-Non-linear function has been simulated (using the Virtual Photonics Inc. software), and the resulting eye diagrams are shown in Figure 2.46 right bottom), with the purpose of comparing the symmetry and noise variance between the different levels, as well as the eye opening for each transition. It can be observed that the IM-DD case presents a noise that is highly dependent on the signal amplitude. Note that the main difference between the SQRT and the Non-linear function eye diagram is the variance of the symbol with lower energy: while the Non-linear function maintains it with respect to the other symbols, the SQRT does not.

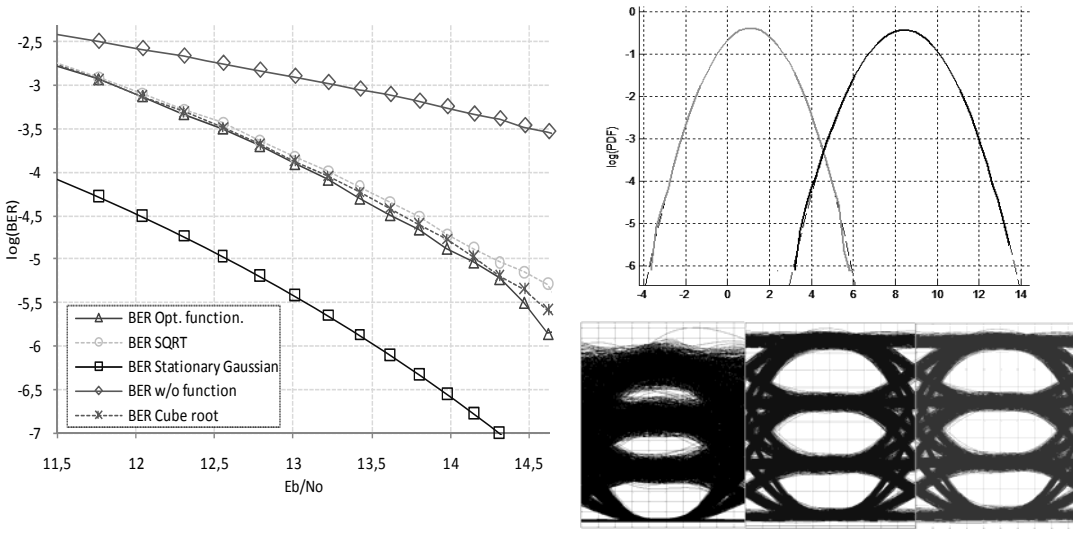

Figure 2.46. Left: BER logarithm versus ratio E_b/N_0 assuming infinite ER with n = n_e = 10, normalized noise system, δ =5 and without CD for 10^7 transmitted pulses. Right: Top) Logarithmic PDF for E_b/N_0 = 13.01 dB, infinite ER, n = ne = 10 spectral modes, δ=5 and 10^7 transmitted pulses and Bottom) Four level eye-diagram for IM-DD (left), AM-SQRT (in the middle) and AM-non-linear function with n_e=4, γ=0.001 and δ=5 (right).

2.4.3.3.2. BER Analysis with MLSE

For the second procedure used to compute the BER, a simulator implementing the Viterbi algorithm has been used. The simulator takes files directly generated by OPTSIM (system simulator). The bit rate used is 10.7 Gb/s, NRZ modulation with ER of 12 dB, filtered by a 5-pole Bessel filter of 7.5 GHz bandwidth. The fibre has been modelled by an ideal fibre Bragg grating with total dispersion DL, with D=17 ps/nm/km and L=400km. Non-polarized system is considered. In the receiver, a 2nd order Super-Gaussian optical filter with bandwidth 35 GHz and a post-detection electrical filter: 5-pole Bessel filter with a bandwidth of 7.5 GHz are considered. After that, the electrical signal is sampled using 2 samples per bit. The MLSE algorithm has been implemented with 2^{20}-1 bits, 2 samples per bit and 128 Trellis states. Simplified or stationary Gaussian branch metric is used.

The number of modes per polarization (2M) can be calculated from the ratio between optical and electrical filter bandwidths ($2M = B_o/B_e$). Here, 2M = 4.67 and n= 2pM = 9.34 (where n is the number of degrees of freedom including both polarization states). As the Hastings-Dillard approximation only permits integer numbers for modal parameter n_e, then the values considered have been: 2M = 4 or 2M = 5 and $n_e = 8$ or $n_e = 10$ respectively. We have compared both cases.

To get the optimum γ noise parameter, a BER versus γ sweep has been generated. After that, the best value has been chosen. Regarding δ, and following the results of last sections, δ=5 has been taken. Figure 2.47 displays the BER logarithm at the MLSE output with respect to the noise parameter γ for the non-linear function in the two selected cases of $n_e = 8$ (triangles) and $n_e = 10$ (crosses), with the SQRT (in dashed line) and cubic root (point-dashed line) as reference lines.

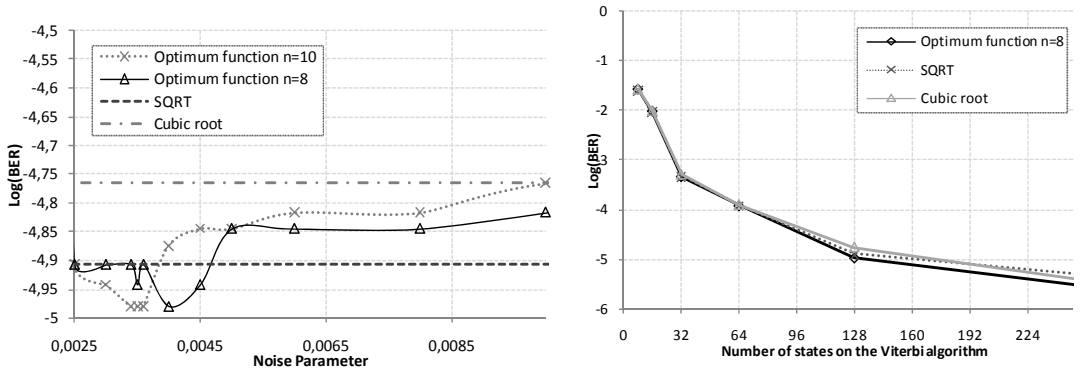

Figure 2.47. Left: Log(BER) for optimum function (ne=10 or ne=8, and δ=5), SQRT and cube root, with 128 Trellis states MLSE versus noise parameter γ for 400Km. Right: BER Logarithm with MLSE algorithm versus number of states or different cases like optimum function (ne=8, γ= 0.004 and δ=5, SQRT and cube root, after 400 Km.

It can be observed that if the noise parameter is correctly chosen, the best results are effectively obtained with the non-linear function. However, other values of noise parameter can give worst BER. Comparing the two functions, the one with modal parameter n_e= 8 presents slightly better performance than n_e = 10. However, they achieve the same minimum BER value in different noise parameter points: $\gamma = 0.004$ for $n_e = 8$ and $\gamma = 0.0035$ for $n_e = 10$.

Once the optimum noise parameter is known, the behaviour of the non-linear function versus the MLSE complexity (Trellis states) has been examined and compared with the SQRT and cubic root (Figure 2.47 right). The best results are always obtained with the non-linear function, although the difference is small: only 0.2 to 0.5dB.

2.5. Conclusions of Chapter 2

In this chapter, the process of photodetection in conventional IM-DD has been evaluated and modified. There are impairments produced in the optical fibre which are linear in terms of optical field (like Chromatic Dispersion) that after photodetection become non-linear. In ASE dominant systems, the noise becomes signal dependent following a chi-square distribution. These effects limit the performance of electronic equalizers, increasing the required complexity.

The use of a non linear module after the photodetector, capable of performing the mathematical operation square root (SQRT) partially compensates the square law characteristic of the photon-electron conversion. A new method of transmitting the signal, more linear with the optical field has been proposed and called amplitude modulation (AM) instead of intensity modulation (IM).

It has been demonstrated that incorporating a SQRT at the receiver reduces the harmonics and intermodulation products in analogue radio over fibre (RoF) systems and reduce the complexity of electronic equalizers in digital systems.

As a mode of example, in RoF, the use of SQRT and AM allows ideally to transmit twice the distance until achieve the same levels of 2^{nd} harmonic and 3 times longer distance until achieving the same level of 3^{rd} harmonic (or transmitting $\sqrt{2}$ and $\sqrt{3}$ times at higher frequency respectively).

With respect to digital systems, the incorporation of the SQRT allowed the use of a simplified metric in MLSE receivers with very low computational complexity, needing only one parameter per branch metric. The nature of this parameter allowed tracking the channel changes very fast, especially as compared to the histogram approach, then simplifying the implementation of large processors with many states. The first transmission over more than 1000 km at 10 Gb/s without optical dispersion compensation has been reported using this technique.

The SQRT module can be analogue as an electronic circuit placed after detection or a mathematical digital operation, after the analogue to digital (A/D) converter. In all cases this technique is a low cost completely colourless solution. Two analogue electronic circuits have been implemented to approximate the SQRT response:

- The first one has been developed using discrete components soldered in a microstrip line, approximating the response of a Schottky diode to the required function adjusting the

appropriate voltage bias. The measured bandwidth was 7 GHz and performed the required SQRT behaviour with accuracy to input signals with ER up to 10dB.

- The second consist of a MMIC chip based in GaAs 0.2um technology demonstrating the potential capability of being integrated together with the photodiode. The SQRT response is achieved by using HEMTs and GM diodes. 3 circuits were included in the chip. Two of them were tested; the measured BW was around 20 GHz and the maximum ER was around 14 dB for the circuit with 6-HEMT and 21dB for the circuit with 6-GM diodes.

The behaviour of analogue and digital SQRT has been compared. In conventional conditions, the analogue performs better than the digital because the operation is done before the quantification process, although in some specific cases, improvement can be obtained for the digital SQRT by applying clipping.

Finally, a theoretical statistic analysis has been performed to optimize the non-linear transformation. The SQRT transforms the chi-square distribution in a Ricean. This implies to obtain a signal with statistics quite similar to Gaussian in the entire region except close to the origin. A mathematical study has been performed and the optimum non-linear function has been achieved, capable to transform the detected signal in Gaussian and signal independent. Due to the followed mathematical process, the optimum function slightly depends on the optical system channel (optical noise and number of spectral modes) and the signal energy (SNR). For this reason, the optimum equalization is obtained after a previous calibration (training sequence). Although the obtained function is always the best in terms of performance, the improvement compared with SQRT, especially together with MLSE, is not substantial because the SQRT has been demonstrated to be a good equalization and the BER considered is high, FEC limit, due to computational costs.

2.6. References of Chapter 2

[A. JimenezMT] "Funció no lineal òptima per una fotodetecció Gaussiana" Author: A. Jimenez. Supervisors: J. Prat and M. Omella. Master Thesis. 30th Sep 2008

[Bosco 2001] G. Bosco, et al, "A Novel Analytical Approach to the Evaluation of the Impact of Fiber Parametric Gain on the Bit Error Rate", IEEE Trans. on Comm., vol. 49, no. 12, Dec. 2001.

[Bosco08A] G. Bosco et al, "Optimization of Branch Metric Exponent and Quantization Range in MLSE Receivers for Duobinary Systems", IEEE Photon. Technol. Lett.,. vol. 20, no. 11, pp. 924 – 926, June 2008.

[Bosco08B] G. Bosco et al., "Performance Analysis of MLSE Receivers Based on the Square-Root Metric" J. Lightw. Technol., vol. 26, n. 14, pp. 2098-2109, July 2008.

[Brooks95] C. J. Brooks et al., "Integrated-optic dispersion compensator that uses chirped gratings" Opt. Lett., vol. 20, pp. 368-370, Feb 1995.

[Bungarzeanu94] C. Bungarzeanu, "Limitations of dispersion supported transmission over standard single-mode fiber," IEEE Photon. Technol. Lett., vol. 6, pp. 858–859, July 1994.

[Cai 2003] Yi Cai et al, "On turbo code decoder performance in optical-fiber communication systems with dominating ASE noise", J. Lightw. Technol, vol, 21 no. 3, pp. 727–734 March 2003.

[Cai08] Y. Cai, "Coherent detection in long-haul transmission systems," in Proc. Opt. Fibre Commun. Conf. (OFC), 2008, pp. 1–3, Paper OTuM1.

[Castellini97] G. Castellini, et al., "A Continuously Adaptive MLSE Receiver for Mobile Communications: Algorithm and Performance", IEEE Transactions on Comm., vol. 45, no. 1, Jan. 1997.

[Curri04] V. Curri et al., "Electronic equalization for advanced modulation formats in dispersion-limited systems," IEEE Photon. Technol. Lett., vol. 16, no. 11, pp. 2556–2558, Nov. 2004.

[Doerr05] C. R. Doerr et al., "40-Gb/s colorless tunable dispersion compensator with 1000-ps/nm tuning range employing a planar lightwave circuit and a deformable mirror" in proc. ECOC 05 PDP5,

[Ellis06] A.D. Ellis and M.E. McCarthy, "Receiver-side electronic dispersion compensation using passive optical field detection for low cost 10Gbit/s 600 km reach applications" in proc. OFC 2006, paper OT3uE4.

[Fews06] H. S. Fews, et. al, "Experimental Comparison of Fibre and Grating-Based Dispersion Compensation Schemes for 40 channel 10Gb/s DWDM systems", ECOC 2006, paper Th3.2.5.

[Foggi06] T.Foggi, et al., "Maximum-likelihood sequence detection with closed-form metrics in OOK Optical systems impaired by GVD," J. Lightw. Technol., vol. 24, n. 8, pp. 3073-3087, Aug. 2006.

[Fonseca06] D. Fonseca et at., "Optical Single-Sideband Transmitter for Various Electrical Signaling Formats" J. Lightw. Technol ., vol. 24, no. 5, pp. 2059-2069, May 2006

[Franceschini07] M. Franceschini et al, "Post-detection nonlinear distortion for efficient MLSD in optical links", Optics Express, vol. 15, no. 18, Sept. 2007.

[GPON03] Gigabit-Capable Passive Optical Networks (GPON): Physical Media Dependent (PMD) Layer Specification, ITU-T Rec. G.984.2, Mar. 2003

[Gysel90] P. Gysel, R.K. Staubli, ”Spectral properties of Rayleigh backscattered light from single-mode fibers caused by a modulated probe signal”, J. Lightwave Techn., vol. 8, pp. 561-567, April 1990.

[Haykin00] Simon Haykin, “Communication Systems”, 4th edition, John Wiley & Sons.

[Hill97] K. O. Hill and G. Meltz, “Fiber Bragg Grating technology fundamentals and overview”, J. Lightw. Technol ., vol. 15, pp. 1263-1276, 1997.

[Hines84] M.E. Hines, “The Virtues of Nonlinearity-Detection, Frequency Conversion, Parametric Amplification and Harmonic Generation”, IEEE Trans. Microwave Theory and Techniques, vol. MTT-32, pp. 1097-1104, Sep 1984.

[Hueda07] M. R. Hueda et al, “Parametric Estimation of IM/DD Optical Channels Using New Closed-Form Approximations of the Signal PDF”, J. Lightw. Technol vol. 25, no. 3, pp 957-975, March 2007.

[Humblet 1991] P. A. Humblet and M. Azizoglu, “On the Bit Error Rate of Lightwave Systems with Optical Amplifiers”, J. Lightw. Technol. vol. 9, no. 11, pp. 1576-1582, Nov. 1991.

[Kramer04] G. Kramer , "Ethernet Passive Optical Network s," McGraw-Hill Professional, 2004 , ISBN: 0071445625

[Lázaro 2006] J. A. Lázaro et al., “Remotely Amplified SARDANA: Single-fibre-tree Advanced Ring-based Dense Access Network Architecture” In proc. ECOC’06, Cannes, paper We3.P.169 September 2006

[Marcuse 1991] D. Marcuse, “Calculation of Bit-Error Probability for a Lightwave System with Optical Amplifiers and Post-Detection Gaussian Noise”, J. Lightw. Technol, vol. 9, no. 4, pp. 505-513, April 1991.

[Marti97] J. Marti, et al., “On the use of tapered linearly chirped gratings as dispersion-induced distortion equalizers in scm systems,” J. Lightw. Technol., vol. 15, no. 2, pp. 179–187, Feb. 1997.

[May94] G. May, A. Solheim, and J. Conradi, “Extended 10 Gb/s fiber transmission distance at 1538 nm using a duobinary receiver,” IEEE Photon. Technol. Lett., vol. 6, pp. 648–650, May 1994.

[Papagiannakis09] Papagiannakis, et al. “Electronic distortion compensation in the mitigation of optical transmission impairments: the view of joint project on mitigation of optical transmission impairments by electronic means ePhoton/ONe+ project”. IET Optoelectron. vol. 3, no. 2, pp. 73–85, April 2009.

[Penninckx97]D. Penninckx, M. Chbat, L. Pierre, and J.-P. Thiery, “The phase-shaped binary transmission (PSBT): A new technique to transmit far beyond the chromatic dispersion limit,” IEEE Photon. Technol. Lett., vol. 9, pp. 259–261, Feb. 1997.

[Poggiolini06A] P.Poggiolini et al., “Branch Metrics for Effective Long-Haul MLSE IMDD Receivers”, in Proc. ECOC 2006.

[Poggiolini06B] P.Poggiolini et al., “1,040 Km Uncompensated IMDD Transmission over G.652 Fiber at 10 Gbit/s using a Reduced-State SQRT-Metric MLSE Receiver” Post Deadline paper, in Proc. ECOC 2006.

[Prat05A] J. Prat et al., “Square Root Strategy: a Novel Method to Linearize an Optical Communication System with Electronic Equalizers”, in Proc. ECOC 2005, Glasgow, Scotland.

[Prat06C] Josep Prat et al., "Square Root Module to Combat Dispersion-Induced Nonlinear Distortion in Radio-Over-Fiber Systems", IEEE Photon. Technol. Lett., vol. 18, no. 18, Sept. 15, 2006.

[Prat07B] J. Prat, et al., "Electronic Equalization of Photodetection by Means of an SQRT Module" ICTON2007 We.C3.6

[Prat07B] J. Prat, M. Omella, P. Poggiolini, G. Bosco, R. Killey A. Teixeira, R. Sousa "Electronic Equalization of Photodetection by Means of an SQRT Module" ICTON2007 We.C3.6

[Proakis01] "Digital Communications" Author: John G. Proakis. McGraw-Hill. Fourth Edition 2001

[Savory07] S. J. Savory et al., "IMDD Transmission over 1,040 km of Standard Single-Mode Fiber at 10Gbit/s using a One-Sample-per-Bit Reduced-Complexity MLSE Receiver" OFC 2007

[Savory07] S. J. Savory, et al., "Electronic compensation of chromatic dispersion using a digital coherent receiver," Opt. Express, vol. 15, pp. 2120–2126, 2007

[Schrenk09A] B. Schrenk, et al., Employing Feed-Forward Downstream Cancellation in Optical Network Units for 2.5G/1.25G RSOA-based and 10G/10G REAMbased Passive Optical Networks for Efficient Wavelength Reuse, in proa. ICTON 2009, paper Th.B3.4

[Sieben99] Sieben et al., "Optical Single Sideband Transmission at 10 Gb/s Using Only Electrical Dispersion Compensation" J. Lightw. Technol ., vol. 17, no. 10, pp. 1142-1149, 1999.

[Stahl04] D. Stahl, P. J. Winzer, C. R. Doerr, and S. Chandrasekhar, "Extending the chromatic dispersion tolerance by optical equalization at 43 Gb/s," in Proc. OFC 2004, Los Angeles, CA, vol. 2, Paper ThU5.

[Vengsarkar93] A.M. Vengsarkar and W. A. Reed "Dispersion-compensating single-mode fibers: efficient designs for first- and second-order compensation" Opt. Lett., vol. 18, pp. 924-926, June 1993.

[Yoneaka95] K. Yonenaga, et al., "Optical duobinary transmission system with no receiver sensitivity degradation," Electron. Lett., vol. 31, no. 4, pp. 302–304, Feb. 1995.

[Yu06] Q. Yu, A. Shanbhag, "Electronic Data Processing for Error and Dispersion Compensation", Journal of Lightwave Technology, vol. 24, no. 12, Dec. 2006.

[Zhao08] J. Zhao et al., "Electronic dispersion compensation using full optical-field reconstruction in 10Gbit/s OOK based systems", Opt. Express, vol. 16, pp. 15353–15365, Sept. 2008.

[Zhao10] J. Zhao et al., "Chromatic Dispersion Compensation Using Full-Field Maximum-Likelihood Sequence Estimation", J. Lightw. Technol., vol. 28, no. 7, pp. 1023-1031, April 2010

3. Rayleigh Backscattering Mitigation

3.1. Introduction

Access networks need to evolve according to the increasing demand of bandwidth. The network providers had to upgrade their access networks without increasing revenue because of the competition and increased demand for bandwidth. Scalability and efficient use of the available resources are two main goals in access Passive Optical Networks (PON), therefore the wavelength agnostic Optical Network Units (ONU) with only one wavelength per user have been the focus of thorough investigation.

One step beyond consist on the use of only one fibre per ONU with the same wavelength for upstream and downstream. Bidirectional transmission over optical fibre networks may yield a large cost improvement because of the reduction of the network infrastructure and can also provide a cost-effective way to upgrade distribution networks by adding bidirectional channels, increasing the bandwidth efficiency in the network system. This solution has been adopted in PONs where the spectral efficiency has to be kept high, so that each tree can only acquire the use of a single wavelength, on which down- and also upstream data is imprinted for full-duplex transmission. In addition, a single fibre access is intended for each ONU, also reducing user connexion and deployment cost.

However, signals propagating in opposite directions at the same wavelength suffer significant impairment. As a light wave propagates along an optical fibre, it continually loses energy due to Rayleigh scattering created by microscopic fluctuations of refractive index. It is related to the inhomogeneities in the material structure. Part of this energy comes back to the source and it is called Rayleigh Backscattering, usually used for fibre link monitoring by OTDR equipment [Agrawal].

As Rayleigh Backscattering is a degradation produced by the medium itself (optical fibre), it is unavoidable.

When signal and crosstalk from RB effect overlap and are detected by a photodiode, the square-law characteristic results in a photocurrent according to equation [Seimetz04]:

$$I_{ph} = R\left[P_s(t) + P_c(t) + 2\sqrt{P_s(t)P_c(t)}\cos(2\pi\Delta f_{opt}(t) + \Delta\varphi_{opt}(t)\right] \quad (3.1)$$

where R represents photodiode's responsivity, $\Delta f_{opt}(t)$ time dependent differential frequency (beat) of signal to crosstalk optical frequencies and $\Delta\varphi_{opt}(t)$ time-dependant optical phase difference. $P_s(t)$ is the signal power, $P_c(t)$ the crosstalk power (incoherent) and the third term presents the coherent crosstalk, often referred to as a Optical Beat Interference (OBI). If this latter term does not fall within the receiver bandwidth, only the two first terms remain after detection (only incoherent crosstalk affects).

Both incoherent and coherent decrease the signal quality but the coherent crosstalk can have much stronger effect due to the $P_s(t)$ $P_c(t)$ product (normally $P_s(t) >> P_c(t)$ for well designed systems).

The RB power depends on the electrical-optical bandwidth ratio and is proportional to the power emitted by the source. The mean power impact in detection of the backscattered signal follows expression [Arellano07]:

$$\bar{P}_{RB} = \frac{S\alpha_s I_0 \left(1 - e^{-2\alpha_a L}\right)}{2\alpha} \frac{1}{\pi} tg^{-1} \frac{B}{\Delta f} . \qquad (3.2)$$

Where S is the recapture coefficient (dimensionless), α_s is the scattering coefficient (km^{-1}), α_a is the attenuation coefficient (km^{-1}), I_0 is the initial power launched into the fibre, B is the receiver electrical bandwidth and Δf is the optical signal bandwidth. The RB optical power stabilizes for a fibre length around 20km. In that case, the backscattered power is about -34dB of the transmitted power, depending on physical characteristics of the fibre.

Only 33% of RB is polarized [Oskar96], for this reason the practicality of any polarization based mitigation techniques is limited.

According to (3.1) and (3.2), mitigating RB effect can be achieved by adjusting or modifying the spectrum of the transmitted signal in order to minimize the RB and data overlap and also by broadening the optical spectrum (Δf) with respect to the electrical receiver bandwidth B.

Reflections of the transmitted signal in the optical distribution network (ODN) produced, for example, due to non-angled connectors or air gap optical attenuators can give serious penalty as well, especially close to reflexive ONU premises. As a mode of example, in [Cho09] reflection tolerances are measured to be in the range of -42 to -35dB for the downstream signals and -29 to -19dB for the upstream signals, depending on the RSOA gain. Although single (Fresnel), back-

reflections can be prevented by using angled connectors or splices, several techniques focus on minimizing their impact in the detected signal quality.

In DWDM PONs and hybrid DWDM-TDM PONs using Centralized Light Source (CLS), there are two distinct RB contributions, which interfere with the upstream signal at the RX (Figure 3.1). The first contribution, carrier backscattering (CB), arises from the continuous wave (CW) carrier delivered from the optical line termination (OLT) to the customer. The second contribution, signal backscattering (SB), is generated by the modulated upstream signal, which is output from the R-ONU. The signal backscattered light re-enters the R-ONU where it is remodulated and reflected toward the receiver. This relatively low-power signal backscattered light is also amplified by the reflective modulator, which is usually arranged to provide net gain in order to overcome the link loss.

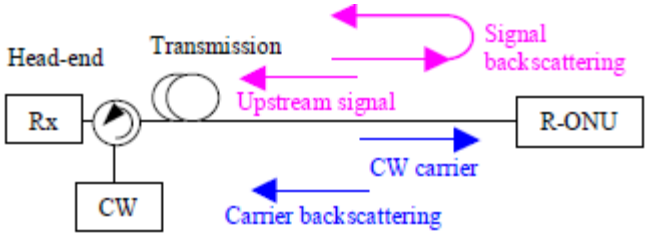

Figure 3.1 RB contributions in a PON system based in reflective ONU

The interferometric noise generated by these two contributions is different due to the different optical spectra. In particular, the CB has the same spectrum as the CW carrier, while the SB contribution is modulated twice by the R-ONU and thus has a broader spectrum.

When dealing with bidirectional transmission impairments in CLS PON systems with reflexive ONU, the ONU gain cannot be chosen arbitrarily. The impact of signal backscattering produced by RB and Fresnel reflections increases significantly with ONU gain, although signal amplification at the ONU increases the signal to CB ratio. As reported in [Fujiwara06] and [Arellano09], an optimal value for the gain at the ONU must be properly selected depending on the link losses. In this kind of scenarios, the transmission performance is maximized when the gain of the ONU equals the transmission loss -1.5 dB. [Fujiwara06]

In literature, RB penalty has mostly been minimized if either the signal or the RB has broad spectrum while the other is narrowband, or by using special modulation formats.

Here, a novel method has been studied and tested. It consists on shifting the incoming lambda at the ONU in order to avoid the overlap of the spectrum while maintaining the new wavelength

inside the same array wave grating (AWG) channel. The coherent crosstalk is avoided and the RB penalty reduced. The crosstalk due to incoherent RB could be removed by filtering optically afterwards. Although this work has been mainly focused on Rayleigh Backscattering, this same technique could be used also to avoid also reflections close to the ONU.

3.2. Approaches to mitigate RB in PON (state of the art)

Diverse modulation techniques can be applied to reduce the spectral overlap. Optical FSK or electrical sub-carrier modulations were demonstrated in previous investigations [Arellano06, Prat06A]. In literature, other interesting solutions can be found, they can be divided in three blocks: the ones in which the penalty is reduced by broadening the source light, the use of special modulations and the high pass filtering at the OLT premises.

3.2.1. Source Spectrum Broadening

Spectrum slicing. In these systems, optical signals are generated by modulating incoherent lights that have broad spectral width, e.g., directly modulating super-luminescent diodes or SOAs. Each of the optical signals is spectrally sliced as they pass through a wavelength multiplexer. The multiplexed signals are transmitted through an optical fibre transmission line, demultiplexed and detected by in a typical WDM configuration.

A well known problem of spectral slicing with incoherent light is the excess intensity noise (EIN) brought about by the spontaneous-spontaneous beat noise that falls within the photoreceiver passband. This noise can be reduced in this system by exploiting the amplitude noise squeezing properties of SOA [Katagiri99]. Amplitude squeezing occurs when an SOA is operated into gain saturation.

Thus, the use of a reflective SOA has been proposed because it performs three functions: (i) amplifying the power in the incident spectral slice; (ii) applying data modulation to the spectral slice; and (iii) squeezing the amplitude fluctuations to reduce the EIN and hence increasing the noise margin of the system. [Healy01]

Phase modulation. By using phase modulation (PM), the optical carrier can be suppressed choosing properly the amplitude of the applied electrical signal. If the modulation index β is

equal to 2.41 or 5.5, then '0^{th}' component in the Bessel function is cancelled ($J_0(\beta)=0$) [Proakis01].

According to Carson's rule, the spectrum bandwidth (B_{PM}) including the 98% of phase modulated signal is [Yoshida06]:

$$B_{PM} = 2(\beta + 1) f_{PM} \qquad (3.3)$$

This means that taking the minimum value of β that cancels the carrier, the bandwidth becomes 6.8 times the rate of the PM. This effect is beneficial for RB mitigation but creates huge penalty to chromatic dispersion.

Having the signal separated from the RB, the later can be filtered using a narrowband optical filter. In [Yoshida06] the CD degradation is reduced by applying an AM-PM synchronized structure, adjusting a phase difference of 45º between the clock signal used for PM and the data NRZ used in the AM, trying to perform an effect on the signal pulse opposite to the generated by the CD.

Chirped modulation. Light chirping can be defined as the instantaneous change of the central wavelength in response to variations in the optical power. We can distinguish two main contributions to the frequency chirp [Bjerkan96]. First, there is a transient chirp component that evolves with the time derivative of the optical power, and is scaled by α, normally called linewidth enhancement factor. Also an adiabatic chirp term is present mainly in lasers, producing a frequency shift proportional to the instantaneous optical power, and scaled, in addition to α, by parameter κ, which is associated to the nonlinear gain. Transient chirp produces phase modulation and adiabatic chirp makes the high '1' to be at different wavelength than the '0' in NRZ modulation. Both cases produce an increment in the signal spectrum bandwidth. In that sense, acting on the chirp of the modulator element can be also thought as a RB mitigation technique. However, as it has been commented before, it creates a penalty in terms of chromatic dispersion.

Laser bias dithering (wavelength dithering)**.** With this technique, the wavelength to be remodulated is changing at the input of the ONU with a period in the order of the round trip delay of the optical fibre which produces the RB, thus the different RB contributions of the different points of the fibre are not at the same frequency and the penalty is reduced. The upstream is narrowband, but moving the carrier with a frequency deviation sufficiently high (in the order of 10GHz). The advantage of this method over other kinds of spectrum broadening is

that instantaneously the upstream is maintained narrowband so there is not degradation in terms of SNR and CD [Lázaro07].

RSOA bias dithering (phase dithering): The signal is modulated in the RSOA by current variations which are a composition of the data signal and a sinusoidal signal at double the data bit rate. This yields a shift of the crosstalk products sufficiently far above the baseband data spectrum in order to allow suppression of this crosstalk by using a filter. [Urban09]

3.2.2. Special Upstream Modulations: CSS-AMPSK

CSS-AMPSK. This technique implies to perform duobinary amplitude modulation together with PM adjusted to cancel the carrier by biasing the modulator at null point. The AMPSK drive signal is generated by modulating a 10 GHz sine clock signal with a 10 Gbit/s duobinary (DB) signal using a microwave mixer. In practice, the DB signal is generated from the NRZ signal using a low pass filter (LPF). By biasing the MZM for minimum transmission, the CW carrier wavelength is suppressed, and two copies of the AMPSK drive signal are translated to sub-carriers at ±10 GHz with respect to the optical carrier frequency. The fundamental frequency shift associated with subcarrier drive of a MZM biased for minimum transmission ensures a frequency translation each time a signal passes through the modulator, ensuring that the upstream signal is shifted away from the backscattered signal [Chow08].

3.2.3. High pass filtering at OLT

In centralized light source PON, the upstream wavelength is generated at the OLT and transmitted as a continuous wave carrier (CW) to the ONU, which modulates it imprinting the up-stream data. At the OLT receiver, the detected up-stream signal mixes with the Rayleigh Back-scattering (RB) mainly caused by the down CW, generating electrical noise; this noise is not spectrally flat but has a main component at low frequencies, resulting from the beating of the two carriers coming from the same laser but with uncorrelated phase noises. This produces a strong noise band centred at DC with a 3 dB bandwidth, which is generally the double of the laser linewidth, in the range of MHz for typical DFB lasers. For this reason, filtering the low frequency components in the OLT receiver can help at reducing the RB signal degradation. The drawback of these techniques is that they do not work for symmetrical full duplex transmission at the same wavelength.

Precoding and high pass filtering

The enhancement is achieved by using 8B10B coding and post-detection high-pass filtering in the uplink. The implementation of this technique does not require additional electro-optical components in respect to typical WDM-PON architecture. It is effective both with CW and modulated remote feeding signals, provided that the network operates asymmetrically (e.g. 10/1.25Gbs) and that a DC-balancing line code is also applied at the downstream signal. [Presi10]. However, this technique requires a transmission with low consecutive number of digits, for this reason it will not be compatible for example with burst mode in TDM-PON.

High pass filtering and low frequency restoration

Here, the proposal is to eliminate the RB by filtering the low frequency components out and restoring them at the receiver by means of electronic Quantized Feedback Equalization (QFE) [Kandikar90]. QFE is a form of Decision Feedback Equalization (DFE) with loop path low-pass filtering. This is a simple technique that allows using standard NRZ signalling with long identical bit sequences without need for precoding. This method is also helpful to simplify the transceivers design as to alleviate the need for DC coupling or very low frequency cut-offs. It offers interesting possibilities for burst-mode hybrid WDM/TDM-PONs. [Prat10]

In this thesis, mitigation of RB has been achieved by shifting the downstream optical wavelength at the ONU, before transmitting back to the OLT. It constitutes a colourless solution which avoids the coherent RB by separating the upstream and downstream wavelengths some GHz. It is transparent to other impairments. Comparing Wavelength Shifting to some previously cited techniques, it does not create any penalty in terms of Chromatic Dispersion nor requires specific data modulation formats, and it allows symmetrical transmission. By optical filtering at the OLT, the RB effect could be not only reduced, but completely mitigated.

3.3. Proposal: Wavelength Shifting as a Method to Mitigate RB

The goal is to shift the wavelength that comes to the ONU from the OLT while maintaining it inside the same AWG channel.

This solution directly improves the transmission without the necessity of optical narrowband filtering. It is completely colourless and transparent to the other impairments (like CD for example) also present in the optical fibre. This implies that it can be applied to long reach PON where the optical power budgets creates low signal to RB crosstalk ratio. It can be obtained with devices capable of being integrated and mass produced, thus applicable to the ONU side, and if it is used together with filtering at the ONU, the RB effect could ideally be completely mitigated.

This is a novel method based on the combination of single-side band (SSB) modulation and carrier cancellation at the ONU, which produces a wavelength shifting over the down-stream carrier, generating a new wavelength which is remodulated with the up-stream data.

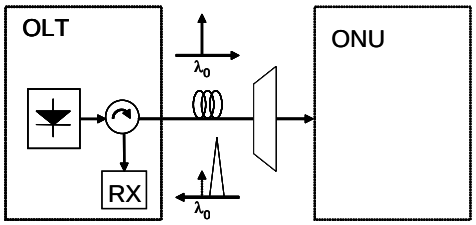

Figure 3.2. Schematic of wavelength shifting

Very recent papers, following our investigations, have used this idea and now apply wavelength shifting to mitigate RB: in [Wang10] a Dual-Parallel MZM has been used to achieve RB noise Mitigation in a carrier distributed PON by performing carrier suppress OSSB, i.e. what here is called wavelength shifting.

And other papers, apply similar techniques, with the same purpose of separating the wavelength used for the upstream to the RB: in [Schrenk_OFC10] all-optical wavelength conversion is used to mitigate the RB by four wave mixing (FWM) in a semiconductor optical amplifier (SOA) placed at the ONU, however it required an interleaver at the ONU and two wavelengths to be send from the OLT.

3.3.1. WS configurations

Different modules capable to perform wavelength shifting have been evaluated in terms of device and input electrical signal complexity and also regarding the shifting purity: spurious free dynamic range (SFDR).

Different possibilities have been considered, and devices based in 1 to 4 arms have been analyzed. Phase Modulators have already been proposed in literature to perform optical frequency translation (although not applying it to RB mitigation until the most recent papers), they are composed of either only one arm or 4 arms. In the first case, the required input electrical signal is a sawtooth, while for the 4-arms based a simply sinusoidal signal can be used. However, for the later case, the sinusoidal electrical signal has to be split in 4 paths with different external electrical adjusted phases, although some devices can incorporate some of them in equivalent push-pull configurations. Devices with 2 and 3 arms are in this thesis proposed as alternative solutions showing its good performance and reduced electrical complexity.

3.3.1.1. One-branch based solution (Serrodyne translation)

Phase modulation of light with an electrical sawtooth of an appropriate amplitude results in an optical frequency shift that is inversely proportional to the sawtooth period. This type of phase modulation, described in detail below, is called serrodyne frequency translation. In literature, it has been used in other applications rather than avoiding RB penalty in bidirectional transmission that is the purpose of this work: fibre optic gyroscopes, lidar velocimeters, spectroscopy, and optical communications shearing interferometry [Powerezhsky05]. The main factor which limits the maximum achievable serrodyne frequency shift has been the difficulty of generating and amplifying a high-speed sawtooth, due to its broad spectrum containing many harmonic components of the fundamental frequency.

Serrodyne frequency shifting is conceptually based on the modulation of the optical phase with a linear waveform $g(t) = a \cdot t$ in an electrooptic (EO) modulator. As a result, the frequency of the modulated optical signal is shifted by the amount proportional to the slope a of the modulating waveform:

$$E(t,z) = E_0 e^{j(\omega t - kz + g(t))} = E_0 e^{j((\omega + a)t - kz)} \qquad (3.4)$$

Here, E is the electrical field of a monochromatic optical signal, E_0 is its amplitude, w is the initial angular frequency, k is the wavevector, and z is the direction of propagation.

Of course, an infinitely long linear signal is not physically realizable, so an alternative waveform must be used for frequency shifting. Phase modulation with an electrical sawtooth can produce frequency translation of either CW or pulsed optical signals. To ensure phase continuity, the peak-to-peak amplitude of the modulating sawtooth must be an integer multiple of $2V_\pi$.

Phase modulation with a sawtooth with fundamental frequency f_s and peak-to-peak amplitude $2m\ V_\pi$, where m is a positive integer, produces a frequency shift of mf_s. An upshift or a downshift is achieved depending on the slope of the ramped portion of the sawtooth.

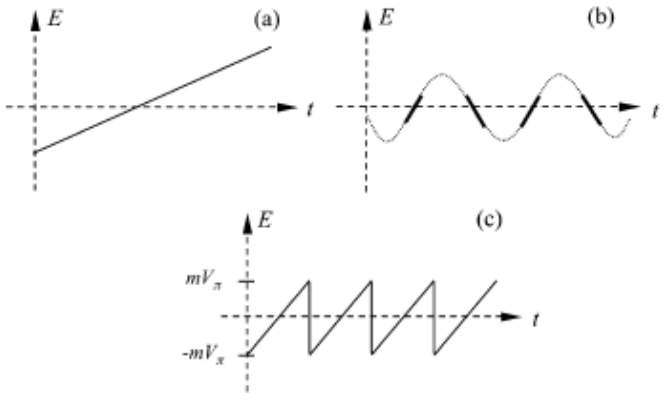

Figure 3.3. Electric field temporal responses that can be used for e/o WS. a) linear electrical field , linear parts of a sinusoid and c) sawtooth with amplitude $2mV_\pi$

In literature, serrodyne translation at Gb/s has been demonstrated [Poberezhskiy05] and [Johnson 2010]. In [Powerezhsky05] an RF-photonic arbitrary waveform generator (PAWG) is implemented to produce a continuous high-power electrical sawtooth signal, obtaining a frequency translation of 1.28 GHz. A passively mode-locked fibre laser with a 20-MHz repetition rate emitted a train of 200-fs pulses that were then spectrally broadened to over 100 nm in a supercontinuum (SC) fibre, by using a combination of nonlinear optical effects such as self- and cross-phase modulation, four-wave mixing, and Raman scattering were utilized.

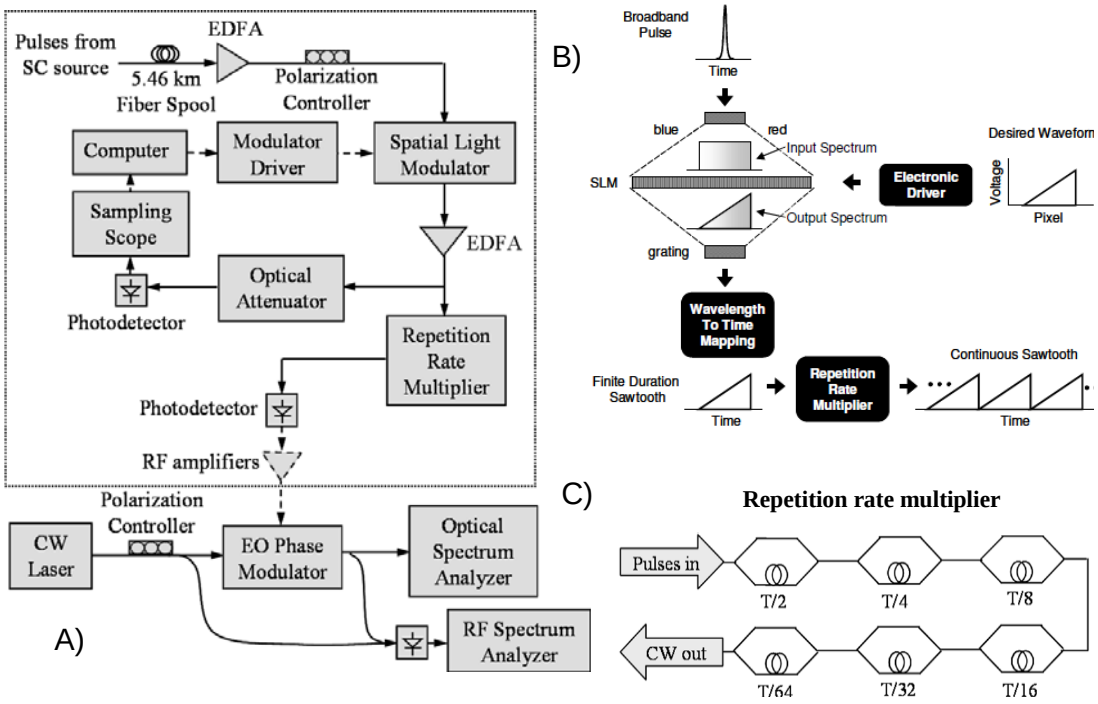

Figure 3.4. Serrodyne frequency translator and details of the repetition rate multiplier and spatial light modulator

The spectrally broadened pulses are temporally and spatially dispersed by using SMF-28 and a diffraction Grating respectively. Then, crystal spatial light modulators (SLMs) are used, where the spectral modulation is transformed into temporal modulation. Figure 3.4 shows the set up with details of the spatial light modulator and the repetition rate multiplier.

Another technique used in literature is phase modulation with linear regions of a sinusoid. [Farías05] as it can be seen in Figure 3.3(b). However, this method is limited to frequency translation of short optical pulses. As the frequency of the sinusoid increases, its linear portion has a greater slope yet shorter duration, therefore, this approach requires a trade-off between the magnitude of the shift and the duration of the optical pulses that can be shifted.

The conceptual operation is presented in Figure 3.5, where the optical pulses are aligned to interact with only these parts of the sinusoid. Nearly uniform frequency shift can be achieved [Poberezhskiy03][Farias03]. However this solution presents several disadvantages. First, the optical pulse train and microwave sinusoid have to be produced simultaneously, so the frequency shifter is not transparent to the repetition rate of the optical pulses. Second, the duty cycle of the optical pulses is often small, so most of the microwave power does not contribute to the frequency shifting. It does contribute, however, to the heating of the device, thus limiting the maximum power that can be applied. Third, synchronization itself presents a technical challenge, since it often involves generating multiples of high frequencies and is vulnerable to drift and phase noise.

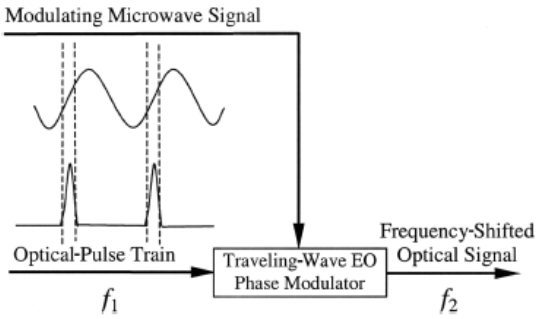

Figure 3.5 Frequency shifting obtained by taking the linear parts of a sinusoid.

Nowadays, arbitrary waveform generators are commercially available in the market which could conceivably be used to produce high-quality gigahertz sawtooth waves. However, they are very expensive instruments and the amplitude of the generated signal is too small to directly modulate the PM with the required multiple of $2V\pi$. Then, it requires the use of very broadband RF linear amplifiers with high optical output afterwards.

In [Johnson 2010] 200 MHz to 1.6 GHz sawtooth waveforms are generated by using an electrical nonlinear transmission line (NLTL). In an NLTL, an electronic signal experiences an amplitude dependent propagation speed. This effect results in a steepening of the input waveform as the higher amplitude components catch up with the lower amplitude components. This effect is used to achieve a sawtooth waveform from a sinusoidal signal. [Rodwell94]

3.3.1.2. Two-branches (AM-PM structures)

As it can be demonstrated, it is not possible with a two arm standard modulator to obtain a spurious free wavelength shifting. Any change in the operational parameters (phase or amplitude misalignments, modulation index, etc) or known electrical function allows generating OSSB and CS at the same time without producing other components as well. In this section, novel structures are presented as devices with high integration capability and low fabrication cost.

In order to obtain the optimum function to achieve spurious free wavelength shifting, we focus our study on a dual-arm MZM structure driven by the electrical function $d_1(t)$:

$$E_{out}(t) = \frac{E_{in}(t)}{2\sqrt{2}}\left(e^{jd_1(\omega t)} + e^{jd_1(\omega t+\theta)}e^{j\phi}\right) \tag{3.5}$$

where θ and ϕ are, respectively, the electrical and optical phase difference between one arm and the other. For $\theta = \phi = 0$ the optimum function $d_1(\omega t)$ is found to be a sawtooth signal; this is redundant in our analysis as can be implemented in a single arm modulator, as it has been explained in the previous section. Here, two cases are possible and have been analyzed:

In the first case, $\theta = \phi = \pi/2$, which is the typical configuration for single sideband modulation, [Fonseca06] the carrier suppression has to be then obtained by electrical amplitude increase adjustment to achieve the phase modulation index of $\beta = 2.4$. In the second case, carrier cancellation is assured by fixing $\theta = \phi = \pi$ and the single sideband modulation has to be then achieved by a proper design of the introduced electrical waveform function.

A. Carrier cancellation by amplitude adjustment

The study is targeted on finding a simpler continuous signal rather than the discontinuous sawtooth. In general, a phase modulation in each arm can generate a high number of spectral components as its modulation index increases. The first step is to try to obtain a modulation function $d_1(\omega t)$ that is able to generate only the three central components λ_0, $\lambda_0+\Delta\lambda$ and $\lambda_0-\Delta\lambda$, independent of the input power. Afterwards, the driving amplitude will be fine-adjusted to achieve the point of carrier cancellation. Finally, as it has been mentioned previously, by introducing 90º phase difference between the two arms (optically and electrically), a single sideband is obtained, that means an ideal wavelength shifting at the RF fundamental frequency. Thus the equation (3.5) is expressed as

$$E_{out}(t) = \frac{E_{in}(t)}{2\sqrt{2}}\left(e^{jd_1(\omega t)} + e^{j(d_1(\omega t+\pi/2)+\pi/2)}\right) \tag{3.6}$$

In general, any function capable of being discomposed in sinusoidal terms can be expressed as follows [Proakis01]:

$$e^{j\beta d_1(\omega t)} = \sum_{k=-\infty}^{\infty} a_k(\beta) e^{jk\omega t} \tag{3.7}$$

Here, we impose $a_0 = a_k = a_{-k} = 0$ for $k>1$ and only $a_1=a_{-1}=a$. By substituting equation (3.7) in equation (3.6) and introducing the values $a_0(2.405)=0$ and $a_1=a_{-1}=a$, it can be deduced that the desired $d_1(\omega t)$ function corresponds to:

$$d_1(\omega t) = \ln\left(2ja\cos(\omega t)\right)/2.405j \tag{3.8}$$

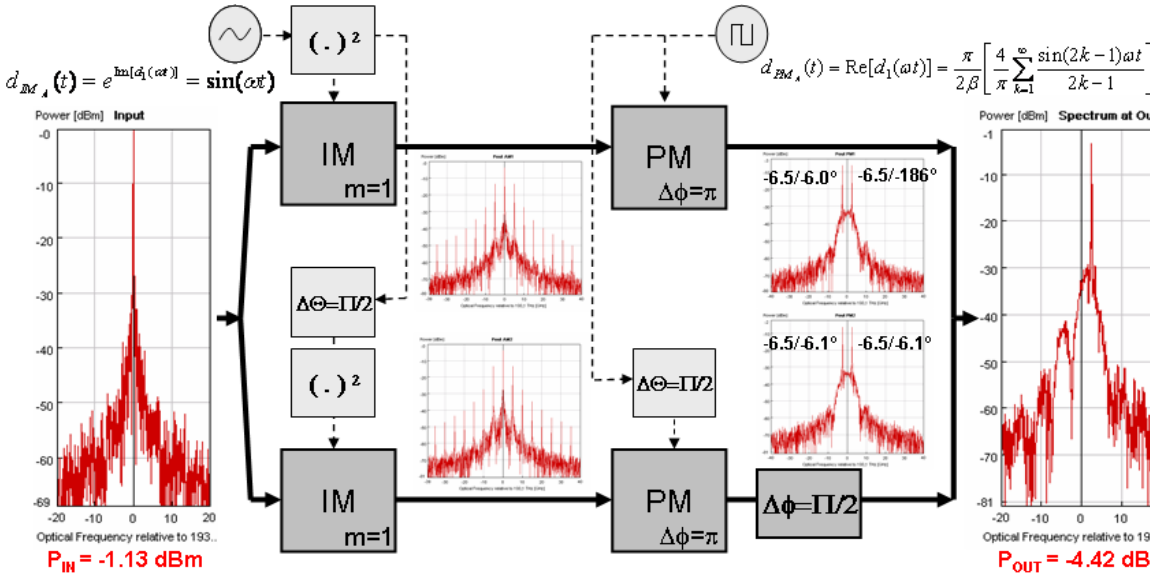

Figure 3.6. Wavelength shifter based on a dual arm modulator with AM and PM modulation in each arm and with electrical and optical phase difference between both arms of π/2. The input signals are a RF tone and a square signal for the intensity and phase modulator respectively. Spectra at the input, after each modulator, and at the output are provided.

This function is complex; it means that with phase modulation only, it is not possible to achieve the requirements. Its real part, $Re[d_1\omega t)]$, corresponds to a square modulation function with an amplitude $\pi/2\beta$. On the other hand, the imaginary contribution, $Im[d_1\omega t)]$ leads to an amplitude modulation of the electromagnetic field of the signal for the special case a = ½ . Both phase and amplitude modulation can then be produced by the design shown in Figure 3.6. It is important to note that the sine is square raised because an intensity modulator modulates the power and not the optical field.

Effectively, using Virtual Photonics Inc. (VPI) program, the system has been simulated and the obtained output signal shows a completely spurious free wavelength shifted spectrum (Figure 3.6 right).

The square signal is composed of a sum of odd integer harmonics; it means that, in order to have a precise wave form, it must be amplified with a wideband electrical amplifier.

B. Carrier cancellation by phase adjustment

Another way to cancel the optical carrier can be achieved by introducing an optical phase difference of π between the 2 arms. Following this concept, another configuration based also on phase and amplitude modulation has been derived, where only sinusoidal signals are needed to obtain an almost spurious free shifted signal.

The starting point is to solve the following expression, where an optical and electrical π phase difference between both arms is considered:

$$e^{j\beta d_1(\omega t)} + e^{j\beta d_1(\omega t)} e^{j\pi} = e^{j\omega t} \tag{3.9}$$

If $d_1(x+\pi) = -d_1(x+\pi)$, then

$$e^{j\omega t} \equiv e^{j\beta d_1(\omega t)} - e^{-jd_1(\omega t)} = 2j\sin(\beta d_1(\omega t)) \tag{3.10}$$

so the obtained function is:

$$d_1(\omega t) = \arcsin(-0.5j \cdot e^{j\omega t}) \tag{3.11}$$

Again, the required function is complex, so it has to be discomposed into its real and imaginary parts which do not have a simple analytical solution. A good approximation of this can be obtained by the proper adjustment of the parameters in the modulators. The series expansion of arcsin(x) can be used:

$\arcsin(x) = x + \frac{x^3}{6} + \frac{3x^5}{40} + ..$ with x = $-0.5j \cdot e^{j\omega t}$

Operating to separate the real and imaginary parts, we find that real part can be approximated by:

$$\mathrm{Re}\left[d_1(\omega t)\right] \approx 0.5\sin(\omega t) - \frac{0.5}{20}\sin(3\omega t) \tag{3.12}$$

$$\text{and} \quad e^{\mathrm{Im}(d_1(\omega t)} \approx \sqrt{0.5 + 0.5(c_1 - c_2\cos(\omega t))^2} \tag{3.13}$$

which can be implemented with an intensity modulator whose electrical input is square raised: Note that the response of an ideal intensity modulator is:

$$E_{out} = E_{in}\sqrt{(1-m) + md(t)} \tag{3.14}$$

where m is the modulation index (with values from 0 to 1). The VPI simulation shows that with these sinusoidal signals, a wavelength shift is achieved with a Spurious Free Dynamic Range (SFDR) of more than 48 dB when the two tones of (3.12) are introduced in the phase modulators (Figure 3.7), for $c_1 = 1$ and $c_2 = 0.86$ in the equation (3.13). More than 37 dB of SDFR can be obtained for a simpler configuration, only taking the first term in equation (3.12) for $c_1 = 2$ and $c_2 = 1$ in the equation (3.13), as it can be seen in Figure 3.8.

Evaluating the optical peak power of the input and output signals of Figures 3.6, 3.7 and 3.8, it can be observed that the last approach presents the lowest intrinsic optical loss of only 1.27dB, (it is 5.1dB with the two tones and 3.3dB with the ideal square signal). This last case constitutes the best trade-off between simplicity, bandwidth requirements and performance.
The shifting frequency fs can be defined as:

$$f_s = \omega / 2\pi \tag{3.15}$$

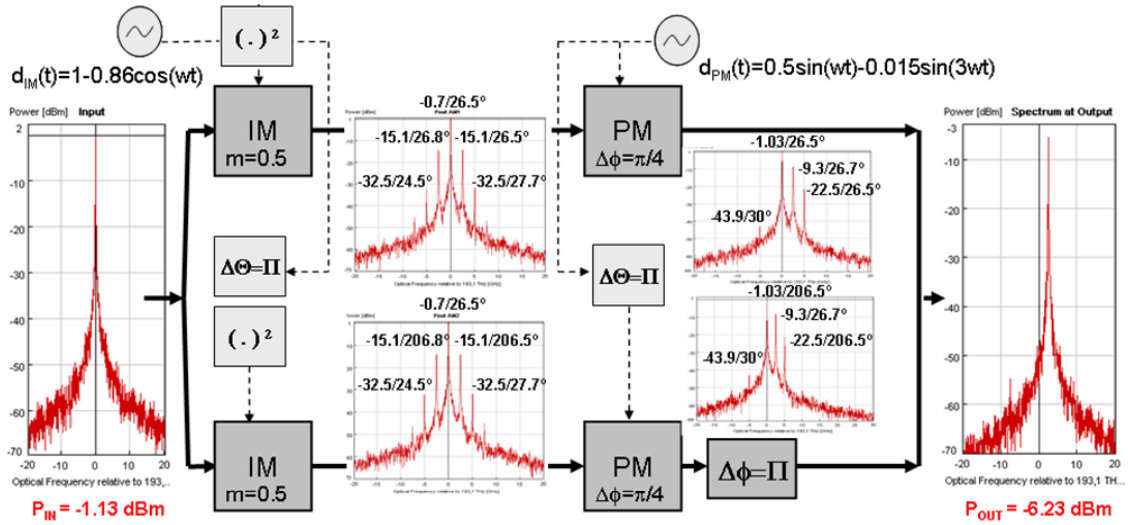

Figure 3.7. Wavelength shifter based on a dual arm modulator with AM and PM modulation in each arm, with electrical and optical phase difference between both arms of π and with two RF tones introduced in the PM. Spectra at the input, after each modulator, and at the output are provided

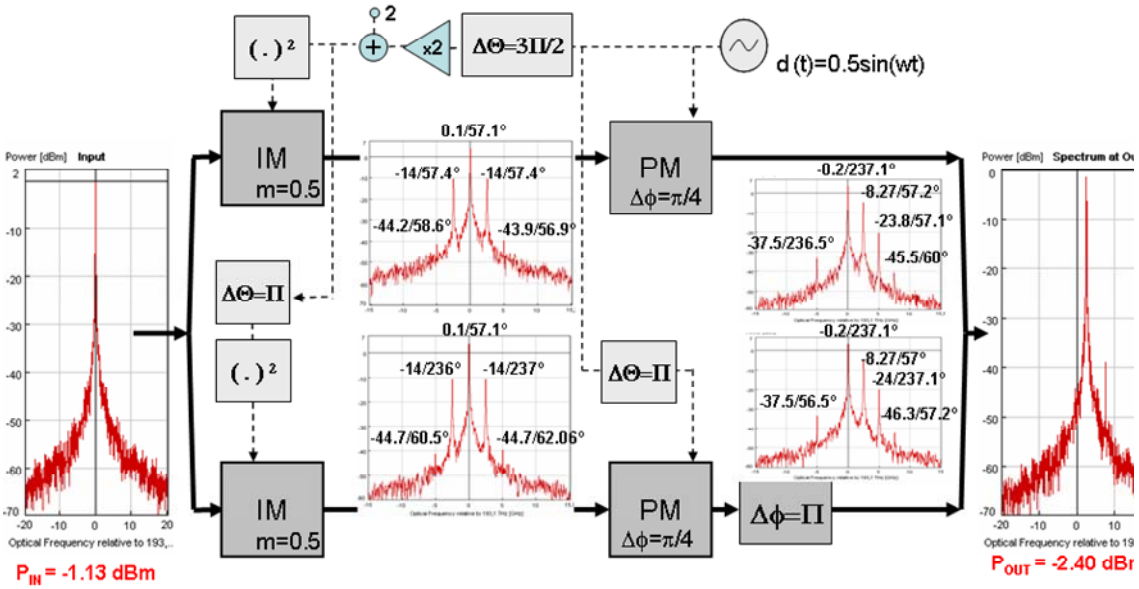

Figure 3.8. Wavelength shifter based on a dual arm modulator with AM and PM modulation in each arm, with electrical and optical phase difference between both arms of π. and with only one RF tone introduced in the PM. Spectra at the input, after each modulator, and at the output are provided.

As it can be seen in Figure 3.9, a comparison of the maximum SDFR versus the requirements in bandwidth (BW) of an RF amplifier has been simulated, taking up to 10 upper and lower harmonics. With an ideal sawtooth, signal and the single phase modulator a BW of 7 times fs is necessary to get a SDFR higher than 20dB, while with the square signal configuration it is achieved with a BW of 3fs, With this last configuration, using only one sinusoidal signal for the

IM and another one for PM, we can get more than 37 dB of SDFR independently of the BW, and with the 2 tones it is 48dB.

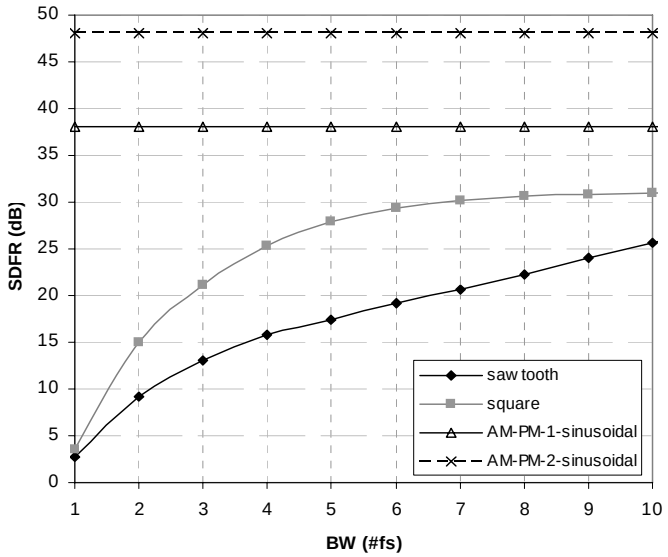

Figure 3.9. Bandwidth requirements comparison between a sawtooth signal followed by a single phase modulation, the dual arm with square modulation of section A) and the dual arm of section B) with 1 RF tone and with 2 RF tone.

These simulations have been performed with an ideal RF amplifier followed by an electrical Bessel filter of 4th order, with signal amplitude optimized for each case.

3.3.1.2.1. Dual arm conventional MZ approximation

As the 2 arm structures with AM-PM combination are not commercially available, a suboptimal solution with a commercial MZM has been adopted in order to prove the concept and to see the improvement of wavelength shifting in the Bit Error Ratio (BER) performance when RB is present. This implies performing only the PM.

A. Theory and simulations

Introducing the tone into the two branches, with a difference in phase at determinate amplitude, it is also possible to achieve a shifted wavelength with respect to the input one. The process cancels the carrier wavelength and generates a single sideband, although with spurious higher order harmonics. A one-branch modulator is mathematically expressed as:

$$E_{out} = A_c E_{in} e^{j\omega_0 t} e^{j\beta \sin(\omega_e t)} \tag{3.16}$$

Since $e^{j\beta \sin(\omega_e t)}$ is periodic, it can be presented in Fourier series coefficients like:

$$C_n = f_R \int_0^{1/f_R} e^{j\omega_0 t} e^{j\beta \sin(\omega_e t)} dt = \frac{1}{2\pi} \int_0^{2\pi} e^{j\beta \sin u - nu} du = J_n(\beta) \tag{3.17}$$

Identifying terms on the Bessel functions, E_{out} in one arm is approximated as:

$$E_{out1} = E_{in} A_c \sum_{n=-\infty}^{\infty} J_n(\beta) \cdot \cos(\omega_0 + n\omega_e)t) \tag{3.18}$$

As said above, SSB can be obtained with a dual arm MZM by inserting an electrical differential delay of 90º between both arms plus a differential optical delay of also 90º. The last can be achieved by means of introducing a DC voltage into the modulation equal to $V_\pi/2$. Then, the optical field at the output of the 2nd arm is:

$$E_{out2} = E_{in} A_c \sum_{n=-\infty}^{\infty} J_n(\beta) \cdot \cos(\omega_0 t + \frac{\pi}{2} + n\omega_e t + n\frac{\pi}{2}) \tag{3.19}$$

It can be approximated that, for low values of beta, the principal components are between 3 and -3. Furthermore, the higher modes can be filtered out. When interfering at the MZM the two modulations we have:

$$E_{out} = E_{out1} + E_{out2} = \\ E_{in} A_c \left\{ \begin{array}{l} 2 \cdot J_{-3}(\beta) \cos((\omega_0 - 3\omega_e)t) + \\ J_{-2}(\beta)(\cos((\omega_0 - 2\omega_e)t) - \sin((\omega_0 - 2\omega_e)t)) + \\ J_0(\beta)(\cos(\omega_0 t) + \sin(\omega_0 t)) + \\ 2 \cdot J_1(\beta) \cos((\omega_0 + \omega_e)t) + \\ J_2(\beta)(\cos((\omega_0 + 2\omega_e)t) - \sin((\omega_0 + 2\omega_e)t)) \end{array} \right\} \tag{3.20}$$

The 90º phase produces the cancellation of the -1 and +3 terms. An appropriate signal level has to be used in order to cancel the carrier. The first point of cancellation is close to J_0 null at $\beta = 2.4$. The problem is that other harmonics are generated. The variables are then optimized to reach one dominant up-stream shifted carrier, with enough down-stream optical carrier suppression together with reduced high order harmonics.

In Figure 3.10, it can be seen that by proper optimization of the input electrical voltage, a point close to $\beta=1.8$ can be found where all the components, including the carrier, present at least 8 dB of attenuation with respect to the desired component J_1. This will be a suboptimum version of wavelength shifting.

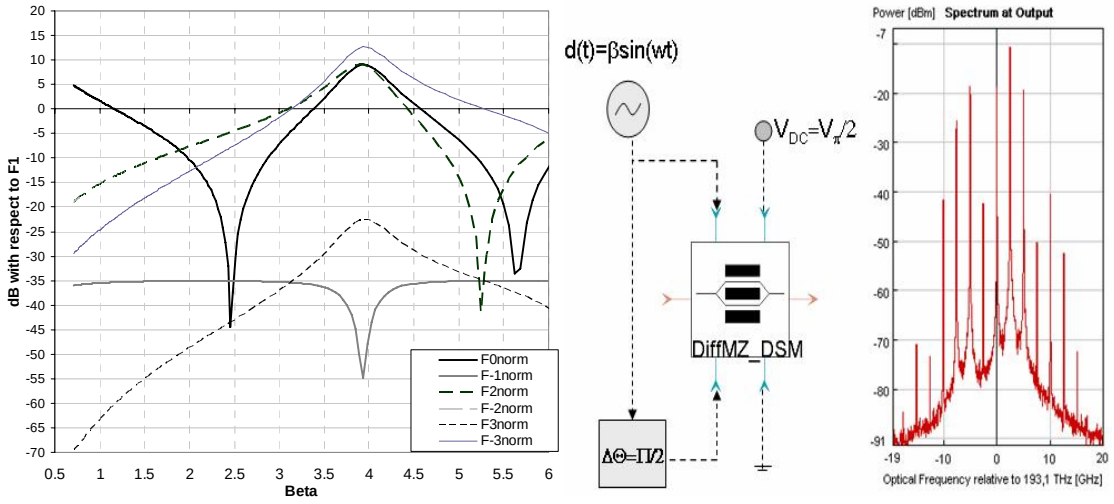

Figure 3.10. left: level of the optical carrier signal, the lower side band, and the second and third harmonic components with respect to the fundamental signal after MZM when a phase difference of $\pi/2$ is applied, electronically and optically between its two arms. Right : VPI simulation of a conventional MZM fixing the optical phase difference of $\pi/2$ by adjusting the DC bias at $V_{\pi/2}$ and spectra results.

B. Experimental results

Figure 3.11 shows the set-up of the measured WDM-PON system, detailing the proposed ONU design. An unmodulated downstream optical carrier is considered in this analysis. In order to demonstrate the concept, the ONU has elements that are not optimized for cost efficiency

It has a loop-back configuration with an optical circulator. First, the RF generator power, frequency and differential delay and the MZM bias are optimized for best spectral quality of the wavelength shifter. The RF frequency was set to 2.5 GHz and the V_{π} of the MZM is 5.5 Volts.

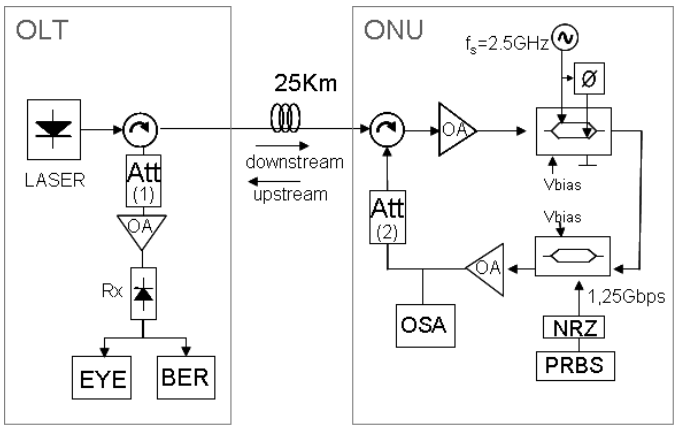

Figure 3.11. Experimental setup used to measure the BER improvement using a conventional MZM as a wavelength shifter. The shifter frequency is 2.5GHz and the bit rate 1.25Gbps

The optical spectrum is measured by means of an optical heterodination for high resolution, with a frequency bandwidth of 22 GHz and an intermediate frequency of 13.5 GHz. The spectra of the ONU signals before and after the dual-arm MZM are shown in Figure 3.12. The peak-to-peak input voltage is about 8 Volts. We observe the dominant lower-side band (J_{-1}), located at –fs from the optical down-stream carrier (J_0), which is reduced by 10.5 dB with respect to the lower-side band. It is high enough to be able to neglect the RB effect of the transmission.

At the same time, the upper-side band (J_1, at +fs) is below 15.4 dB with respect to the shifted carrier. Second order harmonics (J_{-2}, J_2) are at -9.7 and -6.5 dB. The third order harmonics are at 27dB and at 12dB respectively. Higher order harmonics, also excited, were not expected, however the J_{-6} is below -4.3 dB, which is not negligible, but is far away from the centre band. This could be explained by a non linear response in the electrical amplifier that should have been better filtered. Table 3.1 compares the results with the simulations.

TABLE 3.1. HARMONICS DB TO J_1 POWER COMPARISON

	J_0	J_{-1}	J_2	J_{-2}	J_3	J_{-3}
SIM	8.5	32.0	8.8	8.2	39.9	12.7
EXP	10.5	15.4	9.7	6.2	27	12

To improve this, the RF frequency could be increased for the harmonics to be sufficiently reduced by the AWG multiplexer, normally located at the PON remote node. However, it is not done it this experiment.

The shifted wavelength is then remodulated with the up-stream data with a single-arm MZM. Being fs higher than twice the bit rate, there is no overlap between down- and up-stream signal spectra, thus the beat noise between the OLT received signal and the RB from the down-stream is uncorrelated at the RX, and the system may become highly tolerant to RB.

By applying the wavelength shifting process, ideally, a system that initially presented both coherent and incoherent RB is converted to an environment with only incoherent RB as it has been explained in the introduction of this chapter. This means that, with an optical signal to RB

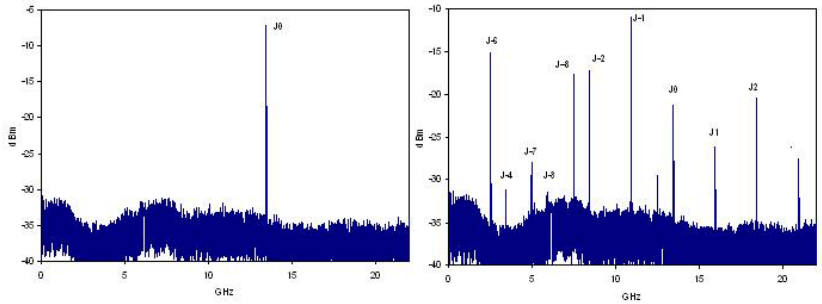

Figure 3.12. Optical spectrum at the input (left) and output (right) of the wavelength shifter measured by means of an optical heterodination for high resolution, with a frequency bandwidth of 22 GHz and an intermediate frequency of 13.5 GHz.

ratio (OSRR) of around 18-19dB the penalty is reduced in about 7-8dB, without filtering.

BER measurements were performed in the up-stream transmission for the single-fibre bidirectional link with that pseudo-reflective ONU, for colourless WDM-capable operation. The experimental set-up for BER measurements is basically the same shown in Figure 3.11, with added polarization controllers and monitors. At the OLT, the transmitted power is 0dBm. The reception branch is composed of a variable attenuator, a 95/5 coupler to monitor the received optical Signal-to-RB Ratio (OSRR), an Erbium Doped Fibre Amplifier (EDFA), an APD photo-receiver and the BER analyzer; an optical circulator separates both branches (isolation is 65 dB). The link consists of 25 Km of SMF, much longer than the RB effective length; the received RB optical power at OLT is -35.5 dBm. The ONU is the loop-based structure placed between two ports of an optical circulator, after an EDFA amplifier and the described dual-arm MZM. The upstream data is generated by applying digital signal at 1.25 Gbps with a PRBS of 2^{11}-1 to the zero chirp MZ modulator. A variable attenuator is also placed into the ONU.

The measurement aims at obtaining the system tolerance against the RB noise. In order to reproduce a scenario where the RB is dominant over the other noise sources (thermal and ASE noise), we fix the input power to the OLT-RX (EDFA included) to a constant value, well over its sensitivity (-34 dBm). For this, we use the two variable attenuators. The result in terms of BER as a function of the OLT input power (which is proportional to the OSRR, except in back-to-back) is represented in Figure 3.13. It can be seen that when the 25 km of fibre is added, the sensitivity is worsened in 14.5 dB, to -20 dBm, because of the dominating RB interference; the signal-to-RB ratio (OSRR) is of 20 dB at BER of $10^{-9.}$ Then, when the dual-arm MZM is switched on, the BER is highly improved. For fs equal to 2.5 GHz, the sensitivity improves in 7 dB, to -27 dBm, with an OSRR of only 13dB. No error floor was observed.

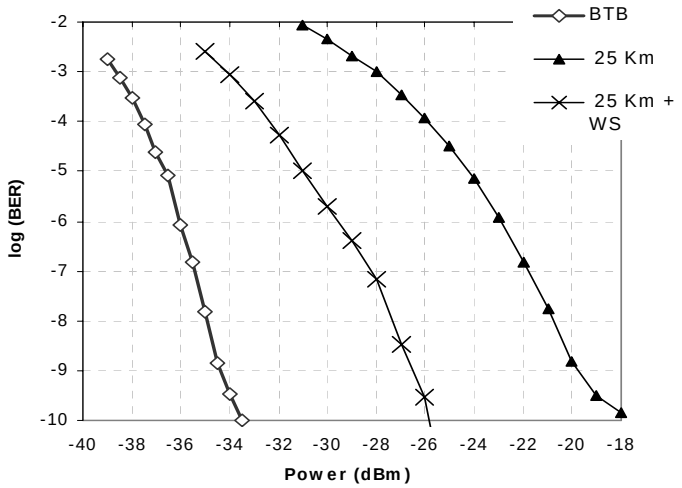

Figure 3.13. Bit error ratio, with respect to received power, for the cases of back to back, 25 Km of single mode standard optical fibre without wavelength shifting and 25 Km of single mode standard optical fibre by applying wavelength shifting.

3.3.1.3. Three-branches

The only reference found which uses 3 branches to perform optical frequency translation is in [Lotspeich1986]. It was achieved utilizing the method of rotating electric field in a channel waveguide by the use of three coplanar parallel channel strip surface electrodes.

Here, using a 3-arm based structure and following the study of the previous subchapter, the requirements for a spurious free wavelength shifter are simpler. The idea is to create a OSSB with two arms, and then use an extra third arm to cancel the carrier by choosing, in a proper way, its relative intensity and optical phase. The modulation index in this case has to be small to maintain negligible second and higher harmonics levels.

Considering that the light is divided in 3 beams with intensity relative levels: $1/(2+\sqrt{2})$, $1/(2+\sqrt{2})$ and $\sqrt{2}/(2+\sqrt{2})$, the two first will be used to create the OSSB. Then, a sinusoidal signal is applied with an electrical phase difference of 90º between them and also an optical difference of 90º between the two arms. The third arm is not modulated and it only consists of a phase delay of 225º. A schematic of the proposed device can be seen in Figure 3.14.

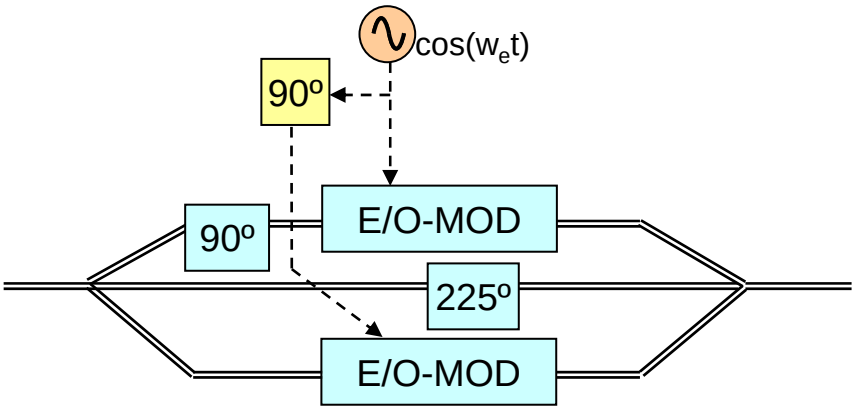

Figure 3.14 Three arm-based wavelength shifter

3.3.1.3.1. AM based modulators

Considering the case where the e/o modulators modify the amplitude and not the phase, and by using the characteristics defined before, the optical field at its output is:

$$E(t)=\frac{1}{\sqrt{2+\sqrt{2}}}\left[\frac{1}{\sqrt{2+\sqrt{2}}}e_o e^{j\omega_o t}e^{j\pi/2}\left(1+m\cdot\cos\omega t\right)^{1/2}\right]$$
$$+\frac{1}{\sqrt{2+\sqrt{2}}}\left[\frac{1}{\sqrt{2+\sqrt{2}}}e_o e^{j\omega_o t}\left(1+m\cdot\cos\omega\left(t+\frac{\pi}{2\omega}\right)\right)^{1/2}\right] \qquad (3.21)$$
$$+\frac{\sqrt[4]{2}}{\sqrt{2+\sqrt{2}}}\left[\frac{\sqrt[4]{2}}{\sqrt{2+\sqrt{2}}}e_o e^{j\omega_o t}e^{j5\pi/4}\right]$$

Assuming that the index modulation is small, the previous expression can be simplified as:

$$E(t)=e_o e^{j\omega_o t}\left\{\frac{1}{\sqrt{2+\sqrt{2}}}\left[\frac{1}{\sqrt{2+\sqrt{2}}}e^{j\pi/2}\left(1+\frac{1}{2}m\cdot\cos\omega t\right)\right]\right.$$
$$\left.+\frac{1}{\sqrt{2+\sqrt{2}}}\left[\frac{1}{\sqrt{2+\sqrt{2}}}\left(1+\frac{1}{2}m\cdot\cos(\omega t+\pi/2)\right)\right]+\frac{\sqrt[4]{2}}{\sqrt{2+\sqrt{2}}}\left[\frac{\sqrt[4]{2}}{\sqrt{2+\sqrt{2}}}e^{j5\pi/4}\right]\right\} \qquad (3.22)$$

Developing the previous expression, it can be obtained:

$$E(t)=e_o e^{j\omega_o t}\left\{\frac{2}{2+\sqrt{2}}\left[j\frac{1}{4}m\right]e^{j\omega t}+0\cdot e^{-j\omega t}+0\cdot e^{0\cdot\omega t}\right\} \qquad (3.23)$$

As it can be observed, the complete cancellation of the carrier is produced, together with the OSSB.

The device defined and mathematically evaluated before can be integrated and in fact an implementation of it has been used in [Doerr07] to achieve a DQPSK Modulator capable to be used at 80Gb/s. It can be seen in Figure 3.15. According to [Doerr07] the device is around only 160μm long.

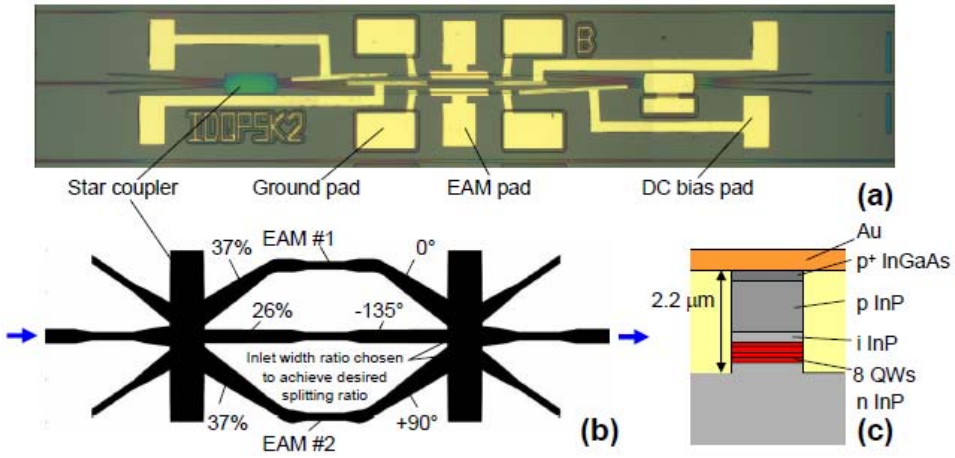

Figure 3.15. Device used in [Doerr07] equivalent to the required 3-arm modulator capable to generate WS

3.3.1.3.2. PM based modulators

In the case of using phase modulators (PM) instead of amplitude modulators (AM), an equivalent wavelength shifter solution can be obtained. Here the beam is divided into three with the following relative intensities: ¼, ¼ and ½. As with the case of AM-based device, the two arms with equal intensities are modulated with an electrical phase difference of 90º and an optical phase difference of also 90º to get OSSB, the third arm is used for cancelling the carrier and needs to have a phase delay of 225º.

Mathematically, it can be modelled as follows:

$$E(t)=e_o e^{j\omega_o t}\left\{\frac{1}{2}e^{j\beta\cdot\cos\omega t}e^{j\theta_1}+\frac{1}{2}e^{j\beta\cdot\cos\omega(t+\frac{\pi}{2\omega})}e^{j\theta_2}+\frac{1}{\sqrt{2}}e^{j\phi}\right\} \quad (3.24)$$

If modulation is small, the previous expression can be approximated as:

$$\begin{aligned}E(t)=e_o e^{j\omega_o t}\left\{\tfrac{1}{2}\left[j^{-1}J_{-1}(\beta)e^{-j\omega t}+J_0(\beta)+jJ_1(\beta)e^{j\omega t}\right]e^{j\phi_1}\right.\\ \left.+\tfrac{1}{2}\left[j^{-1}J_{-1}(\beta)e^{-j\omega t-j\frac{\pi}{2}}+J_0(\beta)+jJ_1(\beta)e^{j\omega t+j\frac{\pi}{2}}\right]e^{j\phi_2}+\frac{1}{\sqrt{2}}e^{j\phi_3}\right\}\end{aligned} \quad (3.25)$$

Then,

$$\begin{aligned}E(t)=e_o e^{j\omega_o t}\left\{\tfrac{1}{2}e^{-j\omega t}jJ_1(\beta)\left[e^{j\phi_1}-je^{j\phi_2}\right]+\tfrac{1}{2}e^{j\omega t}jJ_1(\beta)\left[e^{j\phi_1}+je^{j\phi_2}\right]\right.\\ \left.+e^{j0\cdot t}\left[\tfrac{1}{2}J_0(\beta)\left(e^{j\phi_1}+e^{j\phi_2}\right)+\tfrac{1}{\sqrt{2}}e^{j\phi}\right]\right\}\end{aligned} \quad (3.26)$$

If $\phi_1 = \phi_2 + \pi/2$. For example: $\phi_1 = \pi/2$ y $\phi_2 = 0$ then OSSB is obtained:

$$E(t)=e_o e^{j\omega_o t}\left\{\tfrac{1}{2}e^{-j\omega t}0-e^{j\omega t}J_1(m)+e^{j0\cdot t}\left[\tfrac{1}{2}J_0(m)(j+1)+\tfrac{1}{\sqrt{2}}e^{j\phi}\right]\right\} \quad (3.27)$$

In order to have also CS, then the phase ϕ of the non-modulated arm has to be 225º ($5\pi/4$) and it has to present a coupling factor of $J_0^2(m)/2$.

3.3.1.4. Four-branches

In [Izutsu81] a 4-arm based modulator was presented, together with the first demonstration of optical frequency shifting, which has been carried out using an integrated light SSB modulator of Ti-diffused $LiNbO_3$ optical waveguide.

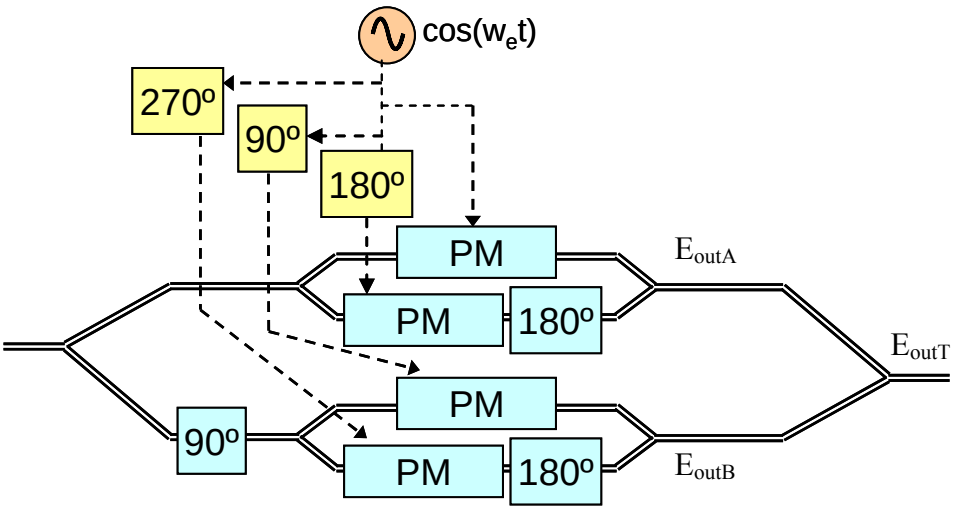

Figure 3.16 Module capable of performing WS in 4 –arm based modulator

According to the Figure 3.16, the optical field expressions for the output of each pair of waveguides (out_A and out_B) and the total output out_T are defined below:

$$E_{outA} = E_{in} A_c \sum_{n=-\infty}^{\infty} J_n(\beta) \cdot \left[\cos(\omega_0 t + n\omega_e t) + \cos(\omega_0 t + \pi + n\omega_e t + n\pi)\right] \quad (3.28)$$

$$E_{outB} = E_{in} A_c \sum_{n=-\infty}^{\infty} J_n(\beta) \cdot \left[\cos(\omega_0 t + n\omega_e t + n\frac{\pi}{2} + \frac{\pi}{2}) + \cos(\omega_0 t + n\omega_e t + n\frac{3\pi}{2} + \frac{\pi}{2} + \pi)\right] \quad (3.29)$$

$$E_{outT} = E_{outA} + E_{outB} \quad (3.30)$$

For low values of beta, the components of higher other than 3 are negligible; furthermore, that modes can be filtered out easily in most of the cases. Expanding the term of expressions 3.28 and 3.29, between 3 and -3 the only remaining terms are:

$$E_{outT} = E_{in} A_c \begin{Bmatrix} 4J_{-1}(\beta)\cos((\omega_0 - \omega_e)t) \\ +2J_3(\beta)\cos((\omega_0 + 3\omega_e)t) \end{Bmatrix} \quad (3.31)$$

As it can be seen, the only spurious able to be generated is the 3rd harmonic which is farther than the sideband of the transmitted signal.

In [Shimotsu01], this 4-port modulator was used and adjusted to perform SSB+CS, demonstrating a 10-GHz frequency shifter, where the only generated spurious was the third order harmonic of the expression 3.31, with a level 20dB lower than the desired frequency.

Very recently, and following our investigations, experiments using an electro-optic modulator to combat RB have been published, using a commercial dual-parallel MZM [Wang10]. In these modulators, the electrical phase difference of 180º between the 1st and 2nd arm and between the 3rd and the 4th, is obtained by using a push-pull configuration, to create electric fields of opposite directions in the upper and lower arm waveguides in each pair, such that they undergo an equal but opposite phase change [Alferness82]. Then, a 90º splitter between the first group of 2 arms and the second is the only required electrical phase shifter, like it can be seen in Figure 3.17

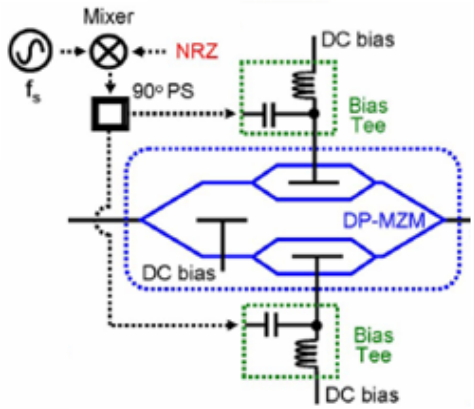

Figure 3.17 Dual drive dual arm MZM to perform SC-OSSB

3.3.2. RSOA-WS

In this subchapter, an RSOA is used to perform wavelength shifting by introducing an electrical square signal with low duty cycle. It constitutes also a new method to obtain a sawtooth signal at GHz, although in the optical domain.

Experimental validation of the increased tolerance to the RB crosstalk is introduced, while maintaining the colourlessness of the network, using an electro-absorption modulator (EAM) plus RSOA configuration. An improvement of around 5dB is obtained when the modulation is applied to the RSOA.

As is has been explained in previous subchapters (3.3.1), in previous work, the optical carrier frequency translation can be obtained by introducing the sawtooth signal in an e/o phase modulator [Powerezhsky05] or by adding a link of highly non linear electrical transmission line [Johnson 2010]. In this experiment, the own phase modulation created by the RSOA's transient chirp produces the translation.

The input signal for the RSOA is generated with a pattern generator with the word "10001000" at a bit rate of 10Gb/s, and after it is amplified by a RF electrical amplifier whose bandwidth (BW) is 10GHz. The optical input power into the RSOA has to be high enough to enter in a partial saturation. The best results have been obtained with an optical power bigger than -10dBm. The RSOA's e/o BW is 1GHz. Figure 3.18 shows the optical output signal in time domain and Figure 3.19 presents a comparative of the spectrum with and without applying the modulation to the RSOA, measured with an Optical Spectrum Analyzer (OSA) with 0.01nm resolution. The wavelength shifting can be observed, with around 8 dB of carrier suppression, but also an increment in its linewidth.

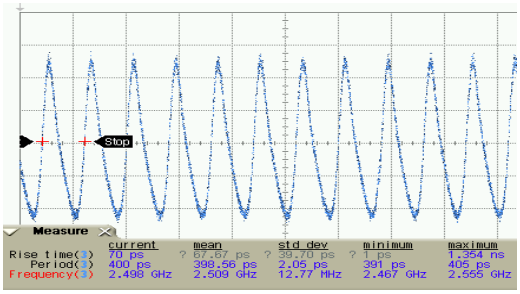

Figure 3.18: RSOA's output signal when the input is a square wave low duty cycle at 10 Gb/s

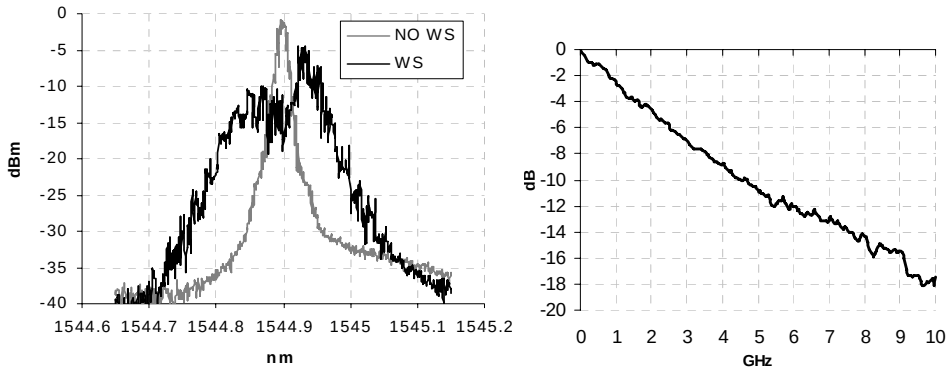

Figure 3.19: a) Spectrum at the RSOA output with and w/o the electrical modulation b) RSOA e/o BW

Experimental set up

In order to demonstrate the concept, and separate the different effects contribution, the ONU consists of several elements that are not optimized for cost efficiency, thus using for example, a RSOA plus an EAM instead of an integrated REAM-SOA chip. The set up is presented in Figure 3.20. A CW signal at 1535nm is introduced from the OLT. Between the OLT and the ONU there is a bidirectional uncompensated link consisted of standard SMF-28 fibre. The laser optical power is fixed to 3dBm to avoid non linear effects in the fibre. At the ONU the CW signal arrives first to the RSOA. The electrical low duty cycle square signal explained in last section, together with a DC bias of 130 mA is applied through a bias-T into the RSOA. The optical sawtooth signal generated by the RSOA enters into the EAM, which is used to modulate the upstream data.

The utilized EAM presents around 15 dB of insertion loss. Its return loss is around -27dB, for this reason, in order to separate the effects of reflections and RB, it has been isolated from RSOA by using circulators and angled connectors.

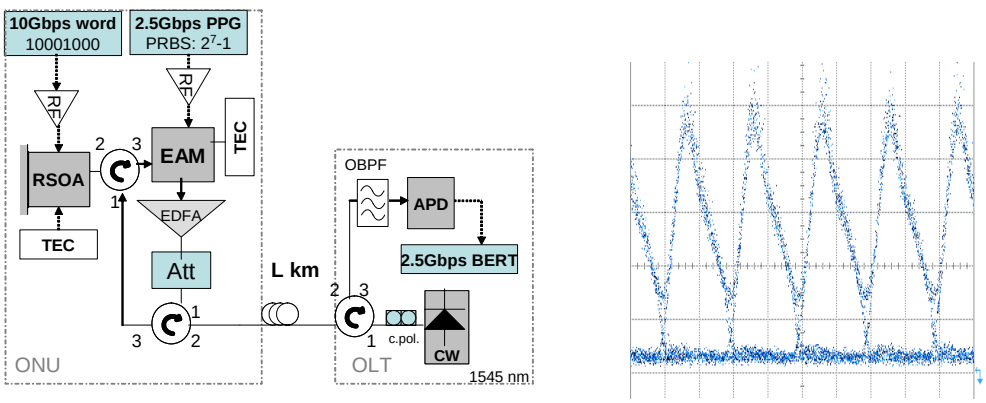

Figure 3.20. Set up (left) and EAM's output (right) after PRBS of EAM and RSOA synchronization

A 2.5Gbps NRZ data stream with PRBS of 2^7-1 is introduced into the EAM modulator. This data will be mixed with the optical signal coming from the RSOA.

In order to create the WS, the input current of the RSOA has to allow a signal with high extinction ratio. This can be a problem for the EAM data modulation because the sawtooth signal can appear as noise in the ones, remaining very little eye opening for the data. To overcome this trade-off between WS quality and ER available for the data, the solution is to synchronize both PRBS, as it is presented in Figure 3.19 right. An EDFA has been introduced in the ONU in order to take complete BER curves for all the cases.

When the modulation in the RSOA is not used, the current of EAM and RSOA have been optimized again. At the OLT, the receiver consist of an optical band pass filter TB9 with a BW of 0.22nm and an APD whose BW is 10GHz.

Experimental Results

The system performance has been evaluated for back to back (BTB), 10.3km and 26.3 km in terms of bit error ratio (BER) versus optical power in the port 3 of the OLT circulator. As the power is changed in the ONU, this received optical power will be directly related with the optical signal to RB crosstalk ratio (OSRR). The measured optical power in that point (port 3 OLT circulator) when the fibre is not connected to the ONU is directly the RB power (plus the circulator losses).

The first step, then, was to identify the values of RB for the fibre spools that were going to be used. It is -29.1dBm for the fibre of length equal to 26.3 km and -30.22dBm for the one of 10.3 km.

The BER curves, shown in Figure 3.20, compare the performance of the system for each

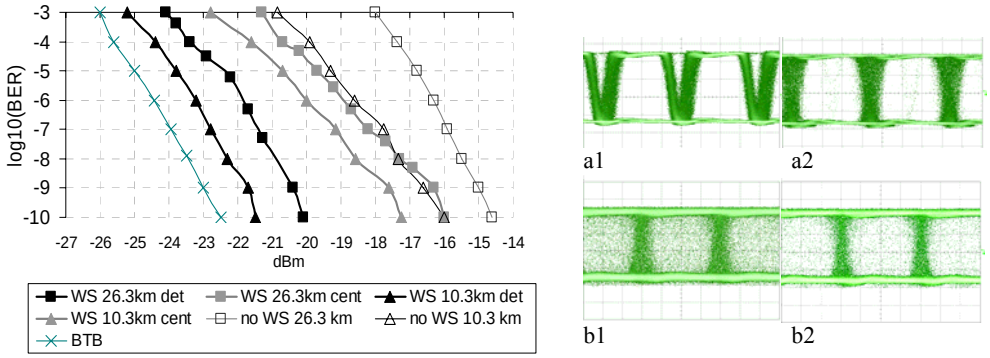

Figure 3.20: BER results (left) and Eye diagrams for 26.3km after APD with a) and without b) WS, with the filter detuned (1) and centered (2) for the same optical power (-20dBm) (right).

distance, taking into account 3 cases: no WS, WS with the filter of the OLT centred in the point of maximum transmission, and WS with such optical filter detuned around + 0.2nm. Detuning the filter without applying the WS, does not produce any improvement because the upstream signal is at the same wavelength than the RB.

As expected, the curves for the 10.3 km spool require less optical power than the ones of 26.3km to achieve low BER due to its smaller RB contribution. The 1.12dB of difference is translated into around 1.5dB of penalty for the fibre of 26.3 km for BER equal to 10-9 if no WS is applied, while it is around 1.2dB for the WS cases.

Without doing WS, the penalty due to RB effects is 8 dB for 26.3 km for a BER of 10-9 and around 6.5dB for 10.3 km, which is translated into a requirement of OSRR of 14.1dB and 13.7dB respectively.

The created WS allows reducing the penalty due to RB by itself, although the big improvement comes when the OLT optical filter filters out part of the RB component. In real networks this could be performed using the periodicity of an array wave grating (AWG) where all the upstream wavelengths come slightly detuned from the channel maximum transmission point.

With the filter in its central position, the system improves around 1.3dB for 26.3km and 1 dB for 10.3 km, thus requiring an OSRR of 12.8dB and 12.7dB respectively. With the filter detuned around 0.2nm, the WS is able to require 5.3dB and 5.1dB less power for 26.3km and 10.3 km to achieve a BER of 10^{-9} compared with the case of no WS. It means an OSRR of only 8.8dB and 8.6dB for 26.3km and 10.3 km respectively.

The electrical eye diagrams after APD receiver, for a length of 26.3 km and an optical power of -20dB, are presented in Figure 3.20 right. The eyes on the left side have been taken with the filter in the central position and the ones on the right for the filter detuned 0.2nm. In the upper ones the WS was activated and the bottom ones are for the no WS case. In the detuned case with WS, it can be observed that although the crossing point is not centred due to the sawtooth signal shape of the transmitter, the eye is open and clear, while if the filter is centred some spots appear in the eye. When the WS is not used, the crosstalk due to RB is too big and the eye is filled with spots.

3.3.3. WS based on Brillouin Effect

Another way to generate a WS with displacement lower than the AWG channel range (50 GHz-100 GHz) can be by stimulating the generation of a Brillouin effect, in a fibre or other Brillouin sensitive media. Then, the Brillouin-effect signal can be modulated to produce a second optical signal having a second carrier wavelength.

The Brillouin effect signal typically propagates in an opposing direction to the propagation of the stimulating optical signal at a wavelength distance of approximately 10-14 GHz of the carrier frequency of the signal used to stimulate the Brillouin. This process is widely colourless. As the carrier wavelength of the stimulating optical signal varies, so does the carrier wavelength of the resulting Brillouin-effect signal; however, the amount of displacement may vary slightly with wavelength.

The input power required to produce a Brillouin effect signal as strong as the input signal is referred to as the spontaneous Brilloun scattering (SBS) threshold. If the input signal is modulated, the SBS threshold is dependent upon the characteristics of the Brillouin media as well as the input signal.

Although scattering is present to varying degrees in standard optical fibres, an optical fibre with an SBS threshold lower than that of standard single mode fibre (SSMF) may be selected. This permits a reduction in the length of the optical fibre otherwise required to obtain a suitable Brillouin effect signal from the same input power. Further reductions in the length of the fibre require increases in the power of the input optical signal in order to maintain a suitable Brillouin effect signal.

We have started to work with this idea, which has been patented [BrillouinWS], however we have not performed measurements yet.

3.4. Conclusions of Chapter 3

Signals propagating in opposite directions at the same wavelength suffer impairment due to Rayleigh Backscattering, significantly reducing the receiver sensitivity.

Several RB mitigation approaches improve the performance by broadening the signal which creates a penalty due to chromatic dispersion at higher frequencies or distances. Other techniques consist on complex modulations and consequent optical filtering. And there is a third group which performs high pass filtering at the ONU which not allows symmetrical IM/IM modulations. Another interesting option is frequency bias dithering but it suffers from reduced efficiency.

Means of wavelength shifting at the ONU can provide a solution because it is a wavelength agnostic and cost and spectrum efficient solution.

Different modules to perform wavelength shifting have been evaluated in terms of device and input electrical signal complexity and also regarding the shifting purity: spurious free dynamic range (SFDR). Different possibilities have been considered, and devices based in 1 to 4 arms have been analyzed.

The simplest devices based in 1 arm require a sawtooth driving signal. Generating sawtooth signals with enough amplitude to perform wavelength shifting at GHz is difficult. Moreover, with an ideal sawtooth signal and a single phase modulator, a BW of 7 times the shifting frequency is necessary to assure a SDFR higher than 20dB.

Solutions based in 2 and 3 arms have been proposed for the first time,

Regarding the 2-arm structures, it has been demonstrated that it is not possible with a two arm standard modulator to obtain a spurious free wavelength shifting (apart from using the sawtooth signal but it is redundant). There is no change in the operational parameters (phase or amplitude misalignments, modulation index, etc) or known electrical function capable of generating OSSB and CS at the same time without producing other components as well.

Novel approaches to achieve spurious free wavelength shifting for colourless ONUs by using a combination of amplitude and phase modulation have been mathematically modelled and simulated. The proposed structures are dual-arm based devices, where each arm is composed of

an IM followed by a PM and offers the possibility of shifting the incoming wavelength accordingly to the electrical signal frequency. Those systems have neither sophisticate signal waves requirements nor the complexity of the four-arm structures. They are not nowadays commercially available but are potentially easy to be integrated with InP. A suboptimal solution using a commercial MZM has been used to prove the concept, obtaining a 7 dB of sensitivity improvement due to the reduction in the Rayleigh Backscattering crosstalk between up- and down-stream signals.

The three-arm structure is basically a conventional dual arm MZM with an added third arm in parallel which only consists of an optical phase delay of 225º. It simply requires a sinusoidal electrical input and an electrical phase of 90º between the modulated arms.

A novel procedure to achieve an optical sawtooth signal at a bit rate of 2.5Gbps has been presented. It only requires a digital electrical signal consisting of a low duty cycle rectangular signal as an input for a RSOA with a BW of 1GHz. This produces a 2.5GHz shifting of a CW carrier because of phase modulation produced in the same RSOA due to its transient chirp. This effect can be used to partially mitigate the penalty of RB in PONs with ONUs presenting small amplification, like SOA-REAM configurations. An experiment has been performed taking an RSOA and an EAM for the proof-of-concept. More than 5 dB of improvement have been obtained with 26.3 Km, requiring less than 9 dB of OSRR to get a BER of 10^{-9}.

3.5. References of chapter 3

[Alferness82] R. C. Alferness, "Waveguide Electrooptic modulators" IEEE Transactions on microwave theory and Techniques, vol. MTT-30, no. 8, Aug. 1982

[Arellano09] C. Arellano et al., "Reflections and Multiple Rayleigh Backscattering in WDM Single-Fiber Loopback Access Networks" J. Lightw. Technol, vol. 27, no. 1, pp. 12-18, Jan. 2009

[Attygalle06] M. Attygalle, et al., "Ultra Dense WDM Passive Optical Network based on RSOAs Facilitated through a Simple and Stable Seeding Source", ECOC'2006, Cannes.

[Bjerkan96] L. Bjerkan, et al., "Measurement of Laser Parameters for Simulation of High-Speed Fiberoptic Systems" J of Lightwave Technology, vol 14, no. 5, 839-850, 1996

[BrillouinWS] "Optical Network Element with Brillouin Effect Colorless Wavelength shift". Inventors: J. Lázaro, J. Prat, M. Omella. Docket No. 74035. P002101. USA,

[Chow07] C. W. Chow et al. "Rayleigh Noise Reduction in 10-Gb/s DWDM-PONs by Wavelength Detuning and Phase –Modulation –Induced Spectral Broadening", Photonics Technol. Lett. pp. 423-425, March 2007

[Chow08] C.W. Chow et al. "Rayleigh noise mitigation in DWDM LR-PONs using carrier suppressed subcarrier-amplitude modulated phase shift keying", Optics Express, vol.16, no. 3 Jan 2008.

[Doerr07] C. R. Doerr, "Compact EAM-Based InP DQPSK Modulator", Photonics Technol. Lett. vol., no. pp. 1184-1186, Aug. 2007

[Farías05]D. A. Farías and J. N. Eckstein, "Dynamic electrooptic frequency shifter for pulsed light signals," IEEE J. Quantum Electron., vol. 41, no. 1, pp. 94–99, Jan. 2005.

[Fonseca06] D. Fonseca et at., "Optical Single-Sideband Transmitter for Various Electrical Signaling Formats" J. Lightw. Technol ., vol. 24, no. 5, pp. 2059-2069, May 2006

[Fujiwara06] M. Fujiwara et al., "Impact of Backreflection on Upstream Transmission in WDM Single-Fiber Loopback Access Networks" J. Lightw. Technol, vol. 24, no. 2, Feb 2006

[Gysel90] P. Gysel, R.K. Staubli, "Spectral properties of Rayleigh backscattered light from single-mode fibers caused by a modulated probe signal", J. Lightwave Techn., vol. 8, pp. 561-567, April 1990.

[Healey01] P. Healy, et al., "Spectral slicing WDM-PON using wavelength-seeded reflective SOAs" IEE Electron. Lett., vol. 37, no. 19, pp1181-1182, 2001.

[Henry82] C. H. Henry, "Theory of the linewidth in Semiconductor Lasers", IEEE J. Quantum Electronics, vol.QE-18, no.2, February 1982.

[Izutsu81] M. Izutsu et al. "Integrated Optical SSB Modulator/ Frequency Shifter" J. Quantum Electr., vol. QE-17, no. 11, Nov. 1981

[Jang04] W.-S. Jang, et al. "Suppression of Rayleigh backscattering in a bidirectional WDM optical link using clipped direct modulation" IEE Proc.-Optoelectron., Vol. 151, No. 4, Aug. 2004

[Johnson 2010] D. M. S. Johnson et al., "Broadband optical serrodyne frequency shifting", Optics Letters, vol. 35, no. 5, pp. 745-747, March 2010.

[Kandikar90] M. Kandikar, I. Jacobs, "Analysis of Quantized Feedback Low-Frequency Restoration in Digital Regenerators", IEEE Trans. on Com., vol. 38, no. 8, 1990.

[Katagiri99] Y. Katagiri 'Intensity stabilisation of spectrum-sliced Gaussian radiation based on amplitude squeezing using semiconductor optical amplifiers with gain saturation', Electron. Lett., 1999, 35, (16), pp. 1362-1364

[Lazaro07] J. A. Lázaro et al. "Rayleigh scattering reduction by means of optical frequency dithering in passive optical networks with remotely seeded ONUs" IEEE Photonics Technol. Lett., vol. 19, no. 2, Jan. 2007.

[Lee07] Y. J. Lee, et al., "Reflection Tolerance of RSOA-based WDM PON," Optoelectronics and Communications Conference 2007, paper 11A1-4, Yokohama, Japan, July 2007.

[Lin08] H. Lin et al., "WDM-PON Systems Using Cross-Remodulation to Double Network Capacity with Reduced Rayleigh Scattering Effects" in proc OFC 2008 paper OTuH6.

[Lotspeich86] J. F. Lotspeich, "Improved Electrode Geometry for Electrooptic Frequency Translation in a Channel Waveguide", J. Lightw. Technol., vol. LT-4, no. 5, May 1986

[Omella_10A] M. Omella, et al., "RSOA as a Sawtooth Generator for Rayleigh Backscattering Effect Mitigation" accepted to ECOC'10, in Torino, 19-24 Sept 2010

[Omella_ws09] M.Omella et al. "Driving Requirements for Wavelength Shifting in Colorless ONU With Dual-Arm Modulator", J. Lightw. Technol, vol. 27, no. 17, pp. 3912-3918, Sept. 2009

[Oskar96] M. Oskar van Deventer, "Fundamentals of Bidirectional Transmission over a Single Optical Fibre". Boston, MA: Kluwer Academic, 1996.

[Park07] C. S. Park et al., "Photonic Frequency Upconversion Based on Stimulated Brillouin Scattering", Photonics Technol. Lett., vol. 19, no. 10, pp. 777-779, May 2007

[Parmigini08] F. Parmigiani et al., " Efficient Wavelength Conversion Using Triangular Pulses Generated Using a SuperStructured Fiber Bragg Gratting" Proc. OFC'08, paper OMP3

[Peters65] C. J. Peters, "Optical Frequency Translator Using Two Phase Modulators in Tandem", Applied Optics, vol. 4, no.7 July 1965.

[Poberezhskiy05] I Y. Poberezhskiy, et al. "Serrodyne Frequency Translation of Continuous Optical Signals Using Ultrawide-band Electrical Sawtooth Waveforms" IEEE J. Quantum Electr., vol. 41, no. 12, Dec. 2005 pp.1533-1539

[Polo08] V.Polo et al. "Reduction of Rayleigh Backscattering an Reflection Effects in WDM-PONs by Optical Frequency Dithering" in proc. ECOC 2008 Brussels (Belgium) paper P.4.21

[Prat05] J. Prat, et al., "Full-duplex single fiber transmission using FSK downstream and IM remote upstream modulations for fiber-to-the-home," IEEE Photon. Technol. Lett., vol. 17, no. 1, pp. 702-704, Jan. 2005.

[Prat06A] J. Prat, et al., "Frequency-modulated Source Broadening to Reduce Rayleigh Backscattering in Bidirectional Centralized Light Source WDM-PON Access Networks", Proc. ECOC 2006 Cannes (France), We4.5.6, September 2006.

[Prat07A] J. Prat, M. Omella, V. Polo " Wavelength Shifting for Colorless ONU's in Single Fiber WDM PONs" Optical Fiber Communications Conference, OFC/NFOEC'07, Proceedings, OTuG6, Anaheim, USA, March 2007.

[Prat10] J. Prat, "Rayleigh Back-scattering reduction by means of Quantized Feedback Equalization in WDM-PONs" accepted for ECOC 2010.

[Presi10] M. Presi, et al., "Single Feeder Bidirectional WDM-PON with Enhanced Resilience to Rayleigh-Backscattering", OFC/NFOEC'2010, paper OThG2, San Diego.

[Rodwell94] M. J. W. Rodwell et al., "Active and nonlinear wave propagation devices in ultrafast electronics and optoelectronics" Proc. IEEE vol., 82, pp. 1037–1059, (1994).

[Schrenk_OFC10] B. Schrenk, et al. “Wavelength Conversion towards Rayleigh Backscattering Tolerant PONs via Four-Wave Mixing in SOA-Based ONUs”, OFC/NFOEC’2010, paper OThG4, San Diego.

[Seimetz04] M. Seimetz, “Bidirectional Transmission for Optical Access Networks and Conventional Techniques and Novel Alternatives”, Proc. NOC’04, pp.170-179, Eindhoven (NL), June 2004

[Talli08] G. Talli, et al., “Modeling of Modulation Formats for Interferometric Noise Mitigation”, J. Lightwave Tech., vol. 26, no. 17, 2008.

[Urban09] P.J. Urban et al., “Interferometric Crosstalk Reduction in an RSOA-Based WDM Passive Optical Network” J. Lightw. Technol, vol. 27, no. 22, pp. 4943-4953, Nov. 2009

[Wang10] C. H. Wang et al., “Rayleigh Noise Mitigation Using Single-Sideband Modulation Generated by a Dual-Parallel MZM for Carrier Distributed PON” IEEE Photon. Technol. Lett., vol. 22, no. 11, pp. 820-822, June 2010.

[Xu10] J. Xu, et al., “Optical Phase Remodulation for 10-Gb/s WDM-PON with Enhanced Tolerance to Rayleigh Noise”, OFC/NFOEC 2010, paper OThG3, San Diego.

4. RSOA-based ONUs

4.1. Introduction

The massive deployment of FTTH depends on cost aspects. Low cost ONUs and easy upgrading of the network are the key factors. Although a flexible solution would be the use of wavelength tuneable transceivers providing a large power budget, it appears today difficult to align the cost/consumption/control of WDM laser transmitters with the access terminal cost/consumption targets. Therefore, the colourless approach, consisting of wavelength agnostic Optical Network Units (ONU) and remote wavelength feeding, is a very attractive and realistic solution. This is due to its expected cost effectiveness. Firstly, all expensive wavelength complexity is put at the central office and is shared by the network. Secondly, a mass market for colourless ONU can be expected as each customer uses an identical terminal regardless the addressing wavelength.

The RSOA has been demonstrated to constitute an integrated low cost colourless solution because of its capability of amplification and remodulation.

First developed RSOAs presented very low bandwidth, high chirp and/or also high dependence with polarization. However, in the last years, these devices have improved and nowadays commercial RSOAs are used in 1.25 Gb/s upstream transmissions.

The evolution of RSOAs is also towards increasing its real colourless operation, decreasing the differences in performance from one selected wavelength to another in a high margin of wavelengths.

As it has been introduced in chapter 1, the new PON standards that have just been approved (XG-PON, 10G-EPON) propose the upgrading of the network towards symmetrical 10G/10G operation. However, RSOA's bandwidth and chirp still limit the performance at these bit rates.

Here, novel techniques have been studied and experimentally tested, capable of increasing the capacity of the RSOA, allowing its operation as a modulator up to 10Gb/s by using devices with around 1.5GHz of bandwidth and high chirp.

4.2. RSOA devices

A Semiconductor Optical Amplifier (SOA) is an optoelectronic device that under suitable operating conditions can amplify an input light signal. It is very similar to a laser, except it does not have the pair of reflecting facets, so it does not enter into lasing operation. A typical amplifier chip is 0.4 to 2 mm long. It has a central active gain region between two semiconductor layers of different compositions (a p-cladding layer and an n-cladding layer) all of which are epitaxially grown over a binary substrate. An electrical current is what produces the carrier inversion and amplification in the gain region by stimulated emission. A schematic of the device is shown in Figure 4.1.

When the device is driven by an electrical current, the electrons are excited in the active region. The photons travelling through the active region cause the electrons to lose part of their extra energy in the form of photons with the same wavelength an phase as the initial ones (stimulated emission) generating thus a coherent amplification of the incoming signal. Such an SOA structure is polarization sensitive, as the Transverse Electric (TE) mode gain is greater than the Transverse Magnetic (TM) mode gain. The polarization dependent gain effect can be reduced to an acceptable value of 0.5dB by designing the active waveguide nearly square or other techniques, having thus almost the same confinement factor for both TE and TM polarization states. [Doussiere94].

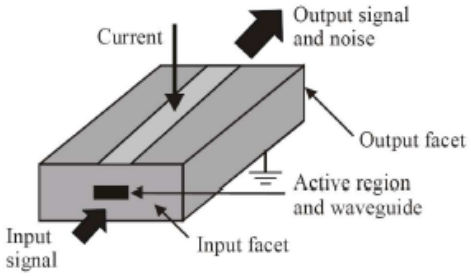

Figure 4.1. SOA chip structure

SOAs are compatible with monolithic integration (hence potential low cost) and offer wide range of applications. Together with the system function of amplification (booster, in-line or preamplifier), these devices present many functional applications due to their non-linearities, fast response and other intrinsic characteristics. For example, a SOA can work as: intensity and phase modulator, wavelength converter, optical switch, logic gate, dispersion compensator or phodetector.

A special type of SOA is the Reflective Semiconductor Optical Amplifier (RSOA). In this structure, one of the facets presents a reflectivity close to 100%. Thus, when the light enters into

the cavity, it is reflected towards the input port, as it can be seen in Figure 4.2. Despite a RSOA has only one optical port, both structures present similar behaviour in terms of gain, optical bandwidth, and noise. However the gain is double in the case of the RSOA because the signal passes twice through the active region. The RSOA is currently being the focus of thorough investigation as a single fibre electro-optic (e/o) modulator at the ONU premises, fact which has produced a higher development in terms of e/o bandwidth compared with SOAs, more focused in other applications.

Figure 4.2. SOA and RSOA comparison.

RSOA response depends on different parameters, like the incoming signal power and the bias current that is injected to the device. In most cases, also temperature is very critical and the RSOA must be connected to a temperature controller.

The bias current in a RSOA device affects its electro-optical BW, gain and also the ER of the generated signal. By increasing the current also the gain and BW enhance. However, the ER may be decreased. An example can be seen about the gain versus current and wavelength in Figure 4.3. In Figure 4.3 right, when the electrical current increases, the eye opens but the zeros move away from the ground level. In bidirectional (full-duplex remodulated) transmissions, as it will be seen in next sections, the bias point has to be carefully adjusted when the upstream bit rate is very high due to the trade-off between ER and BW. Three regions in the response of the RSOA can be defined regarding the operation point of the RSOA, depending on the chosen bias: the transparency threshold, the linear region and the saturation (see Figure 4.3 left).

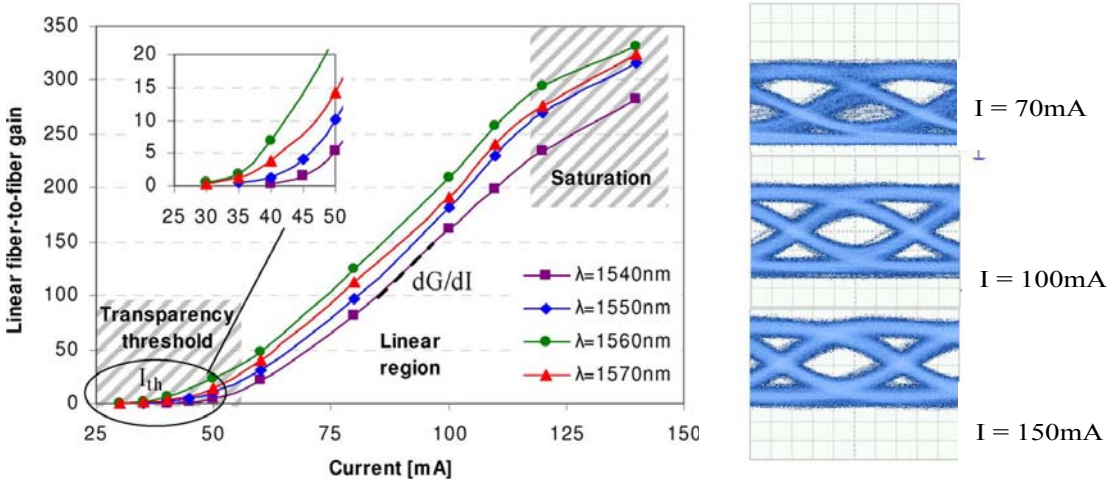

Figure 4.3. Electrical current effects in RSOA operation. Left: Different gain regions with respect current. Right: eye diagrams for different electrical currents.

Regarding the input optical power, the RSOA has also different performance zones, which are the linear and the saturation response regions. For low levels of optical power, the device performs linear amplification, but increasing the optical power derives into gain saturation. The linear region is preferred to use the RSOA as a modulator, as offers the highest extinction ratio. However, optical input also affects the e/o bandwidth and, in specific scenarios, slight saturation is required in order to achieve better performance. Other applications that require optical saturation are Phase Modulation [Lee04] and RSOA photodetection [Prat05]. Again, there is a trade off if the RSOA needs to be used as both, modulator and photodetector to achieve correct performance on both tasks. Also the SNR is different depending on the Optical input power because RSOA operated in gain saturation region can reduce the intensity noise of the optical signal.

Temperature in RSOA affects to the ASE spectrum, ER, noise factor (NF) and gain as it can be seen in Figure 4.4. These are measurements done in the lab with a commercial RSOA. As the temperature increases, the gain in the RSOA is reduced, its peak is shifted toward longer wavelengths and the spectrum is broadened. The optical gain drops with temperature quite similarly in the whole C-Band. Reducing the temperature the gain can be increased. The ER exhibits its maximum around 25ºC and drops when temperature moves away to the edges by both increasing and decreasing. That behavior is quite similarly in the whole C-Band.

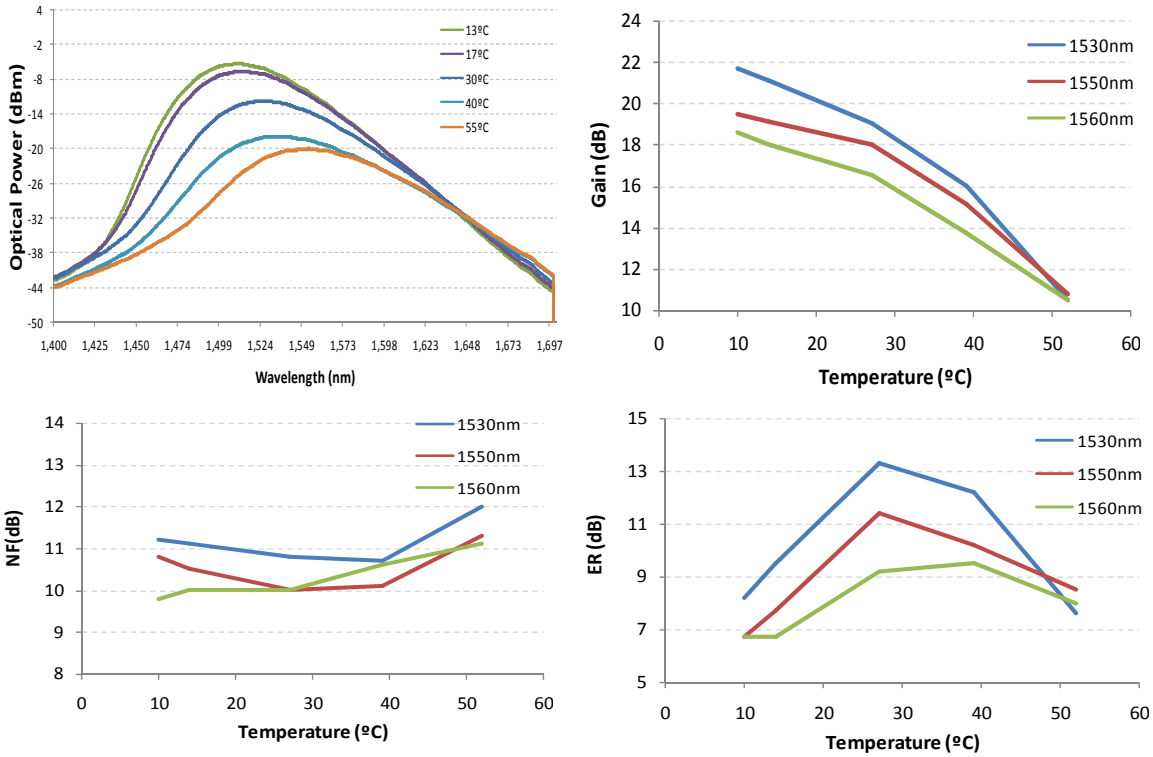

Figure 4.4. ASE spectrum, gain, noise factor (NF) and extinction ratio (ER) with respect to temperature.

4.3. 10G operation with low BW and high chirp RSOA devices

4.3.1. Introduction

When we started to work with the RSOAs in this thesis, to achieve 10 Gb/s transmission in real time and with low BER (10^{-9}) was a challenge.

Until then, we commonly used the RSOA at 1.25 Gb/s, and the maximum reported bit rate had been 5 Gb/s in [Chanclou07]. In [Brenot07] two electrodes based RSOA was proposed in order to increase the modulation bandwidth of the RSOA's from 2 to 6GHz and to reduce the chirp.

In [Omella08] we have applied the RSOA as a simple duobinary transmitter allowing 10G operation up to 10km (limited by the interaction of chirp and CD) and in [Papagiannakis08] a transmission of 85 km at a bit rate of 10Gb/s was achieved by applying detuned offset filtering, according to the RSOA chirp together with electronic equalization, and using a Decision-Feedback Feed Forward equalizer (DFE-FFE), methods that will be deeply explained in this chapter. The first symmetrical full duplex IM/IM 10G transmission with a RSOA at the ONU has also been reported [Omella09] by using the before mentioned techniques, presenting the design characteristics for a symmetrical 10 Gb/s full-duplex bidirectional transmission by using low-cost and low BW RSOAs (1.2 GHz) [Papagiannakis10].

Various sophisticated techniques have been proposed meanwhile, by other research groups, for single (i.e. non-duplex) upstream transmission at 10 Gb/s using RSOAs, like orthogonal frequency division multiplexing (OFDM), achieving a transmission distance of 20 km (at a Bit Error Ratio (BER) of 10^{-9}) [Duong08] or offline processing with the help of Decision Feedback Equalization (DFE) together with Forward Error Correction (FEC) codes [Cho08A], achieving a maximum transmission distance of 20 km at FEC limit.

Last RSOA sample modules in chip form present higher BW and lower roll-off, facts which have allowed to us the transmission at 10 Gb/s by simply applying a RC electronic pre-filter like in our experiments in [Bernhard10]

Several techniques are proposed in this thesis with the aim of enhancing the RSOA's e/o bandwidth to allow 10Gb/s upstream operation. The simplest, in the electrical domain, consist on the pre-emphasis of the upstream signal by means of an electronic circuit based in a capacitor

(C) and a resistor (R) to cut the low frequencies in order to flatten the e/o response. This solution, together with a full wave rectifier, has allowed performing duobinary modulation. However, the RSOA's chirp limited the performance. A more sophisticate technique has allowed 10G transmissions through long distances even performing full duplex 10G/10G remodulation: it consists on applying detuned optical filtering and DFE-FFE equalization at the OLT. An equivalent technique to the previous offset filtering has been found to be the phase adjustment at the OLT carried out by a programmable optical filter. Finally also MLSE has been introduced and tested comparing a conventional MLSE to a correlation sensitive MLSE.

4.3.2. RC filter based e/o bandwidth enhancement

Ideally, an electrical filter with a response inverse to the e/o RSOA's characteristics could expand the RSOA's BW as much as desired. However, besides the difficulty of implementation of this electronic circuit, this solution would introduce very high losses and it could even damage the device due to the high levels that would be necessary to have at the highest frequency components. A practical approximation however, can be to flatten the e/o response of the firsts 4-8 dB of attenuation with simple electronic circuits based in SMD RC cells. Here, the improvement depends on the original BW roll-off of the specific device.

RC filters have been used to increase the BW of RSOA's with original BW around 1.2 GHz to 2.5GHz (Figure 4.5 left) or for more sophisticates chips, to allow direct 7.5GHz as it can be seen in Figure 4.5 right

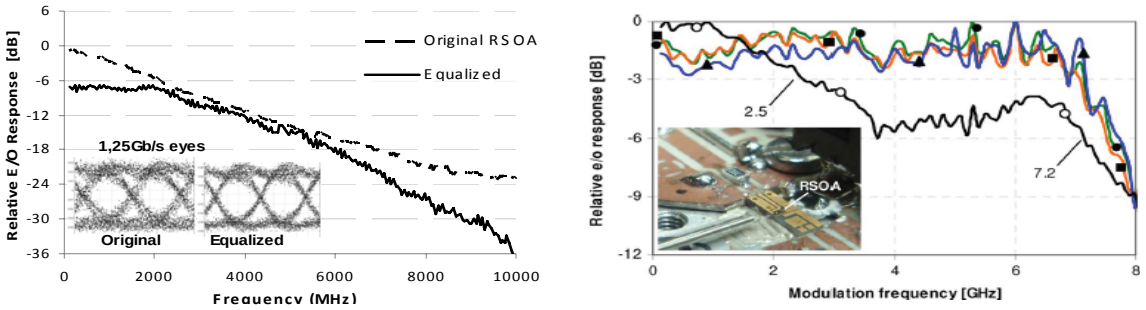

Figure 4.5 Original and RC equalized RSOAs

4.3.3. Special upstream modulations: Duobinary

Duobinary modulation has been experimentally demonstrated to be a simple coding method to increase the transmission distance in bandwidth and dispersion limited systems. It is a scheme for transmitting R bits/sec using around R/4 Hz of Bandwidth. The minimum bandwidth required for a transmitted pulse in order to not to have ISI is R/2. This result implies that duobinary pulses will have ISI. However this ISI is introduced in a controlled manner so that it can be subtracted out to recover the original values. The advantage of this system over simple NRZ is that allowing some ISI the transmitter pulse can be longer in time domain, and hence its spectrum becomes narrower in the frequency domain. With a narrower spectrum, the distortion effects of the channel are also fewer. Another advantage, important here because the bandwidth of the RSOA is limited, is that it requires less bandwidth for the transmitter source.

But the RSOA is too limited in bandwidth, even to act as a duobinary transmitter at 10 Gb/s, for this reason, its electro/optical bandwidth had to be enhanced. A passive microstrip RC pre-equalizer was optimized to combine the RSOA characteristics and the electrical filter producing a resulting electro-optic bandwidth adjusted to match the response of a 2.5GHz cut-off 4th order Bessel filter. That allowed the binary signal to be converted into duobinary three-level signal for transmission at 10 Gb/s. After reception, an electrical full duplex rectifier recovered the original 2-level input data. The implemented full-wave rectifier is based on a couple of balanced high frequency diodes, and a highly linear differential amplifier.

As it can be seen in figure 4.6 the recovered data is not exactly the same and additional decoding (differential) should be applied. In practice, however, a PRBS sequence differentially encoded is the same PRBS, only delayed, so it can be directly decoded and recognised by the BER tested in our experiments. The experimental set up is shown in figure 4.7.

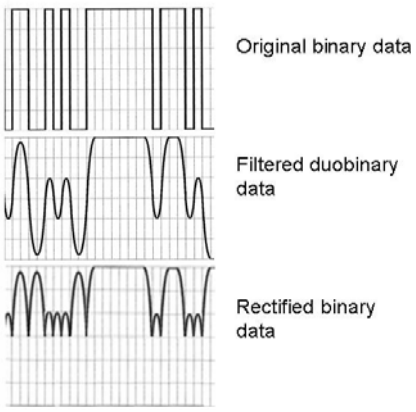

Figure 4.6. Details of the original binary data, the duobinary signal and the recovered after rectifier.

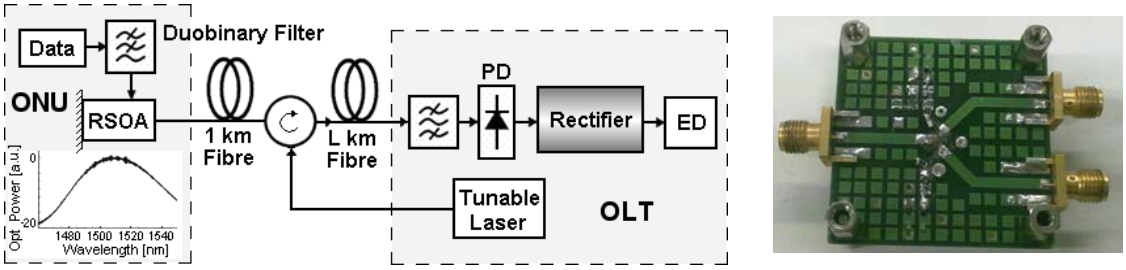

Figure 4.7 Duobinary system set up. Photograph of the rectifier, two small diodes are soldered, one in each spitted arms, in opposite directions.

Measurements have been done at different bit rates, comparing the case of the duobinary at 10 Gb/s with the binary operation at 5Gb/s, 2.5Gb/s and 1.25Gb/s. In back-to-back, using a variable attenuator at the RX input, the electrical equalizer penalizes the sensitivity with 2 dB for the 1.25Gb/s transmission relative to the original RSOA response, due to the amplitude reduction in the low frequencies once the bandwidth has been enhanced. The penalty for 2.5Gb/s is 3dB as it is expected because of doubling the bit rate, while it is up to 11dB for 5Gb/s. From these, 6dB are due to receiving 4 times the bit rate and the other 5dB because now the bandwidth starts to close the eye. At 10 Gb/s, the rectifier is inserted, and 16dB penalty is obtained for the duobinary signal (D+EQ in the legend). The duobinary's penalty is 9dB because of having 8 times the bit rate and 7dB because of the compression of the signal and rectifier process. No BER floor is found in any case. The summary of the measured bit error ratio (BER) from 1.25 Gb/s up to 10 Gb/s is presented in Figure 4.8.

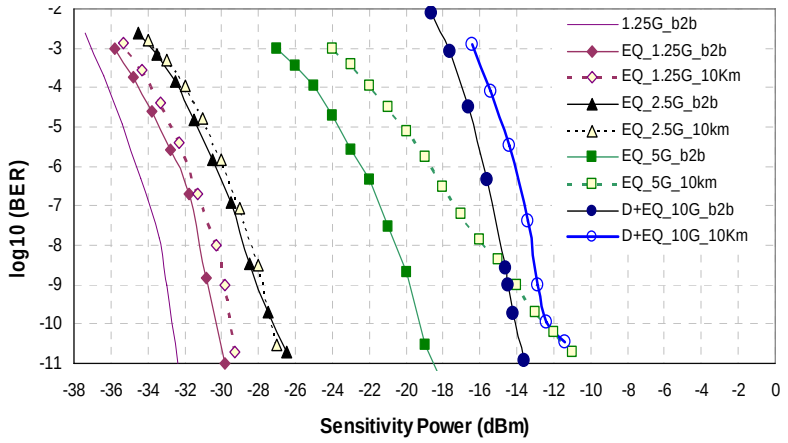

Figure 4.8 BER versus sensitivity power for different bit rates and distances

Figure 4.9 shows the sensitivity of the RSOA device as a function of the bit rate for several optical input power values of the RSOA. From the measured results we can conclude that the RSOA presents good performance at 1.25Gb/s and 2.5Gb/s even for the lower input power of -

20dBm, while it demands higher input power to transmit at 5Gb/s and even more (Pin = -10 dBm) to permit 10Gb/s transmission.

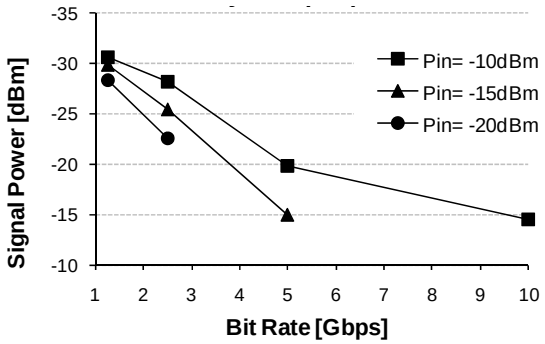

Figure 4.9 .Receiver sensitivity for different bit rates and RSOA's input power

The sensitivity of the RSOA device over the standardized bit rates is presented for several fibre links (see Figure4.10). We have achieved transmission up to the standard maximum of 20km at 2.5Gb/s. The 5Gb/s and the duobinary 10Gb/s transmission allow to achieve a few more than 10+1km with this set-up. This is due to the high chirp of our RSOA which in combination of the chromatic dispersion present in the fibre close fast the eye. The 3-level signal of the duobinary case is so highly degraded after more than 10 km that the rectifier is not able to recover the data.

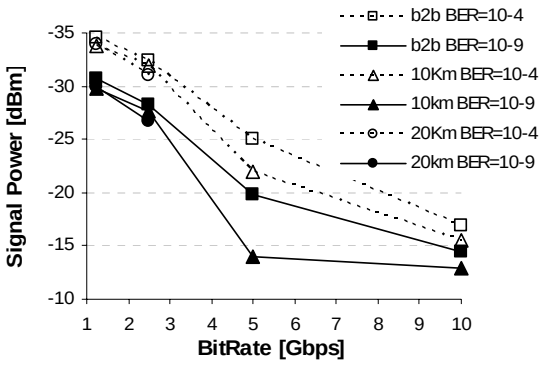

Figure 4.10. Distance sensitivity for different bit rates considering BER equal to 10-9 and 10-4

As a conclusion, duobinary modulation in the RSOAs constitutes an enabling technology for ultra-low cost 10Gb/s RSOA upstream transmission adding only few cheap electronic extra components; nowadays, chirp interaction with CD limits the maximum reach at 10Km.

4.3.4. RSOA offset filtering and DFE equalization

In this section, a technique which directly deals with the chirp is presented. The slope characteristics of a properly detuned optical filter can be used to take advantage of the RSOA chirp to increase its e/o bandwidth. The system is further improved using DFE-FFE equalization. The optimum design characteristics and the transmission performance limits of an intensity modulation full-duplex bidirectional transmission system at 10 Gb/s are also experimentally studied and presented for application in NG-WDM PON. The same RSOA as the used for the duobinary experiment has been utilized at the ONU. Its remodulation properties and performance are examined for both continuous wave (CW) and modulated downstream signal, stemming from the optical line terminal (OLT). The extinction ratio of the downstream signal and the driving operation point of the RSOA are examined experimentally in order to find the optimum conditions for the bidirectional transmission. Moreover, the impact of patterning effects in the performance of the system is evaluated. Finally, the additional performance improvement that is achieved with the use of DFE technique is shown in detail in the following sections.

4.3.4.1. General characteristics of the system

The experimental set-up is shown in Figure 4.11. The ONU is based on an RSOA transmitter fed by the downstream light. The gain peak of the RSOA is at 1510 nm. The upstream signal is introduced through a bias-T and a resistor-capacitor (RC) filter circuit, which in combination with the RSOA provides an enhancement of the effective BW from 1.2GHz to 2.3 GHz at the RSOA based ONU, when biased with 60 mA DC current and modulated with a current of ± 35 mA. The input power into the RSOA is adjusted to -10 dBm by making use of a variable optical attenuator. A chirp parameter of $\alpha = 9.8$ has been measured according to the methodology shown in [Devaux93]. At the OLT, a CW signal at 1532 nm is introduced into a Mach Zehnder modulator (MZM) where a 10 Gb/s non-return-to-zero (NRZ) downstream signal is applied with pseudorandom bit sequence (PRBS) of either 2^7-1 or 2^{31}-1. The impact of the pattern length in the overall system performance is analyzed later.

With respect to the transmission medium, the studies on bidirectional transmission consider only the fibre plant of (L1), whereas for the case of single upstream transmission an additional

unidirectional fibre (L2) was used. In both cases, the utilized fibre type is G.652 SMF-28™ and no optical dispersion compensation is employed in the link. The launched optical power at the OLT output is always fixed at 0 dBm in order to minimize the nonlinear impairment effects. The gain peak of the RSOA used in these experiments is at 1510 nm. However, this work focuses on C-band as required by new generation PON networks such as in SARDANA. Therefore in these experiments the operating wavelength is at 1532 nm, resulting in a limited gain of 10 dB in the RSOA. In this study, the most important parameters that were investigated further in order to find the optimum design rules for bidirectional transmission are the optical filter position at the OLT and the ER of the downstream signal (ER_d) in the full duplex experiments.

In both receivers (ONU and OLT) in the experiments, an optical signal-to-noise ratio (OSNR) emulator, consisting of a variable optical attenuator and an EDFA, was used to alter the OSNR. The signal is detected by a PIN receiver or an APD.

At the OLT, a JDSU-TB9 tuneable optical BPF, with 28 GHz BW at -3 dB and low group delay, was placed before the photodiode. After the detector at the OLT, integrated electronic dispersion compensation (EDC) circuit was used. The EDC circuit had an FFE part and a DFE which were independently controlled by 5 and 2 taps respectively. The values of the taps were adjusted through a controller and in terms of optimum BER for each of the measured cases.

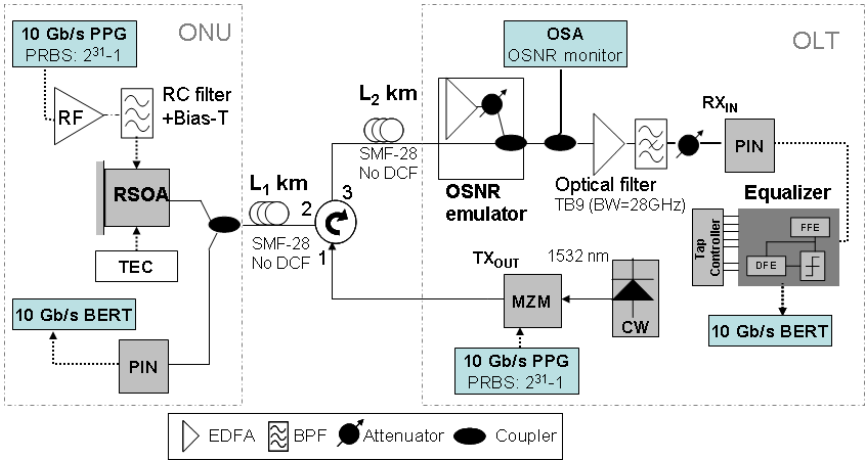

Figure 4.11. The general experimental set up used for the results obtained and discussed in section 3 for both cases of single (unidirectional) downstream transmission (examined over various lengths of L_2 fiber in section 3A) and bidirectional transmission (examined over various lengths of L_1 fiber in section 3B).

4.3.4.2. Offset filtering process

The filter position plays a key role in the detection because of its interaction with the transient chirp generated due to refractive index changes in the RSOA. This chirp effect produces a fast complementary phase modulation (PM) along with the intensity modulation (IM) when the electrical data current is applied. The optical filter detuning transforms the phase derivative (frequency) variations into amplitude variation, and the constructive addition of the IM and the transformed PM generated in the RSOA result in an increase in the bandwidth of the received data.

Blue shifted detuning is applied into a band-pass optical filter located at the output of a RSOA (in our case in the receiver part at the OLT) in order to decrease the time recovering from different intensity level transitions like it has been in some SOA based wavelength converters [Liu06] . This can be graphically seen in Figure 4.12, where the left down signal represent the bits limited in bandwidth,

- From high to low levels (pulse falling-edge), the RSOA presents a red wavelength shift because of chirp. As we want the signal level to go to the minimum possible one, then we want the maximum attenuation of the optical filter.

- From low to high levels (pulse rising-edge), the RSOA presents a blue wavelength shift because of chirp. As we want the signal level to go to the maximum possible one, then we want the minimum attenuation of the optical filter.

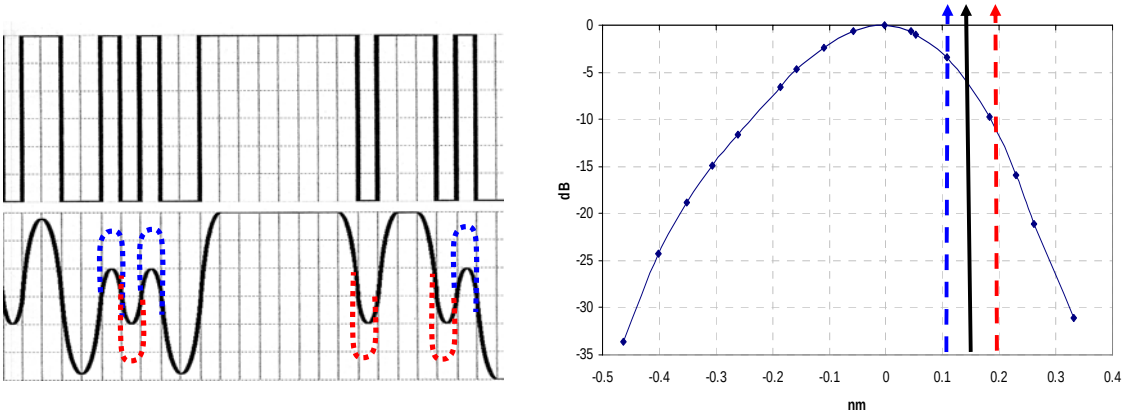

Figure 4.12. Original signal (left up), bandwidth limited signal with coloured filtering effects (left down) and detuned optical filtering right with red and blue walenght shifting due to RSOA transient chirp.

Mathematically, the response of the filter can be defined as:

$$|H(w)|^2 = a + b\Delta f(w) \qquad (4.1)$$

where a, b are the coefficients of attenuation and slope of the filter at the offset wavelength,

respectively. The chirp parameter is defined as in [Watanabe00]:

$$\alpha = 2I\frac{d\phi}{dI} \qquad (4.2)$$

where here I is the RSOA input current intensity and ϕ the phase of the output field. By applying the Fourier transform, the detuned bandpass optical filter transforms (around the offset operating point) the frequency variations (derivative of the phase of the RSOA output field) into intensity variations $P_{opt}(w)$, as:

$$P_{out}(w) = Pout_{RSOA}\left[a + b\frac{\alpha}{2}(jw)\right] \qquad (4.3)$$

The factor with *(jw)* in the second term means a high-pass contribution, coming from the transformation of the PM, created by the chirp of the RSOA, into IM, by using the slope of the filter, thus explaining the extension of the BW of the system. Using a network analyzer we have found that the effective received signal BW of the detected signal increases from 2.2 GHz to around 5 GHz, in back to back configuration. As a result of the interaction between the characteristics of the optical filter and the RSOA chirped signal, the eye reshapes.

4.3.4.3. RSOA driving for 10G operation and ER adjustment

The bias current in a RSOA device affects its electro-optical BW and also the ER of the generated signal as it has been explained in previous subchapters. For this reason, the optimum driving conditions of the utilized RSOA are different if the upstream signal is performed using a CW signal from the OLT, or if it is re-modulated from a downstream signal with limited ER.

By fixing the bias current (I_{bias}) at 70 mA, the RSOA presents a BW of 1.5 GHz. The use of RC filter increases the BW up to 2.5 GHz and after the detuned optical filter, the overall E/O response is around 5.5 GHz. In these conditions, the maximum available ER for the upstream signal is 4.2 dB. This is the best operating point for the RSOA, if the upstream signal is re-modulated from a CW signal coming from the OLT. However, the value of the extinction ratio is too small to have the possibility to re-modulate the signal from a previously modulated downstream transmission.

In order to perform full duplex bidirectional transmission, the I_{bias} has to be reduced to increase the ER up to a value which allows having both downstream and upstream transmission and still being able to detect the upstream signal at the OLT. Unfortunately, by decreasing the I_{bias}, the

BW of the RSOA also decreases. The I_{bias} of 60 mA has been found as a trade-off between ER and BW. The RSOA presents a BW of 1.2 GHz, whereas after the use of RC filter, it is about 2.2 GHz and after the detuned optical filter, it is 5 GHz approximately. However, in this case the ER is 6.2 dB providing a higher value than the case of only upstream transmission (4.2 dB). This operating point has been used for all the full duplex bidirectional experiments. In Figure 4.13, a comparison among the responses for the different cases is depicted in terms of S_{21} E/O BW.

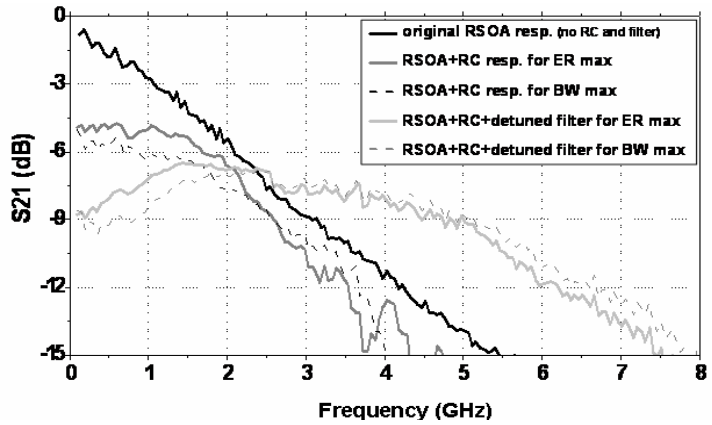

Figure 4.13. Comparison of e/o S21 i) the original RSOA response, ii) the combined RSOA and RC circuit response for max. BW and ER and iii) the combined RSOA, RC circuit detuned optical filter response for max. ER and BW.

Figure 4.14 presents the eye diagrams for the cases of a) single upstream signal (originating from the modulation of a CW signal in the RSOA) with the filter in its optimum detuned position, b) the same signal but with the filter in its central position (i.e. entered with respect to the frequency of the CW signal) and in c) the upstream transmission with the filter detuned and with the presence of a downstream signal whose ER_d is 3 dB. It is evident that the quality of the eye diagrams after bidirectional transmission is decreased with respect to the eye diagrams for only upstream transmission. However, despite the degraded performance, ($BER<5\cdot10^{-4}$) bidirectional transmission is still possible and can be further improved with the use of equalization, as it is studied in the next sections.

Finally, it is important to note that in both cases the optical power in the RSOA was fixed to -10dBm.

The gain in a SOA can be defined [Agrawal]:

$$G = \frac{G_0}{1 + \frac{Popt_{in}}{Popt_{sat}}} \qquad (4.4)$$

where G_0 is the maximum gain, $Popt_{sat}$ is the saturation power and $Popt_{in}$ is the input power to the RSOA. In our case $Popt_{sat}$ is -6dBm, so the gain is compressed in 1.28dB approximately.

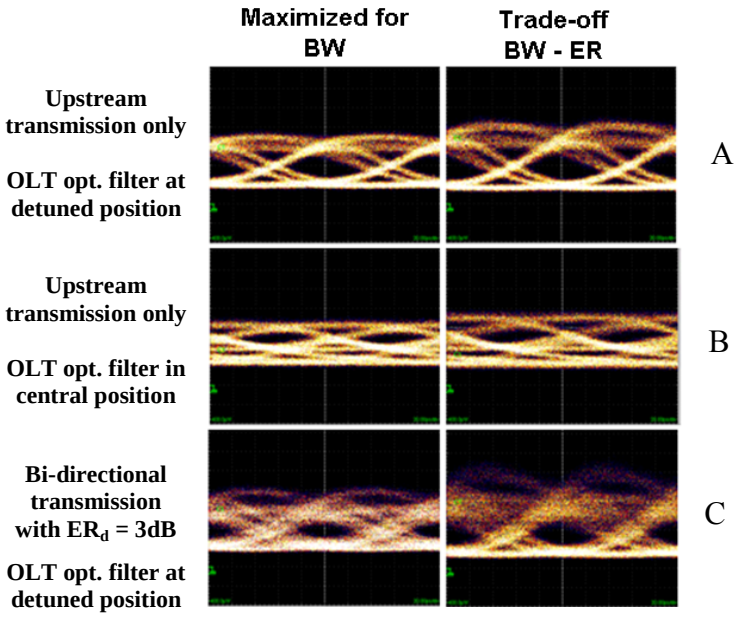

Figure 4.14. Optical eye diagrams of the detected signal at OLT in BTB. Without modulated downstream data and filter at optimum (detuned) A) and non-optimum (centered) B) position. Bidirectional transmission with the filter at optimum position C). The RSOA has been optimized for BW and ER as shown in the two columns respectively.

4.3.4.4. DFE-FFE equalizer

Decision Feedback-Feed Forward Equalizer (DFE-FFE) is a combination of a linear equalizer FFE (as explained in section 2.3.7) where the data signal is delayed by a taped delay line, weighted by tap coefficients C_i and superimposed in a summing unit, and a part of DFE. DFE is basically a nonlinear filter, capable of coping with severe distortions. Its typical working principle is illustrated by a block-diagram in the next Figure 4.15. It superimposes an amount (related to the previous bit decisions together with the B_m weighting factors) to the current bit, trying to eliminate ISI. This causes the eye to reopen, even though the signal's noise is not equalized. In this type of circuit the response speed of the feedback loop is critical: the decision gate, the delay stage and the summing unit all have to comply with performing within 1 bit period, so that the loop response gets fed back to the input. It was found that the high efficiency of FFE can be advantageous for low distortions, as well as the high efficiency of DFE can be fit for strong distortions.

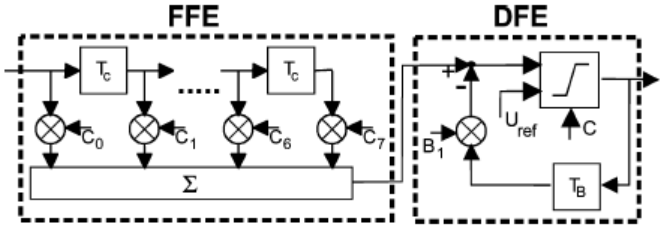

Figure 4.15 - Compound equalizer consisting of series circuit of FFE and DFE

In the following experiments the EDC circuit that has been used had an FFE part and a DFE in series which were independently controlled by 5 and 2 taps respectively. The tap spacing in the FFE/DFE module was half the bit period and the tap weights were adjusted within the normalized range of [-1 1] (which refers to a [0, 3.3V] voltage levels with a logical zero tap value being approximately 1.65 V). The values of the taps were adjusted through a controller and in terms of optimum BER for each of the measured cases.

4.3.4.5. Upstream experiments

This section presents the results obtained for the identification of transmission limit for the upstream case when DFE (5, 2) and optimum filter detuning applies. For these measurements, the fibre of L2 shown in Figure 1 has been varied accordingly. The driving conditions of the RSOA were according to what is presented above. It is noted again that the goal was to maximize the electrical BW of the signal and not the maximum achievable ER of the re-modulated signal. The performance metric that was used in order to investigate the transmission performance was the required OSNR for BER of 10^{-9} (at 0.1nm resolution).

Tolerance to optimum detuning

The first step was to identify the optimum filter position with respect to the central wavelength of the transmitted signal, with and without DFE at the receiver end. Figure 4.16 shows the required OSNR for 10^{-9} BER, at 30 km and 50 km, for various filter offset values with and without DFE (5,2). The input CW power to the RSOA was set to -10 dBm. It is observed that without equalization, the optimum filter detuning value depends on the transmission length (-0.12 nm for 30 km and -0.16 nm for 50 km). This is due to the fact that the chirped signal shape changes because of the dispersion as the signal propagates over various fibre distances. Moreover, it is shown that small filter offset variations around the optimum offset value result in significant signal degradation (or in other words accurate and stable filter tuning is required to assure optimum performance). However, when DFE equalization is used in combination to offset filtering, then a) the link's distance dependency to filter offset is minimized (optimum filter offset at 0.16 nm), b) the system performance is significantly increased (in terms of OSNR performance compared with the case without DFE) and c) the tolerance due to filter offset variations around the optimum value is significantly enhanced.

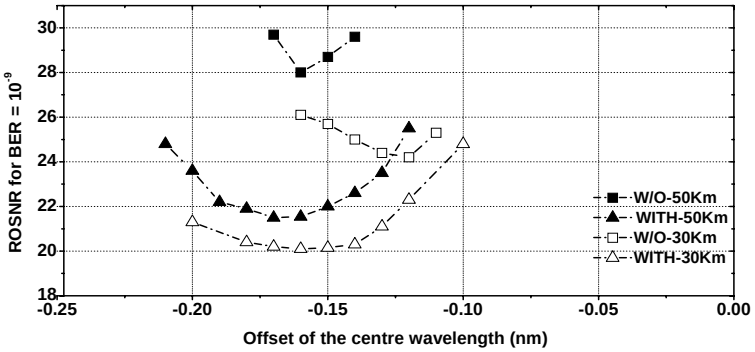

Figure 4.16. Required OSNR for 10^{-9} BER at 30 & 50 Km versus filter offset with and w/o DFE for Pin = -10 dBm.

Maximum transmission distance

The next study focuses on examining the achievable error free transmission distance (in terms of required OSNR for 10-9 BER) when optimum filtering and DFE (5,2) is applied. The measurements shown in Figure 4.16 have been taken for different input power levels of -10 dBm, -13 dBm and -15 dBm at the RSOA, emulating different power budgets for the downstream transmission. Here, the solid symbols refer to the case where only optimum offset filtering is applied at the receiver end. It is noted that without equalization, it was impossible to achieve error free (BER>10-9) operation, for -15 dBm RSOA input power level, mainly due to the fact that the transmitted wavelength (1535 nm) was away from the maximum gain peak of the RSOA (1510 nm). The measured values in Figure 4.17 without the equalizer have been obtained by optimizing the filter position according to the distance, which is a rather impractical approach. For the case of Pin = -10 dBm, the maximum distance is 50 km, whereas for the case of Pin = -13 dBm is 40 km, and the best performance for both cases is achieved at 30 km. This proves that the initial signal from the RSOA is pre-chirped and its interaction with the fibre chromatic dispersion and filtering effect smoothes out signal distortions around 30 km. This is evident also from Figure xx, presenting the received eye diagrams, after various distances with optical filtering at the optimum position.

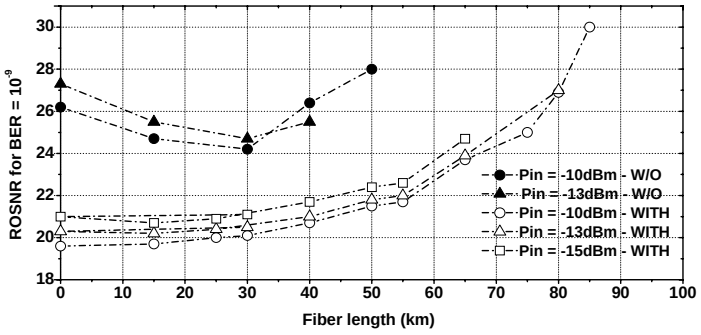

Figure 4.16. Required OSNR for 10^{-9} BER versus fibre length when optimum filter offset combined or not with DFE. Pin refers to RSOA input power (-10 dBm, -13 dBm and -15 dBm).

The curves with open symbols in Figure xx provide the results obtained when optimum offset filtering (now constant at -0.16 nm) is combined with DFE (5,2), examined for three different input power levels at RSOA, -10 dBm, -13 dBm and -15 dBm. According to these results, it can be observed that an additional use of DFE (5,2) relaxes the system from strict design requirements and offers significant transmission improvement achieving error free transmission over 85 km or 80 km or 65 km depending on the input power to the RSOA (-10 dBm, -13 dBm and -15 dBm respectively). This is more than 80% increase in the performance compared with the case of without equalizer. On the other hand, it is important to note that with the use of only DFE and not using optical filtering, it was not possible at any distance to detect with at a BER of 10^{-9}.

In order to study the behaviour of RSOA in combination with optimum offset filtering and at different BER values, the results shown in Figure 4.18 have been obtained after transmission over 30 km and 50 km with or without the use of DFE (5,2). For high BER values (10^{-3}, if FEC is additionally considered), there is an improvement of 2.5-3 dB by using equalizer. On the contrary, for low BER values (10^{-9}), for 50 km the performance improvement is 6 dB, whereas for 30 km, it is 4 dB. The lower penalty for the case of 30 km is due to the fact that the optimum performance was obtained for 30 km without equalizer, as it was previously presented in Figure 4.17.

It is important to comment that obviously, an extended WDM-PON reaching 85km (targeting also a large number of end users) requires strict power budget requirements. Due to the increased losses and the limited gain of currently commercially available RSOAs, these requirements can only be achieved with the use of amplification in the link like for example the remote amplification of SARDANA [Lázaro06]

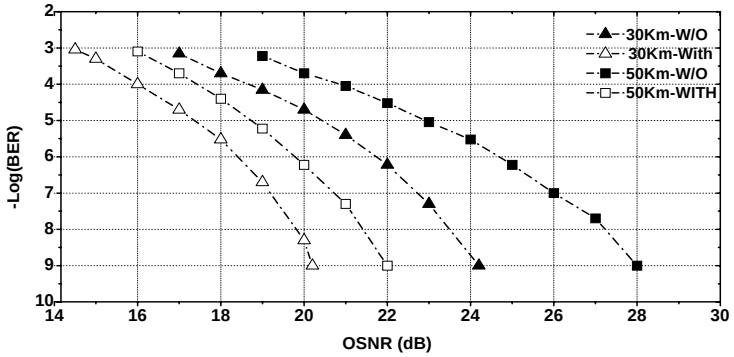

Figure 4.18. BER versus OSNR with and without (W/O) DFE for 30 and 50 Km for Pin = -10dBm.

4.3.4.6. Full duplex experiments

Here the signal which comes from the OLT is already modulated with the downstream. Several considerations have to be taken into account. In general, the RSOAs can be used as:

- *optical amplifiers/detector,* where the optical input is modulated and the output is this same signal but just amplified.
- *electro-optic modulators*, where the input optical signal from the OLT is imprinted with the upstream.

The behaviour of the device is different in E/O and O/O configurations: while modulating the input signal electronically the response is low pass, when amplifying an optically modulated signal, it is high pass, and an example can be seen in Figure 4.19. In the same conditions of optical input power and voltage bias, the RSOA present a high pass response with a frequency cut off at -3dB of 400MHz approximately with an optically modulated input, while the optoelectronic response is low pass, with a frequency cut off around 900MHz

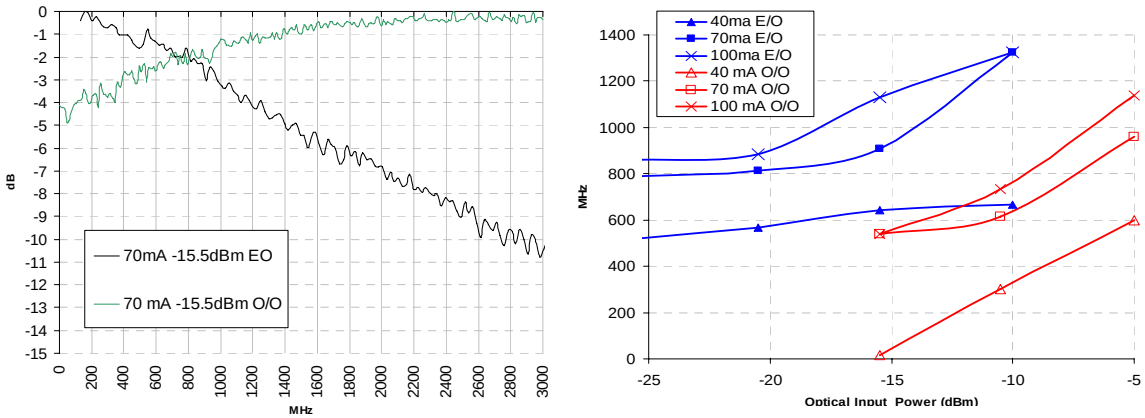

Figure 4.19 Left s21 for 70mA and -15.5dBm in o/o and e/o configuration. Right cut off frequency at -3dB for e/o and o/o configuration for different electrical bias currents.

Patterning effects

The first experimental measurements for the case of bidirectional transmission considered the study of the pattern length effects in the signal performance. This is an important cross-talk parameter in bidirectional WDM-PONs, when upstream and downstream transmission is combined. As the O/O remodulation is high pass; this produces overshoots when many consecutive '1's or '0's arrive to the RSOA and change the dynamics of the RSOA. An example

of this effect is shown in Figure 4.20 which presents the signal directly after amplification in an RSOA and without introducing any upstream signal for remodulation.

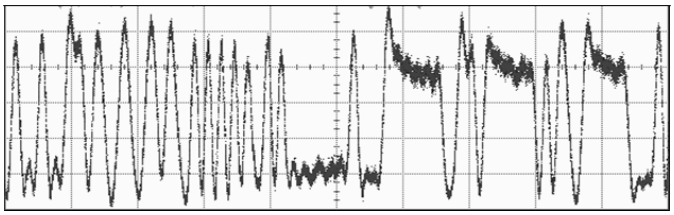

Figure 4.20. A 2^{11}-1 long PRBS signal after passing through the RSOA without injection of upstream signal (i.e. RSOA used as amplification module only)

According to [Inoue97], when a SOA is used to amplify modulated light signals, it can create distortion due to its intrinsic gain dynamics. When intense signals at a bit rate comparable to (or faster than) the gain recovery time are input to an SOA, the signal waveform is distorted due to gain saturation The waveform distortion depends on the bit pattern:

When the input level is switched from OFF to ON after a long OFF period, the leading part of the ON state is amplified with unsaturated gain and the output of the latter part then decreases as the amplifier gain approaches a saturated value. On the other hand, when the input level changes from ON to OFF to ON with a short OFF duration, the amplifier gain does not revert to an unsaturated value during the OFF period and the leading part of the second ON state is amplified with a partially saturated value. Thus, the waveform of an ON pulse after a long OFF duration is much more distorted than it is after a short OFF duration. This suggests that a bit pattern frequently changing between ON and OFF (short PRBS length) causes only a small amount of distortion.

In the case of this experiment, the upstream data will be introduced electrically over a modulated downstream data, which arrives from the OLT and presents low extinction ratio (ER). The impact of this signal over the upstream reception has been evaluated for different values of ER.

From a practical point of view, the PRBS length is important since a low PRBS is applicable for EPON systems and high PRBS for 10G-PON systems. The PRBS of 2^7-1 is a good approximation to Ethernet PON (EPON) systems utilizing eight to ten bit (8B10B) coding [Chi06]. A 2^{23}-1 or 2^{31}-1 PRBS may be necessary to provide the low-frequency content that SONET and SDH telecommunications systems require for the 64B66B coding in 10G-PON.

Figure 4.21 presents the impact of the long sequences of consecutive ones and zeros of the PRBS equal to 2^{31}-1 compared with the case of PRBS equal to 2^7-1 for the back-to-back approach by taking as a performance criterion the required OSNR for 10^{-9} BER and $5{\cdot}10^{-4}$. For the case of 10^{-9} with PRBS equal to 2^{31}-1 it was difficult to obtain measurements for different distances and ER_d values, due to the OSNR limit of this system. Also, it is proven that for the FEC limit ($5{\cdot}10^{-4}$), there is a difference of 2-5dB between the two PRBS. Regarding the 10^{-9} BER, the difference between the PRBS lengths is higher comparing with the previous case, because for low BER, the impact of the patterning effects is more critical in terms of performance.

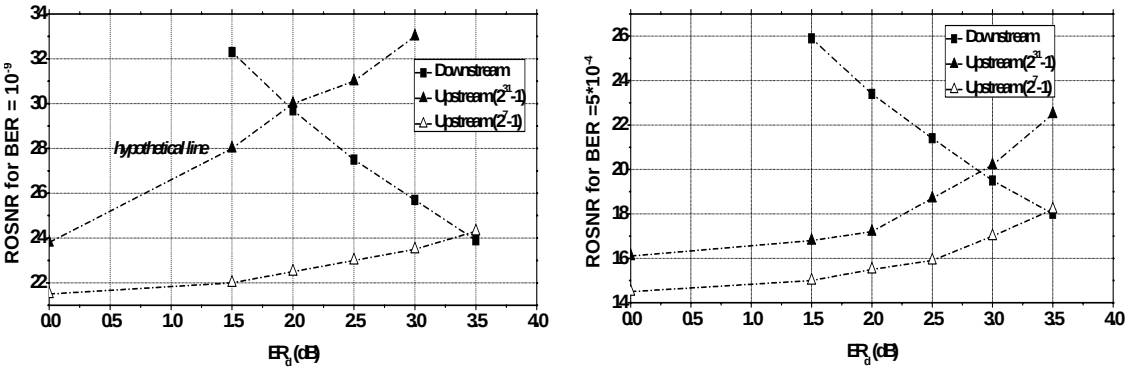

Figure 4.21. ROSNR for BER = 10^{-9} (left) and BER = $5{\cdot}10^{-4}$ (right) versus ER_d for different PRBS of 2^{31}-1 and 2^7-1.

Experimental results for bi-directional transmission

Following the studies on the pattern length limitations, the next performance criterion that was investigated was the optimum value of the downstream ER (ER_d) required in order to achieve simultaneous optimization for both downstream and upstream signals. The studies were performed both with and without the use of DFE equalization, considering different values of ER_d and measuring the required OSNR for BER of 5·10-4 with a PRBS length of 2^{31}-1.Also bidirectional transmission of 25 km has been evaluated at BER of 10^{-9} with fixed ER of the downstream signal at 1.8 dB and a pseudo random binary sequence (PRBS) equal to 2^7-1.

BER of 5·10-4 with a PRBS length of 2^{31}-1 experiments:

Figure 4.22 shows the ROSNR for a BER of 5•10-4 for the downstream and upstream signal, with and without DFE, and considering different transmission distances. This analysis provides the opportunity to identify the optimum ER_d for bidirectional operation with and without equalizer when optimum filter offset is applied for each transmission distance and for each

value of ER_d. This is done by marking the cross point of the downstream line and the line of upstream at which the required OSNR is the same for both transmissions. Figure 4.23 presents the received eye diagrams, after various distances and using different values of ER_d with the optical filter at the optimum position. Observing the results summarized in Figure 4.22, it is evident that the improvement due to equalization increases as the ER_d increases and the fibre length increases. In other words, when the re-modulated signal is more distorted (higher ER_d

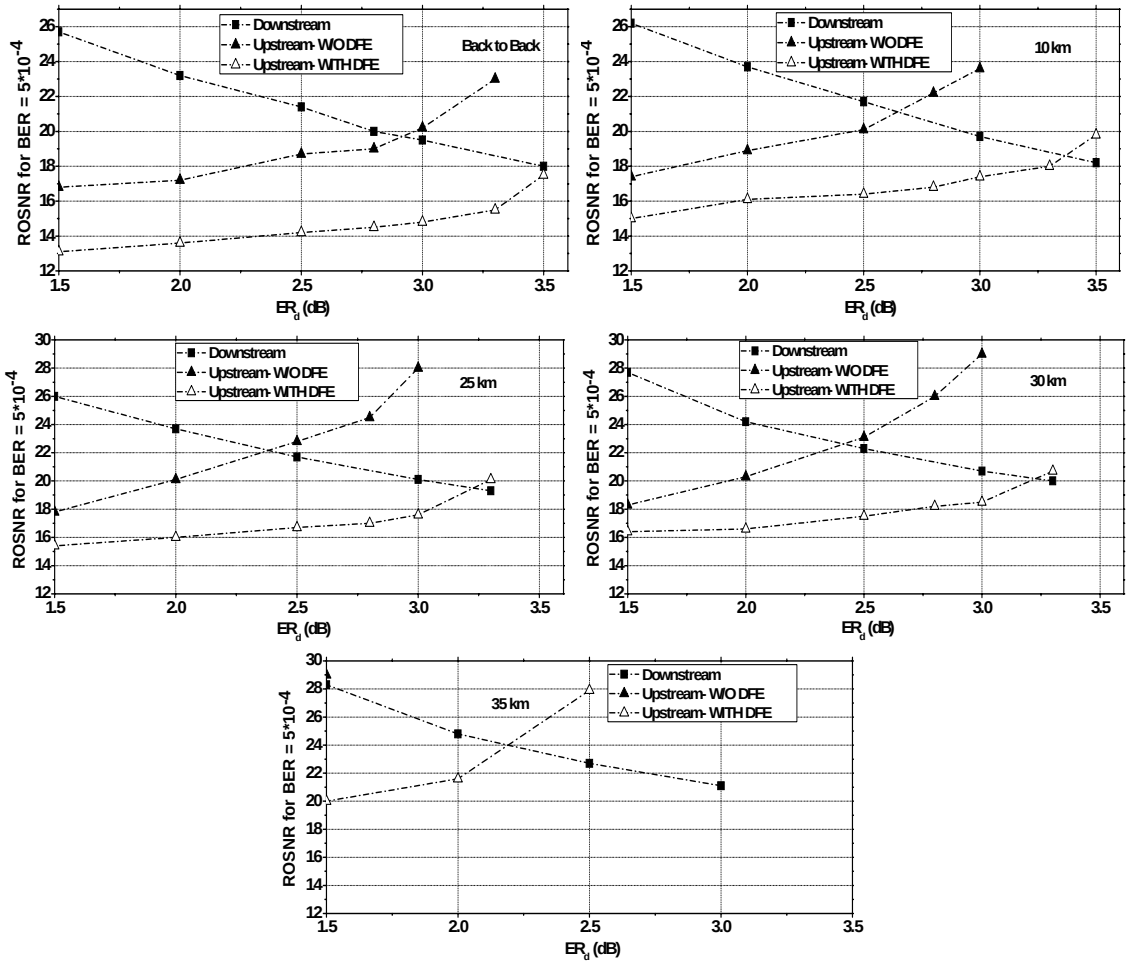

Figure 4.22. Required OSNR (at 0.1nm resolution) for BER=$5 \cdot 10^{-4}$ versus ER_d for different transmission distances for bidirectional transmission (downstream and upstream signal) when optimum filter offset combined or not with DFE for upstream transmission in the OLT side.

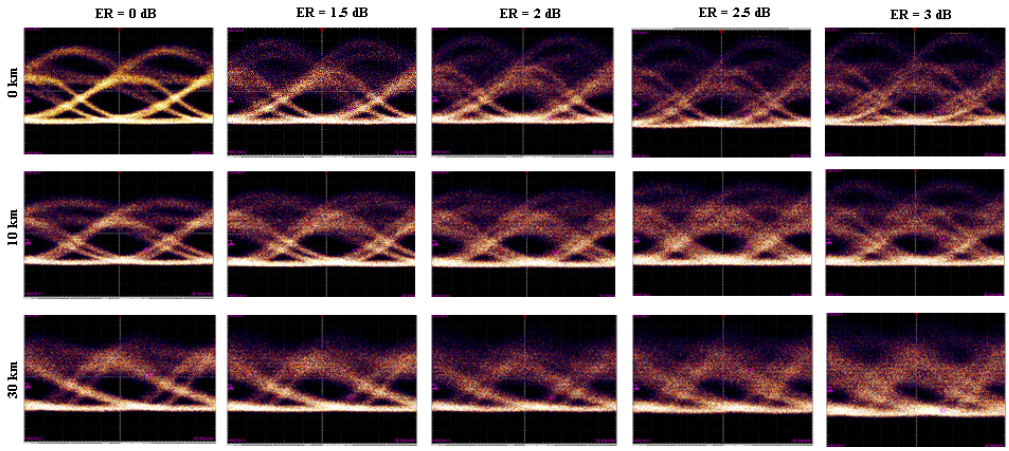

Figure 4.23. Eyes diagrams for various distances and ER_d with detuned OBPF, with window width of 200 ps.

and longer transmission distance) the equalizer performs better than if the signal presents less accumulated distortion. Furthermore, the optimum ER_d decreases as the fibre length increases since the signal is more distorted by the chromatic dispersion in the upstream. The use of DFE allows reducing in more than 2 dB the required OSNR for all the cases. The optimum ER_d is higher due to the fact that the DFE is only in the OLT side, so the downstream is not compensated. Additionally it can be observed that the maximum bidirectional transmission distance that can be achieved without equalizer is 35 km, with ER_d = 1.5 dB and required OSNR of 29 dB, whereas with the use of DFE is the same distance but with higher ER_d of 2.5 dB and required OSNR at 28 dB. Figure 4.24 presents the optimum filter positions with respect to the ER_d for 10 km and 30km, with and without the use of DFE.

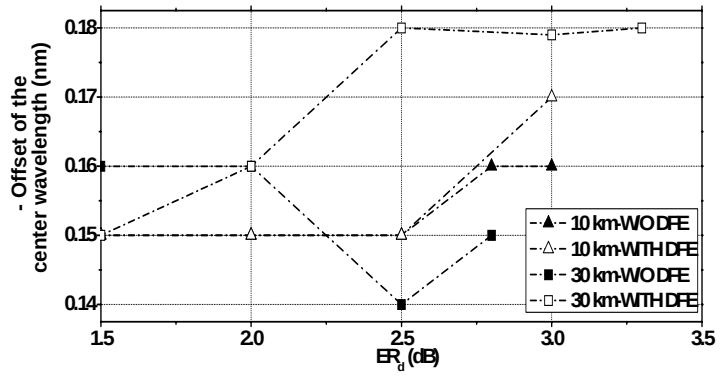

Figure 4.24. Filter offset positions versus ER_d for different transmission distances (10 and 30 km) for bidirectional transmission (downstream and upstream signal) with DFE for upstream transmission in the OLT side.

Figure 4.25 illustrates the summary of the optimum ER_d and the best required OSNR for each fibre length with and without equalizer with the optimum filter position for each case. This graph contains all the necessary information for a bidirectional system in order to be able to achieve the optimum performance. It is observed that the difference in the ER_d between the cases without and with DFE is around 0.6 and 0.8 dB. This difference increases as the fibre length increases. It is important to note that without the use of DFE, the optimum ER_d for 35 km was unattainable. The optical input power in the RSOA for all the cases is -10 dBm. It was impossible to achieve values for Pin = -15 dBm mainly due to the fact that the transmitted wavelength (1532 nm) was away from the maximum gain peak of the RSOA (1510 nm).

In all the cases, the RSOA is optimized for maximum extinction ratio. For this reason, the eye without downstream signal (ER=0) in Figure 10 is not symmetrical. The results have been obtained with fixed values of amplitude and Vbias current, optimized for the back-to-back case. Evidently, the results of only upstream can be further improved if the input current in the RSOA is re-optimized for each transmission distance and according to the resulted trade-off between ER and RSOA BW; however this is a rather impractical approach.

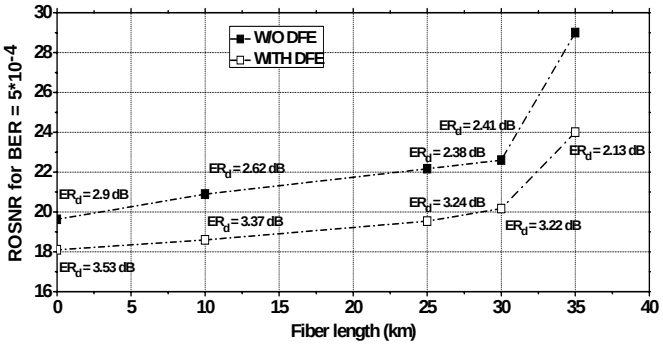

Figure 4.25. ROSNR for BER=5·10^{-4} versus fibre length for bidirectional transmission when optimum filter offset combined or not with DFE and for optimum values of ERd for each case.

Finally, the performance of the received signals has been evaluated in terms of required OSNR for a BER value of 5•10-4 (FEC limit). It should be noted that the clock and data recovery (CDR) circuitry in the equalizer module operates at around 9.952 GHz. Therefore, it was not possible to use a data rate of 10.664 Gb/s for the inclusion of FEC overhead. However the difference in the performance benefit of the equalizer for the mitigation of chromatic dispersion will be negligible at 9.952 Gb/s compared to the case of 10.664 Gb/s. In this manuscript, the main focus is to study the benefit of the equalizer and the difference in the performance improvement with respect to the case without equalization. Of course, it is expected that the absolute numbers of OSNR in all cases (either if equalization is used or not) change slightly since a higher rate affect the shape of the modulated signal coming out of the RSOA.

BER of 5·10^{-9} with a PRBS length of 2^7-1 experiments:

The experimental set-up is shown in Figure 4.26(a). At the OLT, a continuous wave (CW) signal at 1532 nm is introduced into a Mach Zehnder modulator (MZM) where a 10 Gb/s non-return-to-zero (NRZ) downstream signal is applied with pseudorandom bit sequence (PRBS) of 2^7-1.

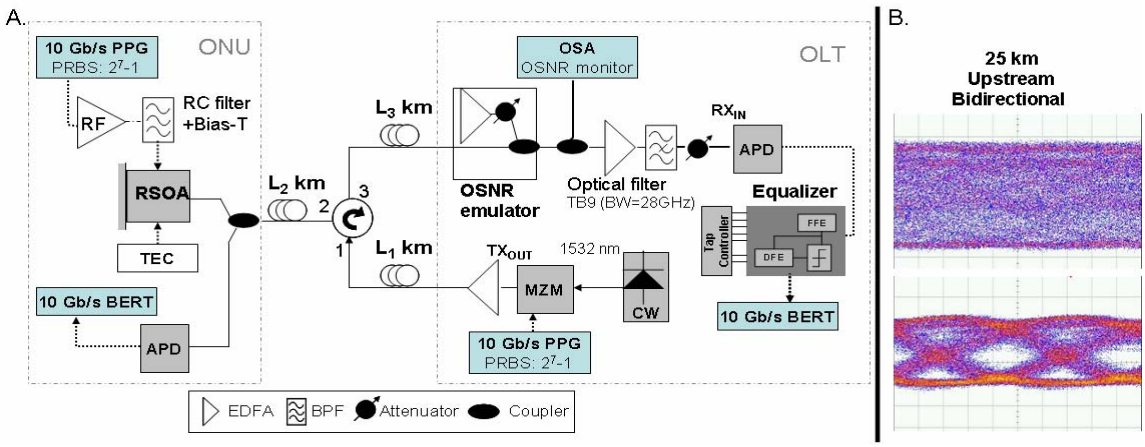

Figure 4.26 Experimental set up and eye diagram

Figure 4.26(b) shows the eye diagrams after 25 km of bidirectional fibre only, with the optical filter placed in its central position (up) and with optimum offset (down). The downstream and upstream signals before and after the RSOA respectively, have been acquired with a PIN diode (after removing the RSOA ASE noise using a wide BW optical filter) in order to measure the ER of the signals more accurately. The optical input power into the RSOA was -10 dBm same as in the final set up. An ER_d of 1.8 dB was selected in order to achieve bidirectional transmission at 25 km and it has been maintained constant for all the studied transmission distances. Higher ER_d would be better for the downstream signal but worse for the upstream signal as we have seen before. Lower ER_d would make the system limited to the downstream transmission. For other distances, the optimum ER_d is different but we have maintained it fixed in all the experiment. Significant cancellation of the downstream modulation because of gain saturation in RSOA is not observed.

For all the measurements presented in Figure 4.27, the spectral position of the filter at the OLT with respect to the central wavelength of the transmitted signal was around 0.16 nm (blue shifted) for both cases with and without equalization of DFE (5, 2) at the receiver end. Regarding the optimum optical filter position, in this experiment, a misalignment of ±0.01nm produces a penalty of 0.5dB in the ROSNR when the DFE is not used, while with the DFE it is necessary to detune ±0.02 nm from its optimum position to obtain this effect. Further misalignment generates strong degradation in the performance. Figure 4.27(a) presents the ROSNR for a BER of 10^{-9} with respect to the bidirectional transmission length L2, for the cases with (open symbols) and without (solid symbols) equalization, with the filter being detuned at its optimum position in both cases. The measured values in Figure 4.27(a) without the equalizer have been obtained by optimizing the filter position according to the distance, which is a rather impractical approach. However, when DFE is used in combination with offset filtering, the optimum offset remains the same (~0.16nm), independent of the transmission distance. Figure 4.27(a) shows that for the case without equalizer the best performance is achieved around 12 km. This proves that the initial signal from the RSOA is pre-chirped, and its interaction with the CD and filtering effect smoothes out signal distortions around 12 km. Additionally, Figure 4.27(b) presents the received eye diagrams, after various distances with optimum offset filtering.

Additionally, it can be observed that the additional use of DFE (5, 2) offers a significant transmission performance improvement by 6 dB in terms of ROSNR at 25 km, which increases for longer transmission distances. It is noted that the same value of ROSNR (26 dB) is needed both for a BER of 10^{-9} in the back-to-back case without equalizer and for 25 km with the use of

equalization. On the other hand, the BER performance is always worse than 10^{-9} if only equalization is used without optical offset filtering as it can be seen in Figure 4.26(b) (top). In the measurements obtained next, the performance of single fibre bidirectional transmission is compared with the case of bidirectional transmission where separate fibres are used for upstream and downstream propagation.

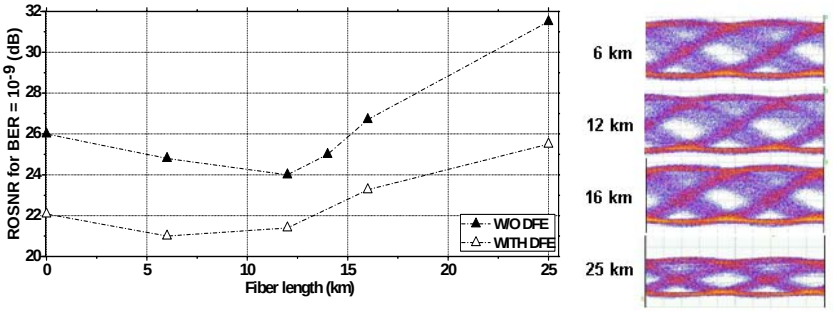

Figure 4.27. (a) ROSNR for BER=10^{-9} versus fibre length for bidirectional upstream and (b) received (electrical) eye diagrams for various distances with detuned optical filter at the receiver (with a window width of 200 ps).

More specifically, Figure 4.28(a) presents a comparison (in terms of BER versus OSNR) between the use of two separate fibres for up- and downstream transmission of lengths L1 = L3 = 25 km and the use of only one bidirectional fibre of length L2 = 25 km. When one bidirectional fibre is used, then the ROSNR to achieve a BER of 10^{-9} increases by 5 dB with respect to the case where two separate fibres are used and without considering equalization. However, with the introduction of DFE, this difference drops to 2 dB. When only one fibre is used without equalizer, there is an error floor caused, due to RB effects, which is partially eliminated when DFE equalization is applied, resulting in better ROSNR values.

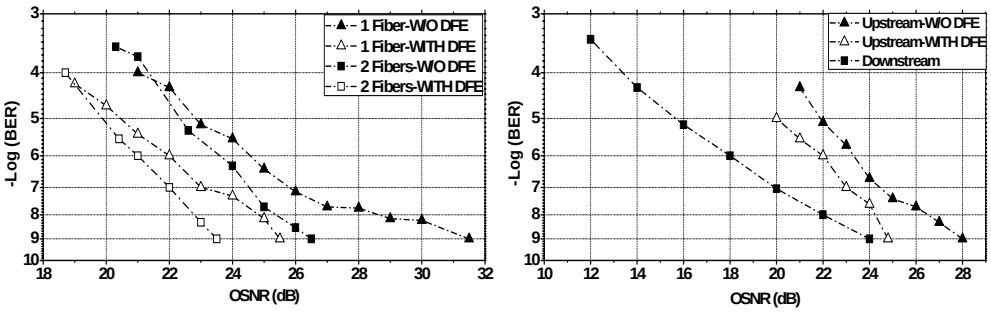

Figure 4.28. (a) Upstream comparison BER versus OSNR with 25 km bidirectional and two fibers of 25 km unidirectional (b) BER versus OSNR with 12 km bidirectional and 2x25 km unidirectional.

It is important to note that the required OSNR for all the BER values of the downstream signal is always more than 3 dB lower than the upstream case reported here. It can be also observed that when DFE is used, the linear tendency of the BER curves shows that no error floor is reached at lower BER values, which is not the case when only one fibre is employed without

applying DFE. In Figure 4.28b, the limit of the downstream transmission is observed. In this case, separated down- and upstream fibre spans, of length L1 = L3 = 25 km are used, with an additional span of a bidirectional fibre of L2 = 12 km. The ROSNR to achieve a BER of 10^{-9} is only 0.7 dB lower for the downstream (without DFE) than for the upstream transmission with DFE. This shows that the performance of upstream transmission in terms of ROSNR is comparable to that of downstream signal only after a total transmission distance close to 37 km (L1+L2), where the CD effect in combination with OSNR and the low ER of 1.8 dB limits the downstream signal quality that is detected at the ONU.

4.3.5. RSOA phase adjustment

This constitutes another technique which deals directly with the chirp as an alternative to the offset filtering. It provides similar results avoiding the loss associated with the detuned filter at l the appropriate slope. Here, only the phase is modified accordingly to compensate both the chirp and the chromatic dispersion present in the fibre.

4.3.5.1. Mathematical analysis

According to [Agrawal], the spectrum of a chirped Gaussian pulse which is broader than the unchirped pulse presents the following expression:

$$E(0,\omega) = E_0 \left(\frac{2 \cdot \pi \cdot T_0^{\,2}}{1 + j\alpha} \right)^{1/2} e^{\left(\frac{\omega^2 T_0^{\,2}}{2(1+j\alpha)} \right)} \qquad (4.5)$$

Here, the '0' means that this field is at the output of the transmitter, just at the input of the optical fibre (L=0 km). T_0 is the pulse half-width at the 1/e intensity point and α is the chirp parameter of the RSOA.

After propagating through the fibre and filtering optically, the expression becomes [Agrawal]:

$$E(L,\omega) = \frac{1}{2\pi} \int_{-\infty}^{+\infty} E(0,\omega) H(\omega) e^{\left(\frac{j}{2} \beta_2 L \omega^2 - j\omega t \right)} dw \qquad (4.6)$$

By expanding the phase of the optical filter transfer function H(ω) in a Taylor series and retaining up to the quadratic term:

$$H(\omega) = \left| H(\omega) \right| e^{j\phi\omega} \approx \left| H(\omega) \right| e^{j(\phi_0 + \phi_1 \omega + \phi_2 w^2)}, \qquad (4.7)$$

where $\phi_m = d^m/d\omega^m$ (m=0, 1, …) is evaluated at the optical carrier frequency w_0. The constant phase ϕ_0 and time delay ϕ_1 do not affect the pulse shape and can be ignored. Then, taking the terms which depend on "ω^2"inside the integral of (4.6) and considering the expression of (4.7), we need to force:

$$e^{\mathrm{Im}\left(\frac{\omega^2 T_0^{\,2}}{2(1+j\alpha)} \right)} e^{j(\phi_2 w^2)} e^{\left(\frac{j}{2} \beta_2 L \omega^2 \right)} = 1, \qquad (4.8)$$

Operating:

$$\frac{T_0^{\,2} \alpha}{2(1+\alpha^2)} + \frac{1}{2}\phi_2 + \frac{1}{2}\beta_2 L = 0 \qquad (4.9)$$

Then, dispersion could be completely compensated by choosing a phase dependent of ω^2 with value:

$$\phi_2 = -\left(\frac{T_0{}^2 \alpha}{(1+\alpha^2)} + \beta_2 L \right) \tag{4.10}$$

4.3.5.2. Optical filter configuration

In order to verify this experimentally, a programmable (in amplitude and phase) optical filter called Waveshaper has been used. It is an optical filter capable of being configured in terms of attenuation and phase. From a basic rectangular filter centred in a specific wavelength defined by the user, a user configured filter is added by means of a text file in which the attenuation and phase are determined in frequency steps relative to the main rectangular filter, being the relative frequency points in terms of THz and the phase in degree. As a first approximation, several filters capable to compensate different link distances (without considering the transmitter) have been implemented.

As a mode of example, let us consider an optical fibre of 25 km. Taking the following expression to calculate β_2:

$$\beta_2 = -\frac{D \lambda^2}{2 \pi c} \tag{4.11}$$

The phase required to compensate L km is found, by isolating it from the following expression:

$$\phi_{2_i} = \frac{1}{2} L \beta_2 (2 \pi f_i)^2 \tag{4.12}$$

A typical filter to compensate 25km of optical fibre can be as it is presented in next Figure 4.29, where the amplitude is flat in all the bandpass, only phase is modified.

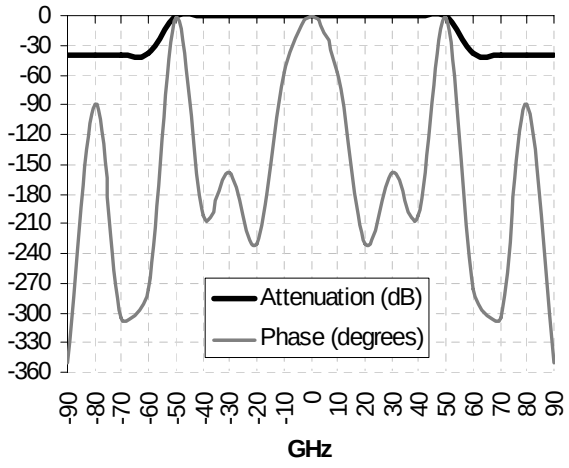

THz	Att.	Phase
-0.09	40	-350.557
-0.08	40	-90.3169
-0.07	40	-305.399
-0.06	39	-275.803
-0.05	0	-1.53002
-0.04	0	-202.579
-0.03	0	-158.951
-0.02	0	-230.645
-0.01	0	-57.6612
0	0	0
0.01	0	-57.6612
0.02	0	-230.645
0.03	0	-158.951
0.04	0	-202.579
0.05	0	-1.53002
0.06	39	-275.803
0.07	40	-305.399
0.08	40	-90.3169
0.09	40	-350.557

Figure 4.29. Optical filter characteristics adjusted to compensate for the RSOA's chirp and optical fibre CD.

The chirp parameter depends on the operating point in the RSOA. In the following experiments, the phase adequate to compensate unchirped 25km was the one which gave better results when the length of the fibre was 10km and the RSOA used as a modulator. The filter which compensates 26km of fibre and RSOA transmission was the one prepared to compensate the dispersion of 40km of SMF. Figure 4.30 shows the chirped pulse in the scope.

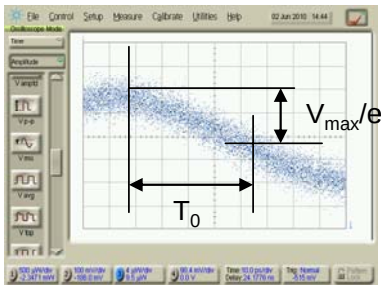

Figure 4.30 Chirped pulse measured in the scope.

This allows calculating approximately the RSOA chirp parameter, by using (4.9) and isolating α:

$$\alpha = \frac{-T_0^{\,2} \pm \sqrt{T_0^{\,4} - 4\left(\phi - \beta_2 L\right)^2}}{2\left(\phi - \beta_2 L\right)} \tag{4.13}$$

$T_{0,}$ the half-width at the 1/e intensity point, has been measured to be $T_0 = 45$ ps. This results in a valid value of $\alpha = 6.57$.

4.3.5.3. Experiment validation

The prepared set up is presented in Figure 4.31. A CW signal laser at a λ=1561nm with 5dBm optical power is sent from the OLT to the ONU. This wavelength is used to modulate the RSOA upstream with a NRZ PRBS 2^9-1 signal at a bit rate of 10.3125 Gb/s with a bias current of 100mA. We have implemented an RC filter which enhances the e/o BW from 1.2GHz to 3GHz. An attenuator is placed between the OLT and the ONU to fix the Power Budget (PB). At the OLT the receiver part is composed by an erbium doped fibre amplifier (EDFA), the optical filter called Waveshaper (Wsh) and an APD with limiting amplifier.

Figure 4.31 also shows the RSOA ASE curve. As it was explained in Chapter 1, 10G-EPON standard proposes the 1574-1580nm bandwidth assignment for the 10 Gb/s downstream [Tanaka 2010]. This new RSOA is precisely centred in those wavelengths, with a 3dB optical bandwidth of 44 nm. The device presents a maximum of 22dB of gain at 100mA and the noise factor is between 6 and 8 depending on the optical power.

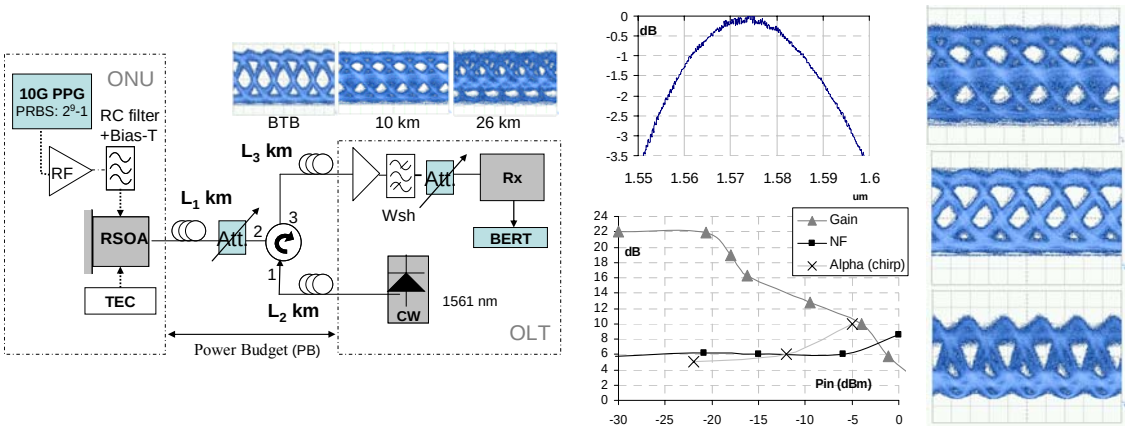

Figure 4.31. Left: Set up and eye diagrams in BTB, and after 10km and 26 km. Middle up: RSOA ASE curve. Middle bottom: RSOA's gain, noise factor and chirp respect optical power. Right: eye diagram comparative after 10km with a simple flat filter centred (top), a filter detuned (middle), the flat filter centred with a specific phase (bottom)

Chirp has also been measured obtaining an alpha parameter of 5 to 10 depending also on the optical power. Finally, the optical fibre has been placed either taking into account RB, only the drop fibre L1 in bidirectional transmission and also by two separated spools L2 and L3 unidirectional. We observed that the chirp of the RSOA closes the eye after 10km at 10 Gb/s being not possible to detect the signal. The eye diagrams of the right column in Figure 4.31 right show a comparative with the signal after 10km with a simple flat filter centred (top), a filter detuned (middle), and the flat filter centred with a specific phase (bottom), we can see how by both techniques the eye opens. Figure 4.32 presents the effect of the Waveshaper (Wsh). The differences between offset filtering and phase were small so only one trace has been plotted for vision simplicity. The chirp, together with the chromatic dispersion, creates null transmission points at around 5.5 GHz for 10km and 3.4 GHz after 26km. The optical filter restores the signal, thus allowing the detection at the OLT.

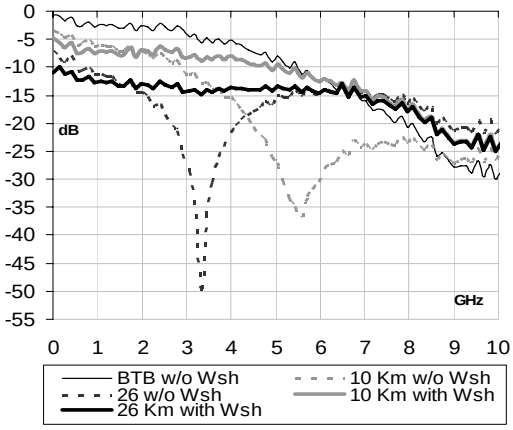

Figure 4.32. e/o response for BTB, 10km and 26km with and w/o Wsh.

Figure 4.33a and 4.33b show the obtained BER for 10.3125 Gb/s for 10km and 26km using the Wsh. Figure 4.33c and Figure 4.33d present the BER for 5.15625 Gb/s (without Wsh) also for 10 km and 26 km. According to the gain presented in Figure 2 and the power of 5dBm from the OLT laser, using only one fibre, the optical signal to Rayleigh Backscattering ratio (OSRR) is around 24.5dB for a PB of 10dB, OSRR=11dB for a PB of 20dB, OSRR=9dB for a PB of 23dB and OSRR=-3dB for a PB of 30dB. The FEC limit of 10^{-3} is considered as in the new standards [Tanaka10]. At 10.3125 Gb/s the maximum PB is 20 dB using a bidirectional fibre and 23 dB if two unidirectional fibres are used, while at 5.15625 Gb/s PB of 23dB can be afforded with 1 fibre as a maximum, while PB of 30dB is possible by using two fibres. As a final remark, using a PB of 10dB, the BER curves present the same behaviour for 1 and 2 fibres approach.

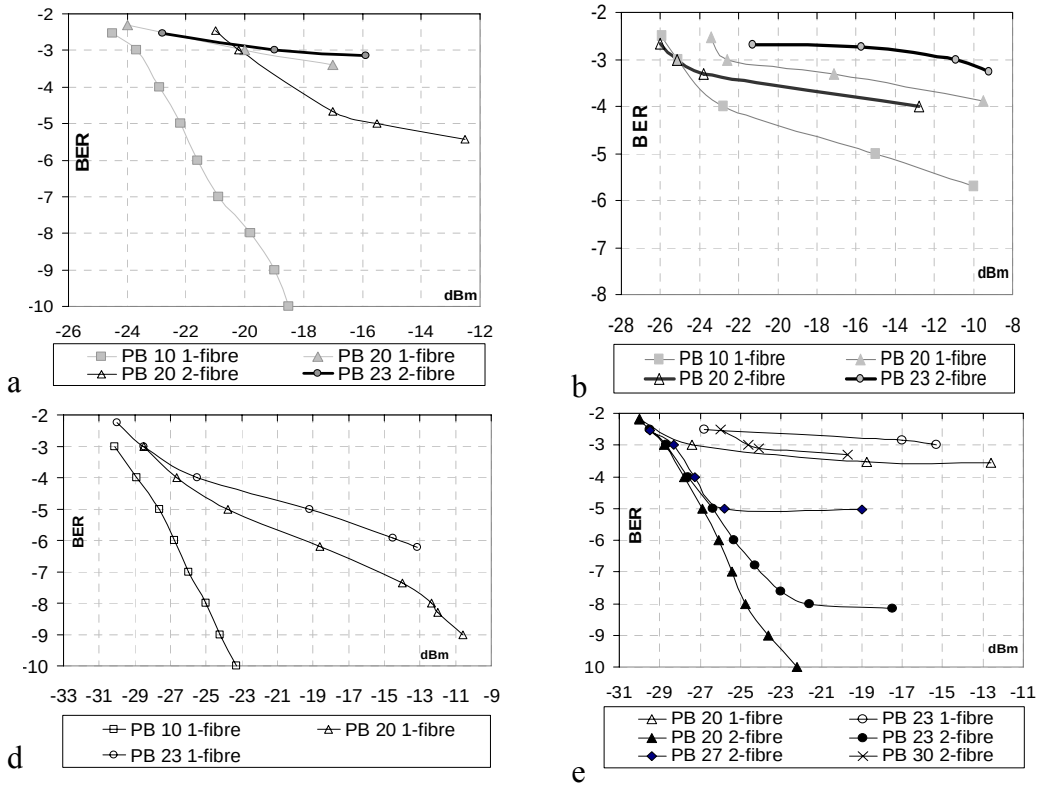

Figure 4.33. BER with respect optical power for 10.3Gb/s and 10km a) 10.3Gb/s and 26 km b) 5Gb/s and 10km c) 5Gb/s and 26km d).

In conclusion, by using this technique we have improved the system increasing its bit rate from 5Gb/s to 10Gb/s.

4.3.6. RSOA and MLSE

In this subchapter, the performance of an RSOA operating at 10 Gb/s in a bidirectional and unidirectional WDM PON system with a conventional MLSE receiver is experimentally studied. Different wavelengths were used to demonstrate its colourless characteristic. Moreover, a comparison between conventional and correlation sensitive (CS) MLSE has been performed.

The set up is presented in figure 4.34 left. A tuneable laser was used for continuous wave (CW) source and its incident power on the RSOA was set to -6dBm. The upstream data was generated with a pseudo-random binary sequence (PRBS) or 2^{15}-1 and modulated by the RSOA at a bit-rate of 10 Gb/s. The RSOA had a modulation bandwidth limited to 2.5GHz and its wavelength band was centred at 1550nm. The output power of the RSOA was set to 0dBm. Single-mode fibre was placed in the unidirectional and directional section of the passive optical network (PON) as shown in Figure 4.34. After the fibre, the signal was filtered by a 300GHz bandwidth optical filter. The receiver was an APD with input power adjusted to -10dBm. The received signal was captured with a digital storage oscilloscope (DSO) with 7GHz bandwidth and sampled at 20Gsamples/s giving 2 samples / bit. The storage time was set to its maximum yielding a total of 2^{17} bits. The samples were then post-processed with a conventional MLSE receiver with 4, 8 and 16 states. The first 2^{15} bits were used for training the trellis and the remaining bits were used for decoding.

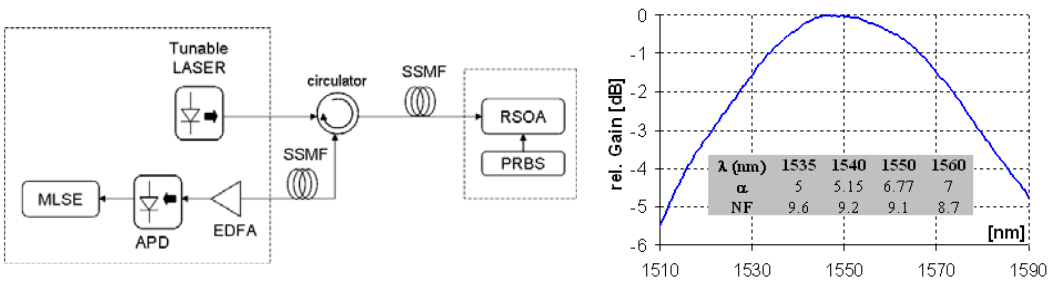

Figure 4.34. set up and ASE curve

The RSOA was first characterized in terms of its gain and noise Figure (NF). The optical bandwidth of the RSOA is 58 nm (at -3dB) as noticed in Figure 4.34. In the considered margin, the gain differed only by -0.8dB (1535) with respect to the centre wavelength (1550). The RSOA modulation bandwidth was 2.5GHz. The NF was around 9dB. The chirp factor was also measured and it varies from 5 to 7 as the wavelength is increased from 1535 to 1560. Consequently, a larger penalty is expected for higher wavelengths.

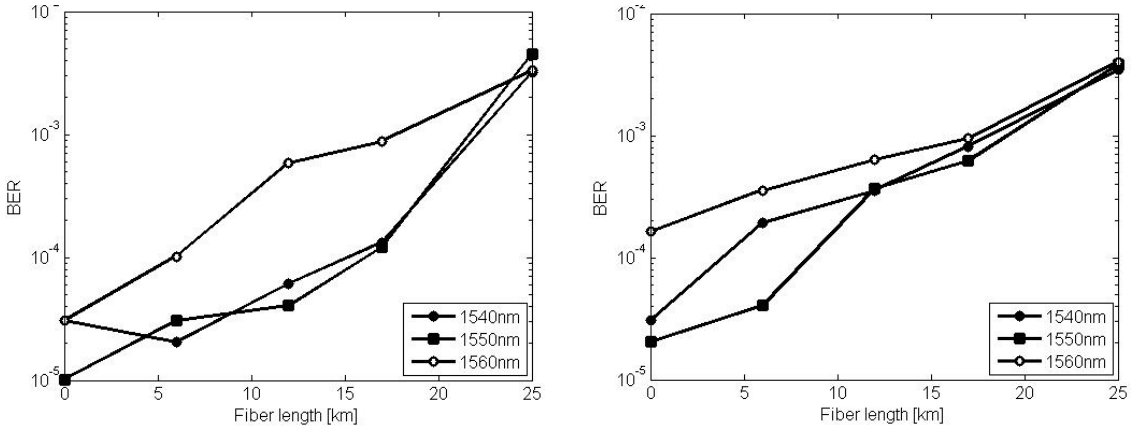

Figure 4.35 BER against fibre length for λ = 1535, 1540, 1550, and 1560 nm using 4 states (left) and 8 states (right) MLSE

We then used the system setup with fibre only in the drop fibre, bidirectional part, with length up to 25Km. The output power of the ONU was adjusted to 0dBm for all wavelengths. The received signal was digitalized and post-processed with a conventional MLSE algorithm. When no MLSE receiver was in place, the bit error ratio (BER) achieved was high above 10^{-2} strongly limiting the system even in back-to-back. Figure 4.35 shows the obtained BER against fibre distance with wavelengths of 1535nm, 1540nm, 1550nm, and 1560nm with 4 and 8 states in the MLSE. We experimented also with 16 states but the overall improvement was minimal compared with 8 states. Due to the limited storage time, the BER could not be lower than 10^{-5}.

It can be observed that MLSE allows to obtain BER lower than 10^{-3} even with the bandwidth limitation of the RSOA. In addition, the curves show similar results for all wavelengths, although a bit worse at 1560nm. Even if the RSOA is centred in 1550nm, the MLSE compensates for the variations in the gain, chirp, and NF allowing a colourless operation. Considering a target BER of 10^{-3}, enough for recovering with forward error correction (FEC), almost 19 Km of fibre are reached with 8 states MLSE at all wavelengths. The performance of the system is severely reduced after 20 Km of fibre, due to the combination of dispersion and Rayleigh back-scattering (RB).

As an extension of the experiment, the fibre is placed in the unidirectional side of the optical system in a two-fibre access configuration. In this case, a longer link length is expected to be reached since there are no reflections and no RB. Figure 4.36 plots the BER against the fibre length for wavelengths of 1535nm, 1540nm, 1550nm, and 1560nm, using 4 and 8 states MLSE.

Considering a target BER of 10^{-3} around 25 Km are reached using an MLSE with 4 states in the worse case. If we increase the number of states to 8 the performance improves considerably, and

with the same target BER the system achieves a total length of almost 125 Km. We processed data also with 16 states MLSE, but the improvement was not significant compared to 8 states.

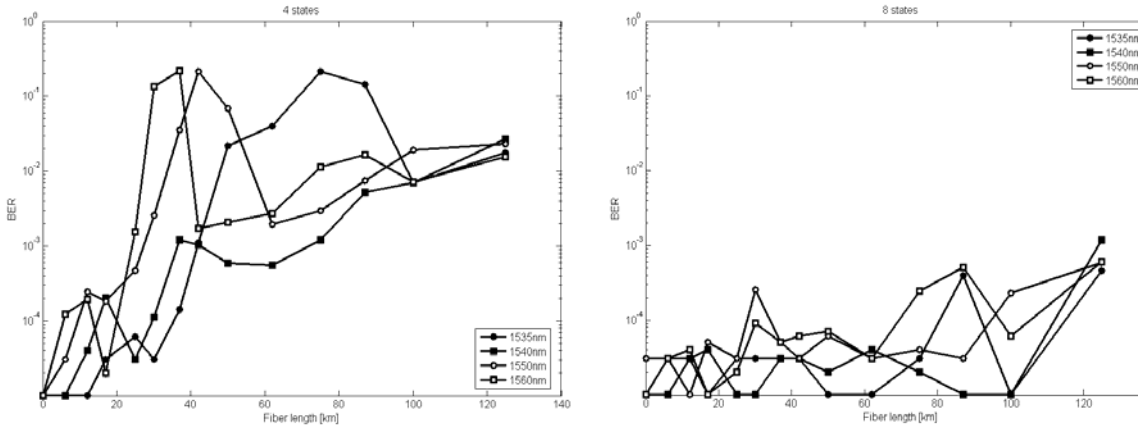

Figure 4.36 BER against fibre length for λ = 1535, 1540, 1550, and 1560 nm using 4 states (left) and 8 states (right) MLSE with system 1b.

Noteworthy, as in the bidirectional case, the results are preserved in the four wavelengths considered, thus MLSE automatically compensates the chirp variation over the wavelength. This allows the RSOA for effective colourless operation. A final remark is that although the RSOA might not give enough power budget for long distances, it can be thought useful for remote amplification networks and long reach WDM-PON like in the project SARDANA [Lázaro06] or with an additional SOA in the input.

Since the RSOA is bandwidth limited compared to the bit-rate, it can be thought to act as a low-pass filter. As a consequence of this narrow filtering effect, the transmitted sequence is correlated. We experimentally studied the performance of a 2.5 GHz bandwidth RSOA operating at 10 Gb/s in a bidirectional WDM PON system. In order to take into account data correlation, we employ a correlation sensitive MLSE (CS-MLSE) based on [Cavcic98]. This algorithm considers the correlation of the samples by assuming that they follow a multivariate Gaussian distribution. It is shown that, with this post-processing, lower number of states and longer fibre length can be reached by the same low bandwidth RSOA than when using only a conventional MLSE.

For the construction of the MLSE program, we considered that the received samples (signal + noise) followed a Gaussian distribution. The branch metric for the trellis is then:

$$V_i = \log\left(\sigma_i^2\right) + \frac{\left(r_j - \mu_i\right)^2}{\sigma_i^2} \tag{4.14}$$

Where r_j is the j-th received sample, μ_i and σ_i are the mean and standard deviation of the received samples in the i-th branch or sequence.

The received samples were later post-processed with the CS-MLSE. For ease of notation, a vector N_i is defined, containing the difference of the received samples and the mean values in the ith branch. The size of vector N_i depends on the number of samples considered for correlation. For L correlation, N_i has (L+1) elements since it considers the current sample and L samples for correlation. It can be expressed as:

$$N_i = \left[(r_j - \mu_i) \quad (r_{j+1} - \mu_{i+1}) \quad \ldots \quad (r_{j+L} - \mu_{i+L})\right]^T \tag{4.15}$$

The last L elements of N_i form vector n_i. Thus, n_i considers the difference between the correlation samples and their mean value in the ith branch. Considering this vector definition, the branch metric is the following:

$$V_i = \log\left(\frac{|C_i|}{|c_i|}\right) + N_i^T C_i N_i - n_i^T c_i n_i \tag{4.16}$$

where C_i is the covariance matrix of the received samples and c_i is the lower principal submatrix of C_i:

$$C_i = \begin{bmatrix} \bullet & \bullet \\ \bullet & c_i \end{bmatrix} \tag{4.17}$$

The same experiments as in Figure 4.35, using bidirectional fibre, have been then performed with the CS-MLSE. As it can be noticed in Figure 4.37b, by using only 4 states with CS-MLSE, the system can reach 18.4Km of fibre for the same target BER, providing 4.2Km more than conventional MLSE with the same number of states but at a price of a more complex metric. This is an increase of 22% of reachable fibre length.

Since CS-MLSE takes into account the memory of the previous states, it can be considered as a higher order MLSE. In order to validate this idea, we plotted together 4 states CS-MLSE and 8 states MLSE lines in Figure 4.37c. The curves are very similar and this shows that CS-MLSE needs fewer number of states to get the same BER. For comparison, we also graphed CS-MLSE and MLSE both with 8 states in figure 2d. In this case, CS-MLSE outperforms by 2.6Km approximately yielding a distance around 19.7Km, i.e. around 15% more fibre. This shows the advantage of considering the correlation of the samples in this system.

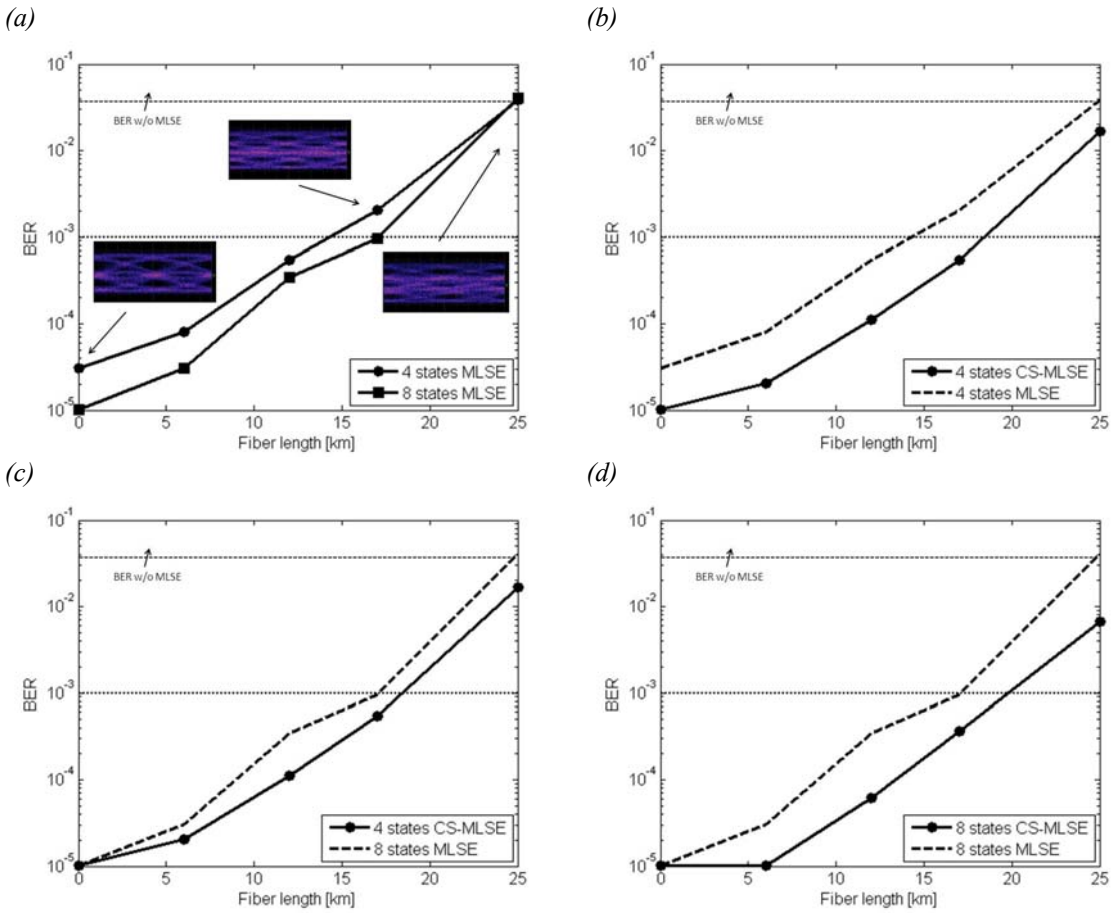

Figure 4.37 BER results against fibre length with: (a) 4 and 8 states conventional MLSE, (b) 4 states CS-MLSE and MLSE, (c) 4 states CS-MLSE and 8 states MLSE, and (d) 8 states CS-MLSE and MLSE

4.4. IM/IM Downstream cancellation using SQRT

As it has been seen in last sections, the simpler solution to achieve full duplex NRZ IM/IM transmission using the same wavelength is to use the optical downstream signal with small extinction ratio and then remodulate it with higher extinction ratio towards the OLT. However there is a sensitivity penalty in the downstream reception, requiring higher optical power at the ONU photodetector.

Other proposed techniques in literature are the following:

Gain saturation.

Loop-back WDM-PON schemes use gain saturated reflective semiconductor optical amplifiers (RSOAs) as remodulators for upstream transmission. In this scheme, through the amplitude squeezing effect in the gain saturation regime of the RSOA, the extinction ratio (ER) of the optical downstream signal injected into the RSOA is suppressed to remodulate with upstream data. However, the magnitude of the suppressed ER is strongly dependent on the optical power into the RSOA as well as the ER of the input optical downstream signal [Lee05]. This means that either low injection power or high downstream ER could degrade the upstream transmission quality owing to the fluctuation of '1' level resulting from the unsuppressed downstream ER. This imposes an upper limit of the allowable link loss from the CO to ONUs and has also limitations at high bit rates.

Wavelength filter detuning

Another solution deals with the adiabatic chirp that is present in direct modulated sources (DML). Due to the adiabatic chirp, the '0' and '1' levels are spectrally separated. The signal should present an ER as high as possible for an optimum downstream detection. On the other hand, to remodulate with the upstream data, ER as low as possible is needed (ideally 0); the level of the 0 has to be high enough to saturate the RSOA. As ER of the downstream increases, the remodulated upstream distorts. A way to solve this problem (Figure 4.38) can be slightly filtering the 1 level in order to have 0 and 1 with the same level. [Yu07] [Lee06]. This filter can be a detuned AWG at the end of the system if it can be considered lineal.

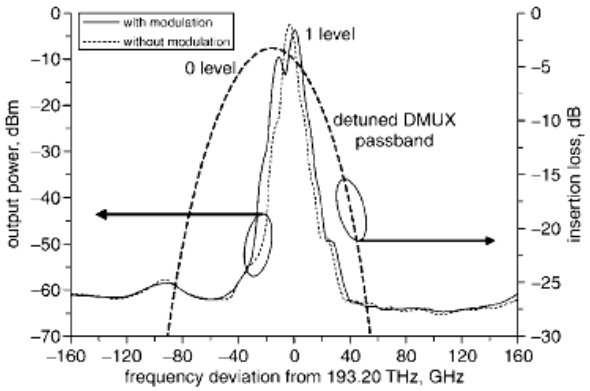

Figure 4.38 Optical spectra of adiabatic-chirped DFB-LD directly modulated [Lee06]

RSOA gain control by feed-forward current injection (FFCI) [Yu07]

In this structure, the total injection current into RSOA consists of two parts:

- Erasing downstream. The amplitude squeezing part to cancel downstream data in the incoming optical carrier.
- Remodulation part: to modulate the optical carrier with upstream data.

First, in the amplitude-squeezing part, the downstream data is inverted and after a limiting amplifier is used to generate the feed-forward current (LDD-I). That is, using the FFCI, the magnitude of the optical gain of the RSOA changes to the opposite direction to the level of the downstream data; this compensates the variation of the RSOA output power caused by the amplitude modulation of input downstream signal. Second, in the RM part, the modulation current with an upstream data and the bias current are injected into RSOA through the LDD-II. The delay paths have to be fine adjusted to cancel properly the downstream data (See Figure 4.39).

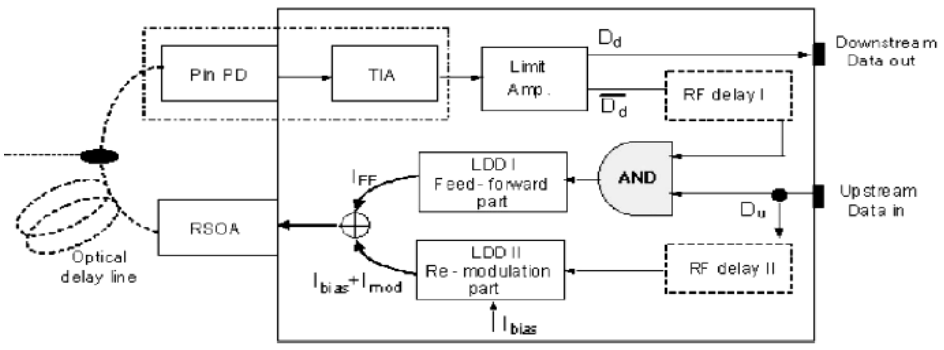

Figure 4.39. FFCI scheme

SQRT proposal

In all cases, the worse trouble in the RM schemes may be the imperfect optical erase of the modulated input light in the RSOA, because the residual interference is reflected on the "1" level thickness of the upstream eye.

An approach to reduce this degrading downstream noise, is to apply the SQRT module to compress the ones level of the received signal at the OLT, while expanding the level of the zeros, in the same way as the SQRT was used to saturate the noise in ASE-limited systems. Downstream cancellation based on FFCI and SQRT equalization in a WDM/TDM-PON using IM and wavelength reuse for asymmetrical 2.5G/1.25G transmission over 100 km reach, and high split, has been demonstrated in [Schrenk09B].

In Figure 4.40 the setup of the experiment, using the SARDANA architecture [Prat2010], is presented. The system is composed of the ONU, the OLT and a remote node (RN) which contains erbium doped fibres to remotely amplify the signal. 10 km of SMF bidirectional fibre separates the ONU and the RN, and two separate fibres of 100km connect the OLT with the RN. The ONU uses a RSOA as a modulator and the detected downstream signal is also inverted and used as a electrical input of the RSOA together with the upstream signal (FFCI technique). At the OLT, the SQRT is placed after the photodetector and the linear RF amplifier which adjust its input signal.

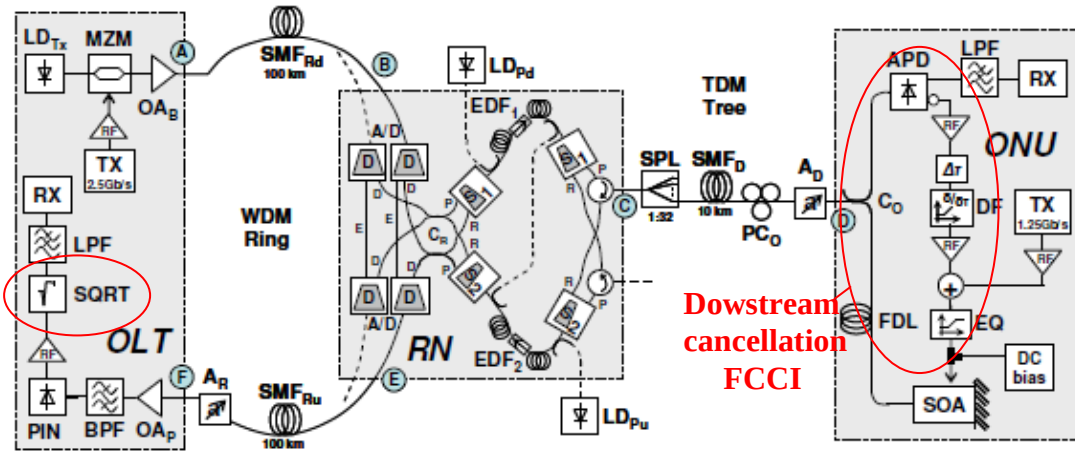

Figure 4.40 Optical spectra of adiabatic-chirped DFB-LD directly modulated [Lee06]

The results in Figure 4.41 show that the use of the SQRT improves the results in all the cases, even when there is not any presence of downstream signal. The SQRT enhanced the transmission for low BERs since there the RSOA induced overshoot is reduced by SQRT and

electrical lowpass filter. For an ER of 3 dB, the sensitivity for a BER of 10^{-10} is -22.6 dBm when using both, FFCI and the SQRT.

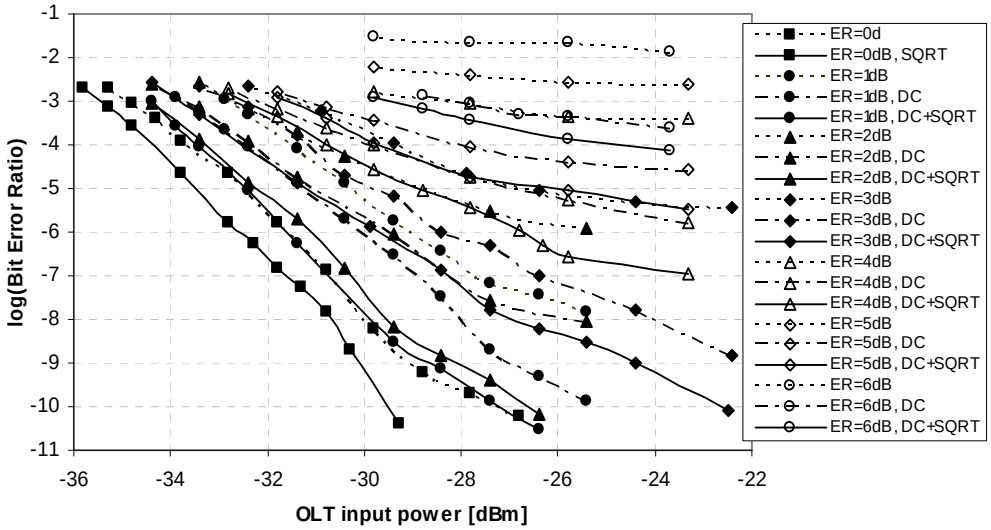

Figure 4.41 upstream BER measurements for feed-forward cancellation (DC) and square root (SQRT)

The added SQRT allows for a BER lower that 10^{-10} with a downstream ER up to 3 dB, while without the SQRT it is not possible unless the downstream is switched off. In this case, the SQRT improves the sensitivity by 2.3 dB.

4.5. Upstream Burst-Mode Reception (SQRT application)

The upstream signal over a PON consists of a rapid succession of packets with varying amplitudes [GPON03]. Hence, the decision threshold needs to make a difference between a received 1 and a received 0 differs from one packet to another packet (see Figure 4.42). Thus, a Burst Mode (BM) receiver has to extract a decision threshold from each incoming packet. This is typically done during a few bits (called the preamble) at the beginning of each packet.

In a conventional receiver for point-to-point applications, the decision threshold can be optimized to obtain a minimum BER for the given constant optical power. Typically, the optimum threshold is situated somewhere lower than half the peak eye opening due to the signal dependent noise. In conventional continuous mode, any dc-offsets can be accurately compensated using averaging measurements on many thousands of bits. For a burst-mode receiver, this is clearly not the case, since the power difference between the optical packets from different homes can be up to 15 dB.

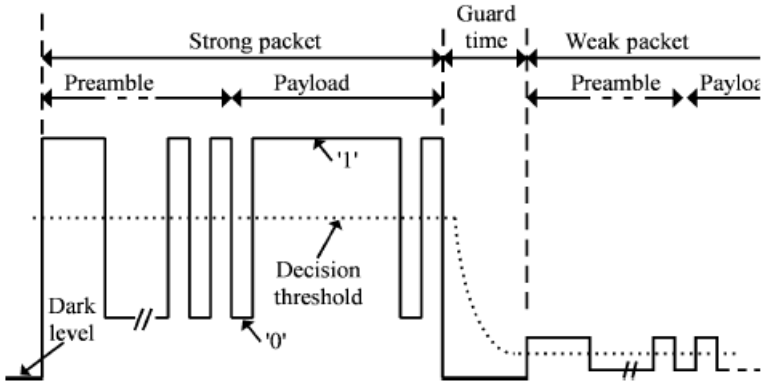

Figure 4.42 Example of BM receiver input signal. The dark level when no light arrives to the photodetector

This signal-dependent noise can be transformed by using the SQRT module, as it has been explained in Chapter 2. Here, the SQRT module can partially compensate the square law characteristic of the photodiode, produce an eye diagram more symmetrical in the presence of Downstream signal, Rayleigh Backscattering and ASE noise to facilitate the optimum threshold adjustment, and also compress the signal of the packets with high optical power to relax the requirements of the limiting amplifiers in the OLT receiver.

In GPON, the BM receiver can handle a guard time as short as 25.6 ns between packets during which all ONU transmitters are turned off. Further complicating the design is the fact that the input signal may contain sequences of up to 72 consecutive identical digits, corresponding to 57.6 ns at 1.25 Gb/s. The combination of a guard time that is shorter than the longest sequence

of consecutive identical digits implies that direct current (dc) coupling is needed. In EPON [Kramer04], where long guard times are combined with 8B/10B coding, simpler alternating current (ac) coupling it is allowed.

Two receivers have been designed, capable to be used in continuous and burst mode conditions, adapted to the OLT Receiver requirements: one AC-coupled and another one DC-coupled.

AC coupled

The AC coupled receiver consist of several blocks: the fotodetector PIN+TIA to detect the optical power and convert it into electrical current, a linear amplifier to adequate the signal power, an electrical module which performs the square root mathematical function over the incoming signal and a limiting amplifier with differential CML AC outputs. (see Figures 4.43 and 2.44). After the SQRT block, the requirements of amplitude adjustment are relaxed for the following elements, and thus the sensitivity of the receiver improves in burst mode conditions.

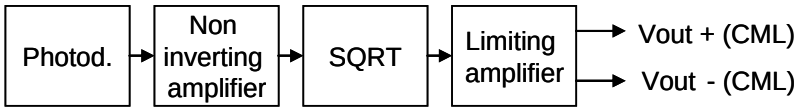

Figure 4.43 OLT AC RX schematic, diagram blocks

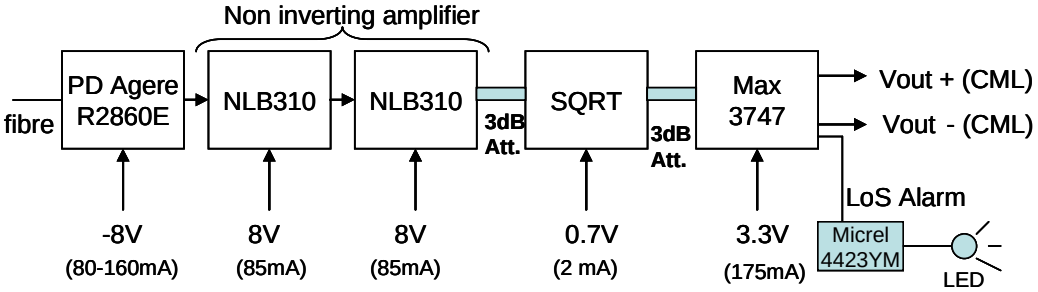

Figure 4.44 OLT AC RX schematic of the components

DC coupled

At the OLT, the optical signal is detected with a photodetector that can be a PIN+TIA, this kind of receivers uses to be AC coupled, they also can be DC coupled but then usually require high impedance at the output. In the first case, the DC and the low frequency components can be obtained through the photodiode voltage feed pad. In the second, the output signal can be divided into two paths, one with high impedance and operational amplifiers and the other with a DC block plus RF amplifiers. After these stages of amplification, the signal has to be combined adjusting the cut frequency and amplitude of both contributions. The next step is to apply the mathematical square root function (mentioned in the AC case). After the SQRT block, the

requirements of amplitude adjustment are relaxed for the following elements. The signal sent passes through different circuits: the burst enable (BE) to determine the end of a packet after more than 72 zeros, the threshold detector and a delay line, to adapt the signal plus the threshold level time and introduce both to a limiting amplifier (see Figure 4.45).

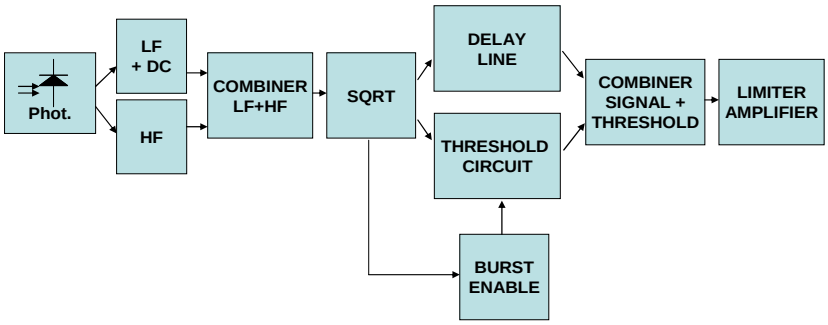

Figure 4.45 OLT DC-Rx block diagram

These devices are currently under construction.

4.6. Conclusions of Chapter 4

This chapter has been mainly focused on the RSOA modulation bandwidth enhancement.

We have demonstrated an ultra low cost implementation of 10 Gb/s transmission by direct duobinary modulation of RSOA together with passive electronic pre-equalization feasible for applications in access networks. The RSOA limits due to the nowadays RSOA technology have been analyzed considering the bit rate, the fibre link length and the optical input power.

The necessary design characteristics of a symmetrical 10 Gb/s full duplex bidirectional transmission by using low-cost and low BW RSOAs (1.2 GHz) have been presented with the introduction of optical offset filtering and DFE/FFE equalization at the OLT according to the chirp characteristics of the utilized RSOAs. The first experimental investigations considered single upstream data transmission by using the RSOA to modulate a CW signal provided by the OLT. A maximum distance of 85 km at 10 Gb/s, and BER of 10^{-9} was obtained, with the assistance of offset filtering and DFE equalization.

With respect to 10 Gb/s symmetrical and bidirectional transmission (i.e., by applying a modulated downstream signal to the RSOA), the system's parameters were optimized in order to increase the overall upstream and downstream transmission. This included the identification of the optimum driving current conditions at the RSOA, which affects the bandwidth and remodulation ER. Measurements of the required OSNR for error-free transmission at the FEC limit of $5 \cdot 10^{-4}$ obtained for different ER values of the downstream signal (ER_d) in combination with optimum filter position and for different transmission lengths. In each case, the optimum ER value was identified to allow the same performance for both upstream and downstream signal transmitted bidirectionally over the same fibre.

It is shown that up to 30 km, full-duplex transmission is possible with an OSNR equal or lower than 20 dB for upstream and downstream, by using the aforementioned

techniques (with ER_d around 3 dB). The proposed scheme allows the use of low BW RSOAs for the realization of colorless PONs achieving bidirectional connectivity (thus, better bandwidth utilization) well beyond the current coverage standards (20 km) of PONs. Additional bidirectional experiments for a PRBS of 2^7-1 have shown error free 10 Gb/s full-duplex bidirectional transmission over more than 25 km with ROSNR for a BER of 10^{-9} equal to 26 dB with a ER_d of 1.8dB.

10G operation with low BW RSOA can be also achieved by adjusting the phase in a programmable optical filter placed before the OLT receiver, capable of compensating both, source chirp and fibre CD.

The performance of a low bandwidth RSOA operating at 10 Gb/s at the highest FEC limit of BER = 10^{-3} has been also enhanced by post-processing the received signal with MLSE in terms of reachable fibre for a target BER. Around 19 km has been achieved by using a bidirectional fibre and 125 km using separate fibres for upstream and downstream. A further improvement is achieved when employing a CS-MLSE to consider the correlation among the samples. CS-MLSE permits to expand the reachable fibre by 22% and 15% for 4 and 8 states respectively in the MLSE processor. In addition, CS-MLSE requires fewer states than conventional MLSE for the same performance.

The upstream signal has also been considered in terms of remodulation and burst mode operation using the non-linearity of the SQRT module presented in Chapter 2. The SQRT is utilized to perform downstream cancellation and to equalize the amplitude level of the packets arriving at the OLT.

As a summary, the novel techniques analyzed and experimentally tested in this thesis provide a path to upgrade next-generation PONs to 10 Gb/s, as new standards (XG-PON, 10G-EPON) propose, using low-cost RSOA-based ONUs, nowadays rated for 1.25 Gb/s operation. By applying the techniques explained in this chapter, RSOA can be taken into account for NG 10G-PON systems (alternatively to DML) with added colourless operation

4.7. References of Chapter 4

[Agata09] A. Agata et al. Study on ISI Mitigation Capability of MLSE Equalizers in RSOA-based 10Gbit/s WDM PON ECOC 2009, 20-24 September, 2009, Vienna, Austria Paper 9.5.5

[Agrawal02] G.P.Agrawal. Fibre-Optic Communication Systems, 3rd ed. New York. Wiley, 2002

[Borghesani07] Borghesani, A. "Optoelectronic Components for WDM-PON" in proc ICTON 07, vol. 1, pp. 305-308. July 2007

[Cano10] I cano et al. "Colorless 10Gb/s extended reach WDM PON with low BW RSOA using MLSE" in proc. OFC2010 San Diego paper OGW2

[Chanclou07] P. Chanclou et al., "Demonstration of RSOA-based remote modulation at 2.5 and 5 Gbit/s for WDM PON", Proc. OFC 2007 San Diego, OWD1

[Chi06] Chi et al. "Improve the Performance of Orthogonal ASK/DPSK Optical Label Switching by DC Balanced Line encoding". J. Lightw. Technol., vol.24 (3), pp.1082-1092, 2006

[Cho08A] K. Y. Cho, Y. Takushima, and Y. C. Chung, "10-Gbps Operation of RSOA for WDM PON", Photon. Technol. Lett., vol. 20 no.18, pp. 1533-1535, Sep. 2008.

[Cho08B] K. Y. Cho et al., "Enhanced Operating Range of WDM PON Implemented by Using Uncooled RSOAs" Photon. Technol. Lett., vol. 20 no.18, pp. 1536-1538, Sep. 2008.

[Deavaux93] F. Devaux, Y. Sorel, J. F. Kerdiles "Simple Measurement of Fiber Dispersion and of Chirp Parameter of Intensity Modulated Light Emitter," IEEE. 11, 1937-1940, (1993).

[Doussiere94] P. Doussiere et al., "1.55 um Polarisation Independent Semiconductor Optical Amplifier with 25 dB Fiber to Fiber Gain" IEEE Photon. Technol. Lett., vol. 6, no. 2, pp. 170–172, Feb. 1994.

[Duong08] T. Duong, et al. "Experimental demonstration of 10 Gbit/s upstream transmission by remote modulation of 1 GHz RSOA using Adaptively Modulated Optical OFDM for WDM-PON single fiber architecture", Proc. ECOC 2008, Brussels, Th.3.F.1.

[Ebrahimi07] .Ebrahimi et al. "A 10-Gbit/s EML link using detuned narrowband optical filtering" Optics Express, vol. 15, no.17, Aug. 2007

[Igarashi08] K.Igarashi and K.Kikuchi. "Optical Signal Processing by Phase Modulation and Subsequent Spectral Filtering Aiming at Applications to Ultrafast Optical communication Systems" J. Quantum Electr., vol. 14, no. 3, pp.551-565 May 2008

[Inuoue97] K. Inoue "Waveform distortion in a gain-saturated semiconductor optical amplifier for NRZ and Manchester formats" IEE Proc-Optoelectron., vol. 144, vo. 6, Dec. 1997

[Kavcic98] A. Kavcic and J. M. F. Moura, "Correlation-sensitive adaptive sequence detection," IEEE Trans. Magnetics, vol. 34, no. 3, pp 763-771, May 1998.

[Lázaro06] J. A. Lázaro et al., "Remotely Amplified SARDANA: Single-fibre-tree Advanced Ring-based Dense Access Network Architecture" In proc. ECOC'06, Cannes, paper We3.P.169 September 2006

[Lee04] U. S. Lee et al., "Optical Single Sideband Signal Generation Using Phase Modulation of Semiconductor Optical Amplifier", Photon. Technol. Lett., vol. 16 no.5, pp. 1373-1375, May 2004.

[Lee06] W. Lee et al. “Frequency Detuning Effects in a Loop-Back WDM-PON Employing Gain-Saturated RSOAs”, Photonics Technol. Lett., vol.18, no. 13, pp. 1436-1438, July 2006

[Lee07] W. Lee, et al. “Optical transceiver employing an RSOA with feed-forward current injection” in proc. OFC 2007 paper OTuH1

[Lin08] S. Lin et al. “Simple approach for bidirectional performance enhancement on WDM-PONs with direct-modulation laser and RSOAs” Optics Opt. Express, vol. 16, no. 6, pp. J. Lightwave Technol 3636–3643, March 2008.

[Liu06] Y. Liu, et al., “Error-free all-optical wavelength conversion at 160 Gbps using a semiconductor optical amplifier and an optical bandpass filter,” J. Lightw. Technol., vol. 24, no. 1, pp. 230–236, Jan. 2006.

[Lyobomirsky03] I. Lyobomirsky, et al. “Interplay of Fiber Nonlinearity and Optical Filtering in Ultradense WDM,” IEEE Photon. Technol. Lett., vol. 15, no. 1, pp. 147–149, Jan. 2003.

[Matsui06] Y. Matsui et al. “Chirp Managed Directly Modulated Laser (CML)” Photonics Technol. Lett., vol.18, no. 2, pp. 385-387, Jan. 2006

[Omella08] M. Omella, et al. “10 Gb/s RSOA Transmission by Direct Duobinary Modulation” ECOC 2008, Brussels, 21-25 September, paper Tu.3.E4

[Omella09A] M. Omella et al., ”Full-Duplex Bidirectional Transmission at 10 Gbps in WDM PONs with RSOA based ONU using Offset Optical Filtering and Electronic Equalization”, OFC09 San Diego, paper OThA7.

[Omella09B] M. Omella, et al., “10 Gb/s full-duplex bidirectional transmission with RSOA-based ONU using detuned optical filtering and decision feedback equalization”, OSA Optics Express, vol. 17, no. 7, pp. 5008–5013 (2009).

[Omella09C] M. Omella, et al., “Design optimization for 10Gb/s full-duplex transmission using RSOA-based ONU with electrical and optical filtering and equalization” ECOC 2009, 20-24 September, 2009, Vienna, Austria Paper 7.5.5

[Omella10B] M. Omella et al., “High Gain RSOA as 10G ONU Transmitter and Optical Phase Adjustment at the OLT” in proc. ANIC’10, Karlsruhe (Germany) 21-24 June 2010, post-deadline paper AThD2

[Papagiannakis08A] Papagiannakis et al., “Investigation of 10 Gb/s RSOA-based Upstream Transmission in WDM PONs Utilizing Optical Filtering and Electronic Equalization” IEEE Photon. Technol. Lett, vol. 20, no. 24, pp. 2168 – 2170, Dec. 2008.

[Papagiannakis08B] Papagiannakis, et al., “Upstream Transmission in WDM PONs at 10Gbps Using Low Bandwidth RSOAs Assisted with Optical Filtering and Electronic Equalization” ECOC 2008, Brussels, 21-25 September, paper We.3.F.3

[Papagiannakis10] Papagiannakis et al., "Design Characteristics for a Full-Duplex IM/IM Bidirectional Transmission at 10 Gb/s Using Low Bandwidth RSOA" J. Lightw. Technol, vol. 28, no. 7, pp. 1094-1101, April 2010.

[Prat05] J. Prat et al., “Optical Network Unit Based on a Bidirectional Reflective Semiconductor Optical amplifier for Fiber-to-the-Home Networks”, IEEE Photon. Technol. Lett., vol. 17, vo. 1, pp. 250 -252, Jan. 2005.

[Rujian08] Rujian Lin, “Next Generation PON in Emerging Networks,” Proc. OFC 2008, San Diego, OWH1

[Schrenk09] B. Schrenk, et al. “Enhanced Transmission in Long Reach WDM/TDM Passive Optical Networks by Means of Multiple Downstream Cancellation Techniques” ECOC 2009, 20-24 September, 2009, Vienna, Austria Paper 8.5.4

[Schrenk10] B. Schrenk, et al., “Direct 10 Gb/s Modulation of a Single-Section RSOA in PONs with High Optical Budget” IEEE Photon. Technol. Lett, vol. 22, no. 6, pp. 392 – 394, March 2010.

[Tanaka10] K. Tanaka, A. Agata, and Y. Horiuchi “IEEE 802.3av 10G-EPON Standardization and Its Research and Development Status”. J. Lightw. Technol., vol. 28, no. 4, Feb 2010 pp. 651-661

[Watanabe00] T.Watanabe, et al. “Transmission performance of chirp-controlled signal by using semiconductor optical amplifier”, J. Lightw. Technol., vol. 8, no. 8, pp. 1069–1077, Aug. 2000.

[Yang09] C. Yang “Simultaneous ER Enhancement and Light Reuse Scheme for RSOA-Based WDM-PONs” in proc OECC 2009 paper ThLP45

[Yiu06] Y. Liu, et al. , “Error-Free All-Optical Wavelength Conversion at 160 Gb/s Using a Semiconductor Optical Amplifier and an Optical Bandpass Filter,” J. Lightw. Technol., vol. 24, no. 1, pp. 230–236, Jan. 2006.

5. Conclusions and future work

This thesis has mainly been focused in low cost solutions to improve the performance of high speed signal in WDM PON with minimum infrastructure.

Maybe the main conclusion that can be extracted from all the proposed techniques and results is that, in most cases, understanding the origin of the degradation is mandatory to find a simple and cost effective solution capable to mitigate it. That solution will improve the signal alone, or with the help of "general solutions" which act over the consequences of these impairments (ISI) to upgrade the performance of a received signal like electronic or optical equalization.

In its origin, CD and ASE noise are linear with optical field. For this reason, returning part of the lost linearity with the SQRT module helps at reducing the complexity of electronic equalizers. As a mode of example, a transmission over more than 1000 km (exceptionally in this thesis long haul scenario) was achieved using MLSE together with the SQRT, without optical dispersion compensation. More focused in PON systems using FFE, simulation results showed that with SQRT the transmission distance can be increased by more than 50% up to 165km for a 2dB penalty at a BER of 10^{-10}. Also in RoF systems the harmonics are highly reduced. After statistical analysis and BER simulation, the signal after the SQRT transformation presented a performance very close to the obtained with the function which was calculated to assure Gaussian distribution after detection in optically amplified (ASE dominant) systems.

This SQRT module has been demonstrated to be a very low cost solution. A first version has been developed with an electronic circuit with discrete components using the non-linearity of the schottky diode, with a BW of 7GHz and 10dB of gain compression; and the second implementation, in a MMIC chip, has shown its integration possibilities together with the photodiode, presenting huge bandwidth (around 20GHz) and gain compression (21dB).

Also, the SQRT module is useful for other applications as downstream cancellation in the upstream signal in bidirectional transmissions, and to reduce the amplitude differences of the different packets in burst mode receivers, relaxing the adjustment requirements for the subsequent limiting amplifiers.

In single fibre, bidirectional systems with the same wavelength for up- and downstream signal suffer impairment because the Rayleigh Backscattering and the upstream signal overlap. By performing wavelength shifting at the ONU, the overlap and thus the coherent RB is avoided. Several wavelength shifter devices have been proposed for the first time, based in 2 and 3 arms capable of translating the wavelength that comes from the OLT in several GHz to avoid the overlap between the upstream signal and the RB, but maintaining the signal in the same AWG channel. These devices are less complex than the 4-arm structures and require simpler signals than the sawtooth that is necessary for the 1-arm phase modulator. Experimental validation of the WS technique for RB mitigation has been performed, first with a commercial dual arm MZM and afterwards by using a RSOA with a low duty square signal with improvements of 5 to 7dB in crosstalk tolerance. As future work, it would be interesting to explore deeper into the optimum remodulation together with wavelength shifting in reflexive configuration for the presented 2-3 arm proposed devices. Also two-section RSOAs can be an integrated solution to perform WS and remodulation at the ONU premises.

In this work, we have proposed some techniques to achieve 10G operation with low cost RSOAs nowadays rated for 1.25 Gb/s operation, the main ones are: duobinary modulation, detuned offset filtering together with DFE-FFE equalization, phase adjustment at the OLT with a programmable optical filter and MLSE.

After the experiments of duobinary modulation, it was clear that the worse limitation of a RSOA was not its BW but its chirp, due to the fact that, after the transmission over few km, the shape of the signal was not with 3 levels anymore to be detected by the rectifier. For this reason, the most impressive results were obtained with the technique that dealt directly with chirp: when applying offset filtering the transient chirp is used to increase the BW by aligning properly the signal in the slope of a filter and in the phase adjustment experiments the chirp and the chromatic dispersion effects of the fibre were mitigated by adjusting properly the phase in an programmable optical filter.

The experiments with offset filtering plus DFE-FFE allowed the first reported transmission done with a RSOA in real time at 10 Gb/s over more than 20km for low BER (10^{-9}). An 85km long upstream transmission has been demonstrated when the downstream wavelength was a CW signal. Full duplex transmission at 10 Gb/s has been also reported for the first time, showing the impact of the patterning effects due to the different dynamics behaviour of RSOAs in o/o and o/e operation. Another way to deal with chirp is restoring the phase; it avoids the attenuation of the filter compared with detuned optical filtering and provides similar results. That has allowed transmitting at FEC limit at a bit rate of 10.3 Gb/s with a power budget of 23dB between the

OLT and the ONU using 26km of optical fibre. Complementary experiments have been performed using the MLSE to directly detect signals at 10Gb/s at FEC limit by applying both a conventional and a correlation sensitive MLSE.

The novel techniques analyzed and experimentally tested in this thesis provide a path to upgrade next-generation PONs to 10 Gb/s, as new standards (XG-PON, 10G-EPON) propose.

It is also left for future works the combination and optimization of techniques used for CD, RB and 10G operation in low cost reflective ONUs in the same experiment.

6. APPENDIX. Research Publications

CONGRESS PUBLICATIONS

1. M. Omella, P. Chanclou, J. A. Lázaro , J. Prat "RSOA as a Sawtooth Generator for Rayleigh Backscattering Effect Mitigation" in proc. ECOC'10, Torino (Italy), 19-24 Sept 2010, paper Mo.1.B.5 .

2. M. Omella, P. Chanclou, J. A. Lázaro , J. Prat "High Gain RSOA as 10G ONU Transmitter and Optical Phase Adjustment at the OLT" in proc. ANIC'10, Karlsruhe (Germany) 21-24 June 2010, post-deadline paper AThD2

3. M. Omella, I. Papagiannakis, D. Klonidis, J.A. Lazaro, A.N. Birbas, J. Kikidis, I. Tomkos, J. Prat. "Design optimization for 10gb/s full-duplex transmission using RSOA-based ONU with electrical and optical filtering and equalization" ECOC 2009, 20-24 September, 2009, Vienna, Austria Paper 7.5.5

4. B. Schrenk, F. Bonada, M. Omella, J.A. Lazaro and J. Prat "Enhanced Transmission in Long Reach WDM/TDM Passive Optical Networks by Means of Multiple Downstream Cancellation Techniques" ECOC 2009, 20-24 September, 2009, Vienna, Austria Paper 8.5.4

5. M. Omella, I. Papagiannakis, B. Schrenk, D. Klonidis, A. N. Birbas J. Kikidis, J. Prat and I.Tomkos," Full-Duplex Bidirectional Transmission at 10 Gbps in WDM PONs with RSOA-based ONU using Offset Optical Filtering and Electronic Equalization", OFC09 San Diego paper OThA7

6. M. Omella, V. Polo, J. Lazaro, B. Schrenk and J. Prat "10 Gb/s RSOA Transmission by Direct Duobinary Modulation" ECOC 2008, Brussels, 21-25 September, paper Tu.3.E4

7. Papagiannakis, M. Omella, D. Klonidis, J. Kikidis, A. N. Birbas, I. Tomkos and J. Prat, "Upstream Transmission in WDM PONs at 10Gbps Using Low Bandwidth RSOAs Assisted with Optical Filtering and Electronic Equalization" ECOC 2008, Brussels, 21-25 September, paper We.3.F.3

8. B. Schrenk, M. Omella, J. Lazaro, J. Prat “Remote Wavelength Generation for Upstream Transmisión in Time and Wavelength Division Multiplexed Passive Optical Networks with C and L-Band Utilization.” Proc.”ICTON2008 Atenas 21-26 June We.B4.7

9. J. Prat, M. Omella, P. Poggiolini, G. Bosco, R. Killey A. Teixeira, R. Sousa “Electronic Equalization of Photodetection by Means of an SQRT Module” ICTON2007 We.C3.6

10. P. Poggiolini, G.Bosco, M.Visintin, P. Bayvel, R. Killey, S. Savory, Y. Benlachtar, J.Prat, M. Omella. “Recent Progress and Fundamental Limitations of Optical MLSE Receivers” ICTON2007 Mo.B1.1

11. J. Prat, J. A. Lázaro, J. M. Fabrega, V. Polo, C. Bock, C. Arellano, M. Omella, “Next Generation Architectures for Optical Access and Enabling Technologies,” OPTOEL’07, Bilbao, July 2007

12. S. J. Savory, Y. Benlachtar, R. I. Killey, P. Bayvel, G. Bosco, P. Poggiolini, J. Prat and M. Omella, "IMDD Transmission over 1040 km of standard single-mode fiber at 10 Gbit/s using one-sample-per-bit reduced-complexity MLSE receiver" Optical Fiber Communications Conference, OFC/NFOEC’07, Proceedings, OThK2, Anaheim, USA, March 2007

13. J. Prat, M. Omella and V. Polo "Wavelength shifting for colorless ONUs in single-fiber WDM-PONs," Optical Fiber Communications Conference, OFC/NFOEC’07, Proceedings, OTuG6, Anaheim, USA, March 2007

14. J. A. Lázaro, V. Polo, C. Bock, M. Omella, J. Prat, “Remotely Amplified SARDANA: Single fibre-tree Advanced Ring-based Dense Access Network Architecture”, Proc. ECOC 2006 Cannes (France), September 2006, We3.P.169

15. J. Prat, M. C. Santos, M. Omella, A. Napoli, “Electronic Distortion Equalization for Dispersion-Limited Radio-over-Fiber Systems”, 13th International Conference on Telecommunications ICT’06-, Madeira, May 2006.

16. J. Prat, A. Napoli, M.C. Santos, M. Omella, P. Poggiolini, “Non-Linear EE to Enhance the compensation Capabilities of Linear EE”, ECOC September 2005, Sunday Workshop.

17. J. Prat, J.M. Gené, V.Polo, M. Omella. “Duobinary-Based CPFSK System with Direct Modulation to Reduce the Bandwidth Requirement of the Laser” Winter School Aveiro2005

JOURNAL PUBLICATIONS:

1. B. Schrenk, G. de Valicourt, M. Omella, J. A. Lazaro, R. Brenot, J. Prat, “Direct 10 Gb/s Modulation of a Single-Section RSOA in PONs with High Optical Budget” IEEE Photon. Technol. Lett, vol. 22, no. 6, pp. 392 – 394, March 2010.

2. Papagiannakis, M.Omella, D. Klonidis, J. A. Lazaro A. N. Birbas, J. Kikidis, I.Tomkos and J.Prat. “Design Characteristics for a Full-Duplex IM/IM Bidirectional Transmission at 10 Gb/s Using Low Bandwidth RSOA” J. Lightw. Technol, vol. 28, no. 7, pp. 1094-1101, April 2010.

3. M. Omella, J.A. Lazaro, V. Polo, J. Prat. Driving Requirements for Wavelength Shifting in Colorless ONU with Dual-Arm Modulator. Journal of Lightwave Technology 2009, vol. 27 pp. 3912-3918.

4. M. Omella, I. Papagiannakis, B. Schrenk, D. Klonidis, J. A. Lázaro, A. N. Birbas, J.Kikidis, J. Prat, and I. Tomkos “10 Gb/s full-duplex bidirectional transmission with RSOA-based ONU using detuned optical filtering and decision feedback equalization”, OSA Optics Express, vol. 17, Iss. 7, pp. 5008–5013 (2009).

5. Papagiannakis, M.Omella, D. Klonidis, A. N. Birbas, J. Kikidis, I.Tomkos and J.Prat, “Investigation of 10 Gb/s RSOA-based Upstream Transmission in WDM PONs Utilizing Optical Filtering and Electronic Equalization” IEEE Photonics Technology Letters, vol. 20, no. 24, pp. 2168 – 2170, Dec. 2009.

6. Papagiannakis, D. Klonidis, V. Curri, P. Poggiolini, G. Bosco, R.I. Killey, M. Omella, J. Prat, D. Fonseca, A. Teixeira, R. Freund, E. Grivas, A. Bogris, A. N. Birbas, and I. Tomkos “A Tutorial on Electronic Dispersion Compensation”. IET Optoelectron. 2009, Vol. 3, Iss. 2, pp. 73–85

7. J. Prat, M.C. Santos, M. Omella, “Square Root Module to Combat Dispersion-Induced Nonlinear Distortion in Radio-Over-Fiber Systems”, IEEE Photonics Technology Letters, vol. 18, no. 18, pp. 1928 – 1930, Sept. 2006

PATENTS:

1. “Wavelength Shifter module for optical fiber access communications and other applications”. Inventors: J. Prat, J. Lázaro, M. Omella. P-200700765.

2. “Optical Network Element with Brillouin Effect Colorless Wavelength shift”. Inventors: J. Lázaro, J. Prat, M. Omella. Docket No. 74035. P002101. USA,

3. “Receiver for optical communications with improved non linear equalizer” P200803431. Inventors: J. Prat, M. Omella, A. Jiménez.

BOOKS:

Collaboration for the book: “Next Generation FTTH Passive Optical Networks. Research towards Unlimited Bandwidth Access.” Editor: Josep Prat. Editorial Springer. ISBN 978-1-4020-8469-0. Co-author of chapter 4: “Enhanced transmision Techniques”.